Characterization of telomere-associated proteins in *Trypanosoma brucei*

-

Charakterisierung Telomer-assoziierter Proteine in *Trypanosoma brucei*

Doctoral thesis

for a doctoral degree

at the Graduate School of Life Sciences,

Julius-Maximilians-Universität Würzburg,

Section Infection and Immunity

submitted by

Nadine Weisert

from

Frankfurt am Main

Würzburg, 2023

Submitted on:

Members of the Thesis Committee

Chairperson: Prof. Dr. Thomas Dandekar

Primary Supervisor: Prof. Dr. Christian J. Janzen

Supervisor (Second): Prof. Dr. Nicolai Siegel

Supervisor (Third): Prof. Dr. Manfred Alsheimer

Date of Public Defense:

Date of Receipt of Certificates:

Affidavit

I hereby confirm that my thesis entitled ‘Characterization of telomere-associated proteins in *Trypanosoma brucei*’ is the result of my own work. I did not receive any help or support from commercial consultants. All sources and / or materials applied are listed and specified in the thesis.

Furthermore, I confirm that this thesis has not yet been submitted as part of another examination process neither in identical nor in similar form.

Würzburg, 2023

Eidesstattliche Erklärung

Hiermit erkläre ich an Eides statt, die Dissertation „Charakterisierung Telomer-assoziierter Proteine in *Trypanosoma brucei*“ eigenständig, d.h. insbesondere selbständig und ohne Hilfe eines kommerziellen Promotionsberaters, angefertigt und keine anderen als die von mir angegebenen Quellen und Hilfsmittel verwendet zu haben.

Ich erkläre außerdem, dass die Dissertation weder in gleicher noch in ähnlicher Form bereits in einem anderen Prüfungsverfahren vorgelegen hat.

Würzburg, 2023

Parts of this thesis are displayed in a drafted publication for a scientific journal (in preparation for submission). Affected figures and tables are additonally marked. The title and the authors of this publication (except Weisert N) can change during the submission process.

Weisert N., Kreß V., Hartleb L., Luko K., Lototska L., Krapoth N. C., Ulrich H., Janzen C.J., Butter F. (2023). TelAP2 links TelAP1 to the telomere complex in *Trypanosoma brucei*.

Parts of this thesis have been presented at international conferences:

09/2020 Novel telomere-associated proteins and their impact on VSG expression site regulation in *Trypanosoma brucei.*
Weisert N (presenting author), Reis H, Schwebs M, Luko K, Dejung M, Butter F, Janzen CJ
Poster presentation at the Molecular Parasitology Meeting by the Genetics Society of America (GSA) **MPMXXI Meeting,** online

10/2019 The impact of novel telomere-associated protein complexes on VSG expression site regulation in *Trypanosoma brucei*
Weisert N (presenting author), Reis H, Schwebs M, Luko K, Dejung M, Butter F, Janzen CJ
Poster presentation at the 14th Eureka International Symposium. **Eureka International Symposium,** Würzburg

04/2019 The impact of novel telomere-associated protein complexes on VSG expression site regulation in *Trypanosoma brucei.*
Weisert N (presenting author), Reis H, Schwebs M, Luko K, Dejung M, Butter F, Janzen CJ
Poster presentation at the 22nd Kinetoplastid Molecular Cell Biology Conference. **KMCB Conference,** Woods Hole, USA

08/2018 Impact of telomere-associated protein complexes on VSG expression site regulation in *Trypanosoma brucei.*
Weisert N (presenting author)
Oral presentation at the Bernhard Nocht Institute for tropical medicine. **DGP 11th Summer School für Parasitologen,** Hamburg

TABLE OF CONTENTS

ACKNOWLEDGMENTS

First, I want to thank my primary supervisor Christian Janzen for giving me the opportunity to be a part of his research group, not only during my PhD but also already during my master thesis. Thank you for your constant support, guidance and motivation and the possibility to work in this interesting field.

I would also like to thank the other members of my Thesis Committee Nicolai Siegel and Manfred Alsheimer for their constructive feedback and input during our meetings.

Furthermore, I am very grateful for my collaboration partner Falk Butter and the members of his group, especially Katharina Luko, Mario Dejung and Albert Fradera Sola for their work on my project and their mass spectrometry expertise. Additionally, I would like to thank Helle Ulrich and Nils Christian Krapoth from the IMB Mainz for their contribution to my project by performing the Yeast two-hybrid experiments and their expertise.

I would like to thank the current and former members of the AG Janzen lab. Thank you for all your support and fruitful discussions as well as for the time we spend together outside of work. My thanks goes especially to Elisabeth, who supported my work immensely with her skills in immunofluorescence and cloning and to Nicole, who was not just a colleague but became a very dear friend of mine. I am looking forward to walking another 100 km (or more!) with you.

I am also very grateful for my students Oliver, Tamara, Verena and Melina who supported my research and were always eager to learn and to work. I enormously enjoyed being your supervisor.

I also want to thank the whole Cell- and Developmental Biology Department. Thank you for a wonderful time, all your help and constructive ideas during TrypClub and all the fun we had inside and outside of lab. I will always remember the laser tag, wine festivals, carnival parties, the hiking, wine tasting, amusement park visits and the obstacle parkour we did together, and I am thankful I had such a great time with you guys in 2018, 2019, 2020 and 2021. Corona lockdown was only half as bad because of this group of people who made work feel like home to me, at least during these years. My thanks goes especially to Kevin (additionally an exeptional neighbour!) and Fabian, who became dear friends and supported me during my most difficult times in and outside of work. Thank you so much.

At last, I want to thank all my beloved friends but especially Maximilian, Lossy and Nina. Without your constant support, your warm words and love, especially during the year 2022, I wouldn't have been able to finish this thesis. You really showed me what the word friendship means and how rare and precious true friends are in a time of struggle and need. I am incredibly grateful to have you in my life and I truly hope this will never change.

Ein Dank auch an meine Eltern für ihre Unterstützung während meiner Zeit als Doktorandin und während meines Schreibprozesses.

SUMMARY

The unicellular pathogen *Trypanosoma brucei* is the causative agent of African trypanosomiasis, an endemic disease prevalent in sub-Saharan Africa. *Trypanosoma brucei* alternates between a mammalian host and the tsetse fly vector. The extracellular parasite survives in the mammalian bloodstream by periodically exchanging their ˈvariant surface glycoproteinˈ (VSG) coat to evade the host immune response. This antigenic variation is achieved through monoallelic expression of one VSG variant from subtelomeric ˈbloodstream form expression sitesˈ (BES) at a given timepoint. During the differentiation from the bloodstream form (BSF) to the procyclic form (PCF) in the tsetse fly midgut, the stage specific surface protein is transcriptionally silenced and replaced by procyclins. Due to their subtelomeric localization on the chromosomes, VSG transcription and silencing is partly regulated by homologues of the mammalian telomere complex such as *Tb*TRF, *Tb*TIF2 and *Tb*RAP1 as well as by ˈtelomere-associated proteinsˈ (TelAPs) like TelAP1. To gain more insights into transcription regulation of VSG genes, the identification and characterization of other TelAPs is critical and has not yet been achieved.

In a previous study, two biochemical approaches were used to identify other novel TelAPs. By using ˈco-immunoprecipitationˈ (co-IP) to enrich possible interaction partners of *Tb*TRF and by affinity chromatography using telomeric repeat oligonucleotides, a listing of TelAP candidates has been conducted. With this approach TelAP1 was identified as a novel component of the telomere complex, involved in the kinetics of transcriptional BES silencing during BSF to PCF differentiation.

To gain further insights into the telomere complex composition, other previously enriched proteins were characterized through a screening process using RNA interference to deplete potential candidates. VSG expression profile changes and overall proteomic changes after depletion were analyzed by mass spectrometry. With this method, one can gain insights into the functions of the proteins and their involvement in VSG expression site regulation. To validate the interaction of proteins enriched by co-IP with *Tb*TRF and TelAP1 and to identify novel interaction proteins, I performed reciprocal affinity purifications of the four most promising candidates (TelAP2, TelAP3, PPL2 and PolIE) and additionally confirmed colocalization of two candidates with *Tb*TRF via immunofluorescence (TelAP2, TelAP3). TelAP3 colocalizes with *Tb*TRF and potentially interacts with *Tb*TRF, *Tb*TIF2, TelAP1 and TelAP2, as well as with two translesion polymerases PPL2 and PolIE in BSF. PPL2 and PolIE seem to be in close contact to each other at the telomeric ends and fulfill different roles as only PolIE is involved in VSG regulation while PPL2 is not. TelAP2 was previously characterized to be associated with telomeres by partially colocalizing with *Tb*TRF and cells show a VSG derepression phenotype when the protein was depleted. Here I show that TelAP2 interacts with the telomere-binding proteins *Tb*TRF and *Tb*TIF2 as well as with the telomere-associated protein TelAP1 in BSF and that TelAP2 depletion results in a loss of TelAP1 colocalization with *Tb*TRF in BSF.

In conclusion, this study demonstrates that characterizing potential TelAPs is effective in gaining insights into the telomeric complex's composition and its role in VSG regulation in *Trypanosoma brucei*. Understanding these interactions could potentially lead to new therapeutic targets for combatting African trypanosomiasis.

ZUSAMMENFASSUNG

Der einzellige Pathogen *Trypanosoma brucei* ist der Erreger der afrikanischen Trypanosomiasis, eine endemische Krankheit vertreten in der Sub-Sahara Zone Afrikas. *Trypanosoma brucei* wechselt zwischen einem Säugerwirt und dem Insektenvektor, der Tsetse-Fliege. Der im Blutstrom des Säugers vorkommende, extrazelluläre Parasit ändert seinen Oberflächenmantel bestehend aus dem ˈvariablen Oberflächenproteinˈ (VSG) in periodischen Abständen, um der Immunantwort des Wirtes auszuweichen. Diese antigenetische Variation wird durch die monoallelische Expression einer einzelnen VSG-Variante, lokalisiert auf den ˈBlutstromform Expressionsseitenˈ (BES), zu einem bestimmten Zeitpunkt erreicht. Diese stadienspezifischen Oberflächenproteine werden während der Differenzierung der ˈBlutstromformˈ (BSF) zur ˈprozyklischen Formˈ (PCF) im Mitteldarm der Tsetse-Fliege stillgelegt und durch Prozykline ersetzt. Wegen der subtelomeren Lokalisation wird die VSG Transkription und Stilllegung teilweise durch Homologe des Säuger Telomerkomplexes *Tb*TRF, *Tb*TIF2 und *Tb*RAP1 als auch durch Telomer-assoziierte Proteine (TelAPs) wie TelAP1 reguliert. Um Einblicke in die Transkriptionsregulation der VSG Gene zu erhalten, ist die Identifikation und Charakterisierung anderer Telomer-assoziierter Proteine von großem Interesse.

In einer vorherigen Studie wurden zwei komplementäre biochemische Versuchsansätze verwendet, um weitere neue TelAPs zu identifizieren. Es wurde eine ko-Immunpräzipitation (co-IP) durchgeführt, um mögliche Interaktionspartner von *Tb*TRF zu identifizieren, sowie eine Affinitätschromatographie unter Verwendung telomerischen Wiederholungseinheiten. Hierdurch wurde eine Liste von potenziellen Kandidaten generiert. Mit diesem Ansatz wurde TelAP1 als neue Komponente des Telomerkomplexes identifiziert, welches an der Kinetik der transkriptionellen BES-Stilllegung während der Differenzierung von BSF zu PCF beteiligt ist.

Um weitere Einblicke in die Zusammensetzung des Telomerkomplexes zu erhalten, wurden zuvor angereicherte Proteine durch einen Screening-Prozess unter Verwendung von RNA-Interferenz charakterisiert. Nach der Depletion von 21 Proteinen wurden massenspektrometrische Analysen der VSG Expressionsprofiländerungen sowie allgemeine Veränderungen des Proteomenprofils analysiert. Mit dieser Methode können Erkenntnisse über die Funktion der jeweiligen Proteine und ihrer Beteiligung an der Regulierung der antigenetischen Variation von *T. brucei* gewonnen werden. Um die Interaktionen von Proteinen zu validieren, welche bei den Co-Immunpräzipitationen mit *Tb*TRF und TelAP1 angereichert wurden, habe ich eine reziproke Affinitätschromatographie mit vier der vielversprechendsten Kandidaten durchgeführt (TelAP2, TelAP3, PPL2 und PolIE). Zusätzlich bestätigte ich die Co-lokalisation von zwei Kandidaten mit *Tb*TRF via Immunfluoreszenzaufnahmen (TelAP2, TelAP3). TelAP3 ko-lokalisiert mit *Tb*TRF und TelAP1 und interagiert potenziell mit *Tb*TRF, *Tb*TIF2, TelAP1 und TelAP2 als auch mit den zwei Transläsionspolymerasen PPL2 und PolIE in BSF. PPL2 und PolIE stehen in engem Kontakt zueinander und nehmen an den Telomerenden unterschiedliche Funktionen ein, da nur PolIE an der VSG Regulation beteiligt ist.

TelAP2 wurde in einer vorherigen Publikation als Telomer-assoziiertes Protein durch partielle Co-Lokalisation mit *Tb*TRF identifiziert und Zellen zeigen nach der Depletion von TelAP2 eine Derepression von zuvor stillgelegten VSGs. In dieser Studie zeige ich, dass TelAP2 mit den Telomer-bindenden Proteinen *Tb*TRF und *Tb*TIF2 sowie mit dem telomerassoziierten Protein

TelAP1 in BSF interagiert und dass die Depletion von TelAP2 zu dem Verlust der Co-Lokalisation von TelAP1 mit *Tb*TRF in BSF führt.

Zusammenfassend zeigt diese Studie, dass die Charakterisierung potenzieller TelAPs dazu beiträgt, Einblicke in die Zusammensetzung des Telomerkomplexes und dessen Rolle bei der VSG-Regulation in *Trypanosoma brucei* zu gewinnen. Das Verständnis dieser Interaktionen könnte möglicherweise zu neuen therapeutischen Ansatzpunkten zur Bekämpfung der afrikanischen Trypanosomiasis führen.

FIGURES AND TABLES INDEX

Figure index

Table index

ABBREVIATIONS

AAT	Animal African Trypanosomiasis
ACD	adrenocortical dysplasia protein homologue (TPP1/TINT1, PTOP, PIP1)
ALT	Alternative lengthening of telomeres
ASF1A	Anti-silencing factor 1A
AT	African Trypanosomiasis
ATM	Ataxia-telangiectasia mutated
ATP	Adenosine triphosphate
ATR	Ataxia telangiectasia and Rad3-related
BARP	Brucei alanine-rich protein
Base J	ß-D-glucopyranosyl-oxymethyluracil
BDF	Bromodomain factor
BES	Bloodstream form expression site
BLE	Bleomycin resistance gene
bp	Base pair
BP	Branch point
BSF	Bloodstream form
C	Celsius
CAF-1	Chromatin assembly factor 1
Cas9	CRISPR-associated gene 9
CITFA	Class I transcription factor A
Co-IP	co-immunoprecipitation
CRISPR	Clustered regularly interspaced short palindromic repeats
CST	CTC1-STN1-TEN1
CTC1	Conserved telomere capping protein 1
DAPI	4’,6-diamidino-2-phenylindole
D-loop	Displacement loop
DMSO	Dimethyl sulfoxide
DNA	Deoxyribonucleic acid
dNTP	Deoxynucleoside triphosphate
DOT1b	Disruptor of telomeric silencing 1b
DSBs	Double-strand breaks
dsDNA	Double-strand DNA
DTT	Dithiothreitol
E. coli	*Escherichia coli*
EMSA	Electrophoretic mobility shift assay
ESAG	Expression site associated genes
ESB	Expression site body
EtOH	Ethanol
FACT	Facilitates chromatin transcription
FAZ	Flagellum attachment zone
FDA	Food and Drug Administration
FCS	Fetal calf serum
fw	Forward
g	Gram
g	Relative centrifugal force
gDNA	Genomic DNA
GOI	Gene of interest
GPI	glycosylphosphatidylinositol
G418	Neomycin
HAT	Human African Trypanosomiasis
HEPES	4-(2-hydroxyethyl)-1-piperazineethanesulfonic acid

HMI-9	Hirumi's modified Iscove's medium 9
HP1	Heterochromatin protein 1
HYG	Hygromycin phosphotransferase gene
Hygro	Hygromycin
I	Input material
IP	Immunoprecipitation
kb	Kilobase pair
kDa	Kilodalton
KO	Knockout
LB	Lysogeny broth
L. major	*Leishmania major*
M	Molar
mA	Milliampere
MeOH	Methanol
MES	Metacyclic expression site
µg	Microgram
mg	Milligram
min	Minute
MiTat1.2	Molteno institute trypanozoon antigen type 1.2
µl	Microliter
ml	Milliliter
µm	Micrometer
µM	Micromolar
mm	Millimeter
mM	Millimolar
MMEJ	Microhomology mediated end joining
mRNA	Messenger RNA
MS	Mass spectrometry
NEO	Aminoglycoside phosphotransferase resistance gene
NES	Nuclear enrichment score
ng	Nanogram
NHEJ	Non-homologous end joining
nm	Nanometer
ORF	Open reading frame
P	Pellet
PAC	Puromycin N-acetyltransferase gene
PAGE	Polyacrylamide gel electrophoresis
PBS	Phosphate-buffered saline
PCF	Procyclic form
PCR	Polymerase chain reaction
PFR	Paraflagellar rod
pH	Potential of hydrogen
Phleo	Phleomycin
POI	Protein of interest
Pol	RNA Polymerase
POT1	Protector of telomeres 1
PPL	PrimPol-like protein
ProtA	Protein A
ProtC	Protein C
PTM	Post-translational modification
PTP	Protein C epitope – tobacco etch virus – protein A epitope
PTU	Polycistronic transcription unit
Puro	Puromycin

PVDF	Polyvinylidene fluoride
rev	Reverse
Rap1	repressor/activator protein 1
Rif	Rap1 interacting factor
RNA	Ribonucleic acid
RNAi	RNA interference
RPA	Replication protein A
rpm	Revolutions per minute
rRNA	Ribosomal RNA
RRNA	Ribosomal RNA locus
RT	Room temperature
SAS	splice acceptor site
SDM	Semi-defined medium
SDS	Sodium dodecyl sulfate
sec	Second
sgRNA	Single guide RNA
SIF	Stumpy induction factor
SL	Spliced leader
SLAB	Spliced leader array body
SMRT	Single-molecule real-time
SOC	Super optimal broth with catabolite repression
SRA	Serum-associated resistance antigen
ssDNA	Single-strand DNA
STN1	Suppressor of CDC thirteen 1
TAE	Tris-acetate-ethylenediaminetetraacetic acid
T. b. brucei	*Trypanosoma brucei brucei*
T. b. gambiense	*Trypanosoma brucei gambiense*
T. b. rhodesiense	*Trypanosoma brucei rhodesiense*
T. brucei	*Trypanosoma brucei*
T. cruzi	*Trypanosoma cruzi*
TDB	Trypanosome dilution buffer
TDP1	Trypanosome DNA binding protein 1
TelAP	Telomere-associated protein
TEMED	Tetramethylethylenediamine
TERC	Telomerase RNA component
TERRA	Telomere repeat-containing RNA
Tet	Tetracycline
TETR	Tetracycline repressor
TEV	Tobacco etch virus
Ti	Tetracycline-inducible
TIN2	TRF1-interacting nuclear factor 2
TLCK	Tosyl-L-lysyl-chloromethane hydrochloride
T-loop	Telomeric loop
TPE	Telomere position effect
TRF	TTAGGG repeat binding factor
TSS	Transcription start sites
TTS	Transcription termination sites
TUB	Tubulin
T7RNAP	T7 RNA polymerase
UB	Unbound
UTR	Untranslated region
V	Volt
VEX	VSG exclusion

VSG	Variant surface glycoprotein
W	Wash
WHO	World health organization
WT	Wildtype
2T1	VSG221 expressing, tagged, clone1
Δ	Deletion

INTRODUCTION

Kinetoplastids

Kinetoplastea (Honigberg, 1963) are unicellular organisms with a kinetoplast, the name giving cell organelle consisting of circular mitochondrial DNA (Shapiro and Englund, 1995). They belong to the phylum Euglenozoa and comprise a group of free-living and parasitic flagellates, found in vertebrates, invertebrates, and plants (Adl et al., 2012). The order *Trypanosomatida* includes the well-known pathogen genus of *Trypanosoma* and *Leishmania* (Lukeš et al., 2014). Both have complex life cycles, alternating between a vertebrate host and an insect vector. Leishmania, with more than 20 species causing leishmaniases in humans worldwide (WHO, 2022), are transmitted by Phlebotominae and exist in amastigote and promastigote forms (Bates, 2007). Notable examples include *Leishmania donovani*, which causes the visceral form of leishmaniasis known as kala-azar, and *Leishmania mexicana* or *Leishmania major* (*L. major*), causing cutaneous forms of the disease (Kevric et al., 2015).The genus *Trypanosoma* infects all vertebrate classes, and among them are the human pathogens *Trypanosoma brucei*, the causative agent of ˈAfrican Trypanosomiasisˈ (AT; ˈAnimal African Trypanosomiasisˈ (AAT), ˈHuman African Trypanosomiasisˈ (HAT)), and *Trypanosoma cruzi*, responsible for causing Chagas disease in South and Central America (Kennedy, 2019, Lidani et al., 2019). While *T. cruzi* is an intracellular organism transmitted by Triatomine bugs, *T. brucei* has adapted to an extracellular lifestyle in the mammalian bloodstream and is transmitted by species of the tsetse fly *Glossina*. The following chapter will give an overview of the pathogen *Trypanosoma brucei*.

Trypanosoma brucei

African trypanosomiasis

Trypanosoma brucei spp. is the causative agent of the devastating disease called ˈAfrican Trypanosomiasisˈ, which is endemic in 36 sub-Saharan African countries due to restrictions imposed by its vector. It was first discovered by Dr. David Bruce in 1895 (Steverding, 2008). *Trypanosoma brucei brucei* is responsible for the livestock disease commonly named Nagana (loss of spirit), which has catastrophic effects on the economy in affected African countries. ˈHuman African Trypanosomiasisˈ, known as sleeping sickness, is caused by *Trypanosoma brucei gambiense* and *Trypanosoma brucei rhodesiense*. The chronic form, caused by *T. b. gambiense*, can remain symptomless for years and accounts for 97% of all cases (WHO, 2022). The acute form acquired through *T. b. rhodesiense* is very severe but only leads to few reported cases of 3% each year. Both sub-species can also be found in domestic and wild animals, acting as a reservoir (Brun and Balmer, 2006). From almost 40,000 reported cases of HAT in 1998, the number dropped to under 1000 reported cases in 2019, with 70% coming from the Democratic Republic of Congo (WHO, 2022). The disease has two main stages. In the early hemo-lymphatic stage, common symptoms include fever, headache, cardiac disorders, swollen lymph nodes, general weakness, and musculoskeletal pains. If parasites cross the blood-brain barrier, the second meningo-encephalitic stage is established, characterized by

neuropsychiatric signs (Franco et al., 2014). If untreated, the disease leads to coma, multiple organ failure and can be fatal.

Up to now, six different drugs are used to treat HAT: two drugs for the first stage, three drugs for the second stage and one drug for both stages (WHO, 2022). The most recent discovered drug, Fexinidazole, represents the first oral treatment for both stages caused by *T. b. gambiense* and has been approved by the 'US Food and Drug Administration' (FDA) in 2021. Another crucial component of the disease control is the reduction of vector populations using traps (Mahamat et al., 2017). As the affected regions in endemic countries are mostly impoverished, the primary prevention technique remains the avoidance of vector bites.

Cell architecture and developmental life cycle

T. brucei is a unicellular organism containing single copies of organelles; including the nucleus, the Golgi apparatus, and the mitochondrion, which are defined in specific positions within the cell. The kinetoplast, the name giving organelle of the class kinetoplastida, contains condensed circular mitochondrial DNA and is located at the posterior end of the cell. One of the most prominent organelles of *T. brucei* is the single flagellum responsible for motility in the bloodstream and closely attached to the trypanosome cell body. It emerges from the flagellar pocket, which is the sole site of exo- and endocytosis of the parasite (Overath et al., 1997, Link et al., 2021). The basal body of the flagellum is linked to the kinetoplast and controls its segregation (Vaughan and Gull, 2015). The attachment of the flagellum to the cell surface along the cell body through the 'flagellum attachment zone' (FAZ) enables a hydrodynamic fluid flow, caused by the directional beating of the flagellum (Engstler et al., 2007). The most prominent surface protein of the 'bloodstream form' (BSF) *T. brucei* is the 'variant surface glycoprotein' (VSG), which is continuously endocytosed and recycled back to the surface (Engstler et al., 2004). This process efficiently clears antibodies bound to VSG and VSGs with bound antibodies reach the flagellar pocket more quickly, enhancing the efficiency of this process. The surface proteins of both stages of *T. brucei*, VSG and the procyclins EP and GPEET, are both anchored to the cell surface by a 'glycosylphosphatidylinositol' (GPI) anchor.

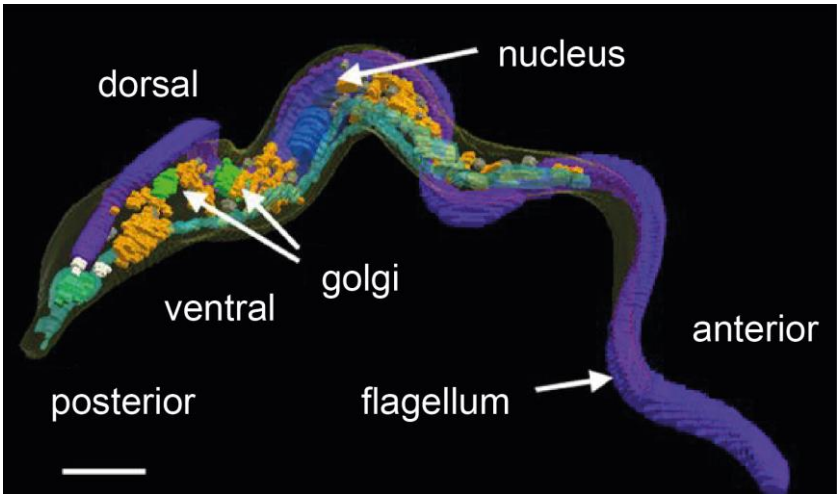

Figure 1: The cellular ultrastructure of BSF *T. brucei*. 3D structure reconstructed by serial block face scanning electron microscopy (SBF-SEM). Image adapted from (Hughes et al., 2017).

The life cycle of *T. brucei* is shaped by the contrast of shuttling between its tsetse fly vector and the mammalian host. Consequently, the parasite must undergo tremendous changes to resist the different extracellular environments and to become infective to the host after passing through the fly.

In the bloodstream, the parasite adopts either a long proliferative slender form or, in response to the quorum sensing 'stumpy induction factor' (SIF), a non-proliferative, cell cycle arrested short stumpy form (Vassella et al., 1997). This change serves as a control mechanism to limit parasite burden, as stumpy forms can only survive for a short time period. It has been proposed that the stumpy form is an adaption to the uptake by the fly and the only stage capable of successfully infect it (Rico et al., 2013). However, recent discoveries question this theory, as a single long slender form is also sufficient to infect the fly and differentiate into the procyclic form of trypanosomes (Schuster et al., 2021). Both bloodstream forms express and periodically change VSGs on their surface to evade the host's immune response. After taking a bloodmeal, BSF trypanosomes are passing through the fly's crop into the midgut. In the midgut, the VSG surface protein is exchanged to procyclins (Roditi et al., 1989). The proliferative procyclic trypanosomes then swim back to the proventriculus and cross the peritrophic matrix to the ectoperitrophic space (Rose et al., 2020). There, they differentiate into the non-proliferative mesocyclic stage or develop into the proliferative long epimastigote stage in the proventriculus. Epimastigotes express another surface protein called 'brucei alanine-rich protein' (BARP) (Urwyler et al., 2007). Asymmetric cell division of the epimastigote form results in a long and a short daughter cell. In the salivary glands, the short epimastigote form attaches to the epithelium via its flagellum and proliferates. They either divide to epimastigotes or undergo another asymmetric cell division. The resulting unattached, cell cycle arrested metacyclic form is the only form capable of infecting the mammalian host and expresses a metacyclic VSG protein on its surface as a pre-adaption mechanism.

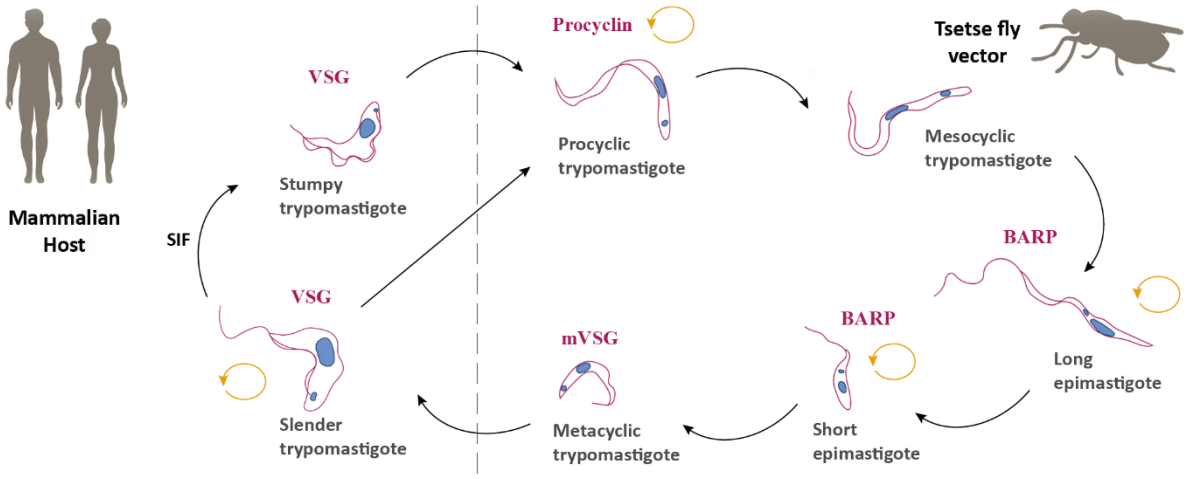

Figure 2: The Life cycle of *T. brucei*. As the environments are changing during the transmission from the tsetse fly vector to the mammalian host, *T. brucei* adapts by differentiation and has proliferative (circular arrow) and non-proliferative forms. Variant surface glycoprotein (VSG), metacyclic VSG (mVSG), brucei alanine rich protein (BARP). Figure adapted from (Borges et al., 2021).

The position of the nucleus, the kinetoplast and the flagellum change during the life cycle of *T. brucei*. Trypomastigote stages of *T. brucei* display the nucleus anterior to the kinetoplast, whereas in the epimastigote stages, the nucleus is posterior. Throughout its elaborated life cycle, *T. brucei* also adapts its metabolism to the different environments it is in. In the 37°C warm bloodstream of the mammalian host, the environment is rich in glucose (5 mM) and has high oxygen saturation levels. Glucose is therefore the carbon source for adenosine triphosphate (ATP) production via glycolysis for BSF trypanosomes.

As BSF replicate faster with a doubling time of 6 to 7 h compared to the 'procyclic form' (PCF) with a doubling time of 12 h and the need for a 10-fold upregulated endocytosis to recycle the VSG protein, the glucose degradation rate and the ATP requirement are high (Smith et al., 2017).

In contrast, in the fly's midgut, glucose levels are low, and the oxidation of amino acids becomes the main primary energy source. Therefore, the mitochondrion is elaborated as the PCF relies on mitochondrial energy production (Dewar et al., 2018). The differentiation of the BSF to the PCF form can also be replicated in vitro by a temperature shift from 37°C to 27°C, addition of cis-aconitate to the culture medium, and removal of glucose (Engstler and Boshart, 2004).

Genome organization

The first published genome sequence of *T. brucei* was the haploid mosaic sequence of the diploid chromosome called TREU927 (Berriman et al., 2005). Recent studies further enhanced our understanding of the genome architecture by using 'single-molecule real-time' (SMRT) sequencing technology on DNA from Lister 427 isolates and Hi-C interaction mapping (Figure 3) (Müller et al., 2018). This work has allowed the precise positioning of the VSG ES and revealed that sub-telomeric regions are highly divergent between the diploid alleles. Both data sets are accessible at TriTrypDB, which provides sequence information on genes, 'RNA interference' (RNAi) phenotypes, proteomic and transcriptomic data, among others (Aslett et al., 2010). Together with TrypTag, providing information about protein localization in procyclic trypanosomes, these databases supply researchers with access to a vast amount of information about the protein of interest (Dean et al., 2017, Billington et al., 2023).

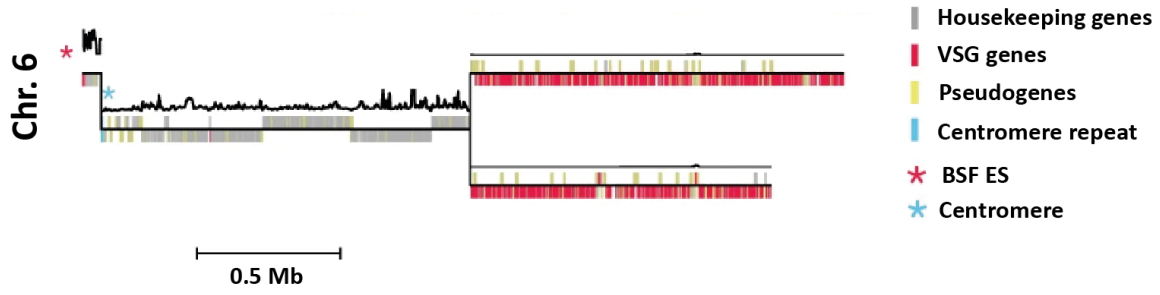

Figure 3: Chromosome organization of *T. brucei*. Chromosome 6 is displayed. The homozygous chromosomal core region containing the housekeeping genes is shown as one chromosome whereas the heterozygous subtelomeric regions are displayed as both chromosomes. The relative transcript level is shown as a black line above the chromosome. Figure adapted from (Müller et al., 2018).

The genome of *T. brucei* is composed of 30-50 megabases including 11 megabase chromosomes, about 5 intermediate chromosomes, and approximately 100 mini-chromosomes (Melville et al., 2000, Wickstead et al., 2004, Berriman et al., 2005). The megabase chromosomes encode for 9068 genes, of which more than 2500 are *VSG* genes (Cross et al., 2014). Most of these genes are located in subtelomeric regions, with 65 found on mini-chromosomes. About 80% of the VSG genome consist of pseudogenes, forming a substantial reservoir crucial for the organism's antigenic variation. Genes are arranged in approximately 190 mostly intron-free ˈpolycistronic transcription unitsˈ (PTU) (Clayton, 2002). While housekeeping genes are transcribed by RNA Polymerase II (Pol II), rRNA genes, VSG, ˈexpression site associated genesˈ (ESAG) and procyclin are transcribed by RNA Polymerase I (Pol I) (Rudenko et al., 1989).

Pol II transcription is initiated at the ˈtranscription start sitesˈ (TSS), which are enriched with histone variants H2AZ and H2BV. These sites can contain GT-rich elements that induce transcription (Siegel et al., 2009, Kraus et al., 2020, Wedel et al., 2017). Recently, a 75 bp core promoter, similar in structure to Pol II promoters in other eukaryotes has been identified. This finding suggests that ˈmessenger RNAˈ (mRNA) levels could be regulated not only by post transcriptional mechanisms but also by transcription initiation (Cordon-Obras et al., 2022). For Pol I transcription, promoters have been identified and characterized for BES, ˈmetacyclic expression sitesˈ (MES), rRNA and procyclin genes (Zomerdijk et al., 1990, Janz and Clayton, 1994, Graham et al., 1998). Termination of transcription occurs at H3V, H4V and DNA base ˈß-d-glucosyl-hydroxymethyluracilˈ (Base J) enriched regions called ˈtranscription termination sitesˈ (TTS) (Schulz et al., 2016). However, the exact mechanisms of termination remain elusive.

Another unique feature of *T. brucei* is its mechanism of trans-splicing, where capping and transcription are decoupled. While cis-splicing requires Pol II transcription, trans-splicing allows the transcription of genes by Pol I (Günzl, 2010). Typically, during the mRNA capping in cis-splicing, capping enzymes interact with the C-terminal region of Pol II. In trans-splicing, capping and transcription are two separate mechanisms and are not linked. For mRNA maturation, a ˈspliced leaderˈ (SL) sequence translated from SL RNA and consisting of 39 nucleotides is attached to the 5'-end of mRNA post transcriptional (Milhausen et al., 1984). As each mRNA requires a SL RNA, the synthesis rate of SL RNA is considerably high. Additionally, SL RNA genes possess a well characterized Pol II promoter motif for transcription initiation (Gilinger and Bellofatto, 2001). Another important factor for RNA splicing are pyrimidine rich regions (poly(Y) tracts) at the 5' untranslated region, which affect trans-splicing efficiency (Huang and Van der Ploeg, 1991, Siegel et al., 2005). The splicing process is conducted by the spliceosome, a complex composed of small nuclear RNAs and proteins that assembles on pre-mRNA (Liang et al., 2003). This assembly is guided by the 5' ˈsplice acceptor siteˈ (SAS), an adenosine ˈbranch pointˈ (BP) positioned upstream of the poly(Y) tract and the 3'splice site (AG-dependent), along with possible enhancer motifs. The only two cis-splicing events necessary for intron removal in *T. brucei* are required for the *PAP1* gene, encoding a poly(A) polymerase and the DEAD box helicase *DBP2B* gene (Mair et al., 2000, Siegel et al., 2010). The primary mechanism regulating mRNA involve post-transcriptional factors crucial for mRNA abundance, including mRNA stability, mRNA processing and mRNA transport (Erben et al., 2014). Alongside trans-splicing, 3'-polyadenylation and RNA-binding proteins also influence these factors (Siegel et al., 2011, Clayton, 2013).

The bloodstream form expression site and antigenic variation

As an extracellular parasite, *T. brucei* developed a sophisticated mechanism to evade the immune system of the mammalian host. Its surface is covered with a 15 nm thick, homogenous protective coat composed of a single copy of a VSG protein, first discovered by George Cross in 1975 (Cross, 1975). This 55 kDa protein comprises approximately 95% of the surface proteins and accounts for roughly 10% of the overall protein amount in *T. brucei (*Grünfelder *et al., 2002)*. Transcription is limited to a single VSG gene at a given timepoint, transcribed from one of approximately 15 'bloodstream form expression sites' (BESs) (Figure 4). The polycistronic transcription units are located at subtelomeric regions and consist of a 50 bp repeat region, a Pol I promoter region, several *ESAG*s, a 70 bp repeat region, and the VSG gene (Hertz-Fowler et al., 2008). It is worth noting that most *ESAG*s are membrane associated or exposed on the parasite's surface.

ESAG3, 5 and *11* encode for membrane-associated proteins. *ESAG4* encodes a receptor-like transmembrane adenylyl cyclase. *ESAG6* and *7* encode the GPI anchored transferrin receptor, essential for iron scavenging in BSF trypanosomes. *ESAG10* is a surface transporter (Pays et al., 2001). The VSG-like 'serum-associated resistance antigen' (*SRA*) is also classified as an *ESAG* and is involved in the adaption of *T. b. rhodesiense* to the human serum (Van Xong et al., 1998). Approximately 20% of the ESAG mRNA is transcribed from silent BES, as the transcription is initiated but attenuated along the BES (Ansorge et al., 1999, Batram et al., 2014).

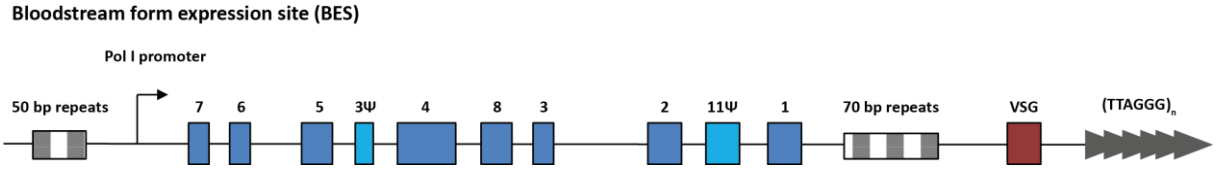

Figure 4: Organization of the VSG BES expression site. Repeat regions are marked by hatched grey-white boxes. Dark blue boxes indicate expression site associated genes (ESAGs), light blue boxes indicate pseudogenes. The VSG gene is red and downstream are the telomeric repeat regions, marked with grey arrowheads. Figure adapted from (Taylor and Rudenko, 2006).

As only one BES is fully active, all others are silenced through various mechanisms to enable monoallelic expression. During an infection, periodical switching of VSG is crucial to evade the immune system and occurs at a rate of 10^{-6} to 10^{-5} switching event per population doubling (Hovel-Miner et al., 2012). This is essential for establishing a reoccurring wave of parasitemia after the host's immune response has adapted to the predominantly exposed VSG variant (Figure 5A) (Mugnier et al., 2016). There are different mechanisms of VSG switching (Figure 5b) (Taylor and Rudenko, 2006, Vink et al., 2012). *In situ* switching refers to a switch by inactivation of the active BES and activation of a previously silent BES, limiting the switch to the BESs. Gene conversion refers to a mechanism where one or several parts of different *VSG* genes or a BES is copied into an active BES, resulting in the loss of the previously expressed *VSG* variant. This mechanism can utilize pseudo-*VSG*s, which lack a complete open reading frame, by converting multiple of them into a mosaic *VSG* (Thon et al., 1989, Taylor and Rudenko, 2006). Crossover, also called telomere exchange, is a mechanism in which homologue regions of the BES are exchanged. The 70 bp repeat region of the BES provide these homologue regions for recombination, and 'homologous recombination' (HR) is crucial for successful antigenic variation. It has been previously established that DNA 'double strand breaks' (DSBs) accumulate at subtelomeric regions and DSBs in the BES trigger antigenic

variation through gene conversion (Glover et al., 2013). Recent studies propose that not all DSBs at the BES are productive; a DSB in the 70 bp repeat region does not directly lead to *VSG* switching but rather undergoes repair through 'microhomology mediated end joining' (MMEJ). Only a DSB directly upstream of the *VSG* gene leads to HR based switching (Thivolle et al., 2021). The 'non-homologous end joining' (NHEJ) pathway, used by most eukaryotes to repair DSBs is non-existent in *T. brucei* (Burton et al., 2007).

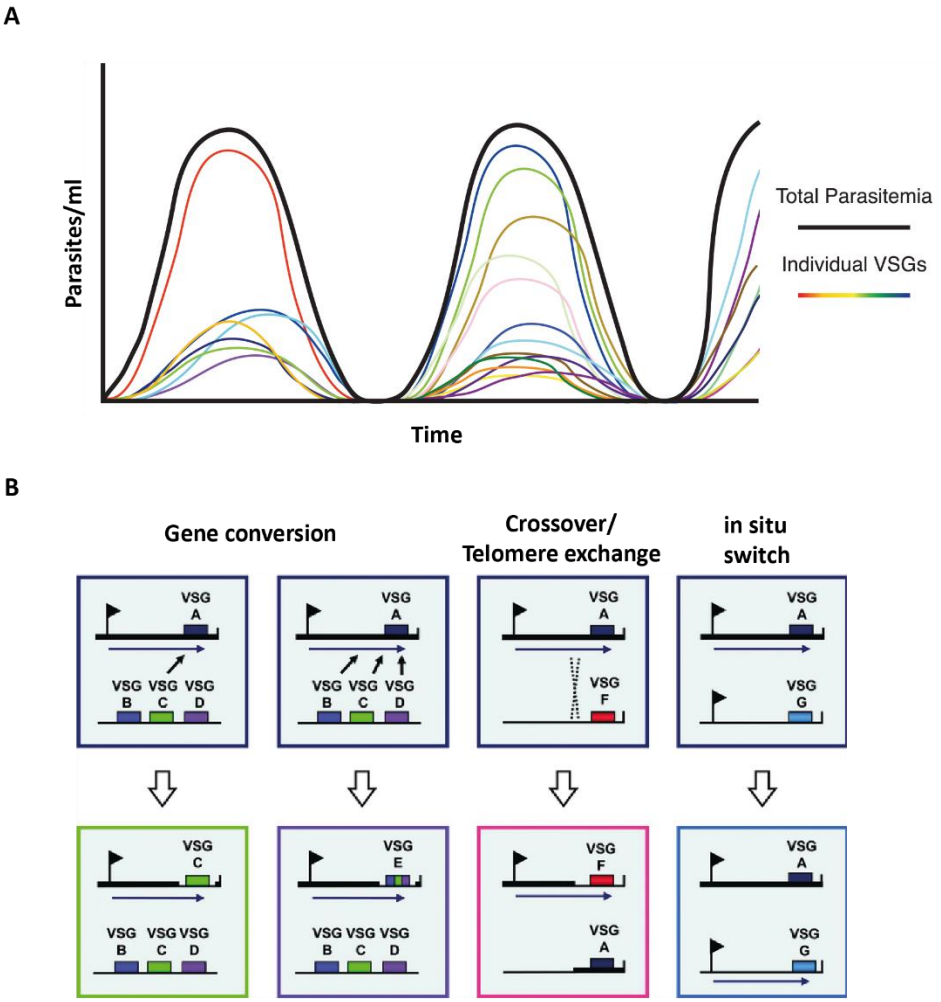

Figure 5: VSG expression and mechanisms of VSG switching. (A) The expression of VSG in BSF trypanosomes is dynamic and a large diversity is expressed at one time in a population. Figure adapted from (Mugnier et al., 2016).**(B)** VSG switching mechanisms. Gene conversion can either be by copying one VSG gene from a reservoir into the active BES or segmental, with parts of VSG genes copied together into the active BES. A crossover event of homologue regions by telomere exchange leads to the expression of a new VSG variant. An *in situ* switch is the transcriptional inactivation of the active BES and activation of a silent BES. A flag indicates the Pol I promoter region of the BES. The blue horizontal arrow marks the active BES. Figure adapted from (Vink et al., 2012).

Regulation of VSG expression

Numerous factors contribute to the VSG expression site regulation, governing transcription initiation, elongation, and silencing. This regulation heavily depends on post-transcriptional mechanisms and 'post-translational modifications' (PTMs) (Clayton and Shapira, 2007, Figueiredo et al., 2009).

While transcription initiation occurs at all BES promoters, elongation is limited to only the active BES at a given time (Kassem et al., 2014). Active BES transcription takes place at an extranucleolar locus containing Pol I foci called the 'expression site body' (ESB) (Figure 6) (Navarro and Gull, 2001). It has also been shown that the VSG gene of the active BES interacts with a SL-RNA locus (Faria et al., 2021). Additionally, three other nuclear bodies ('spliced leader array body' (SLAB), Cajal bodies, NUFIP splicing factor body) have been recently identified, all of which colocalize with the ESB (Budzak et al., 2022). These bodies play essential roles in the production of splicing components for *trans* splicing and processive *VSG* transcription.

Important for Pol I transcription initiation and allelic exclusion is the 'VSG exclusion' (VEX) complex, comprising the proteins VEX1 and VEX2 (Glover et al., 2016, Faria et al., 2019). VEX1 was identified to be enriched in association with the ESB and the active BES while VEX2 was interacts with VEX1, identified via affinity purification. The compartmentalization of the VEX complex is Pol I transcription dependent and recruitment only occurs upon active transcription. Depletion of the VEX complex results in VSG derepression and loss of extranucleolar Pol I foci in the ESB, resulting in impaired monoallelic VSG gene expression (Faria et al., 2019). Another important factor is the DNA replication-associated 'chromatin assembly factor 1' (CAF-1), responsible for the maintenance of VEX1 compartmentalization post DNA replication. One of the subunits of CAF-1, CAF-1b, has previously been described and depletion of this subunit results in VSG depression during S-phase (Alsford and Horn, 2012). Recent studies have shown that VEX1 is also associated with the SL-RNA transcription compartment while VEX2 colocalizes with the *VSG* transcription compartment (Faria et al., 2021). This connection persists during S phase, where the VSG gene and SL-RNA locus separate. The current model suggests that VEX2 is recruited to the BES by Pol I transcription, facilitating the interaction between one VSG gene and the SL-RNA transcription compartment. Moreover, the BES promoter region is highly enriched with SUMOylated proteins and 'Class I transcription factor A' (CITFA), both important for Pol I recruitment and transcription initiation (López-Farfán et al., 2014, Nguyen et al., 2014).

Another striking feature of monoallelic expression regulation involves nucleosome organization and histone modifications (Figure 6). The active BES is nucleosome depleted whereas silent BES are enriched in histones H1, H3, H2A and the histone variant H3V (Figueiredo and Cross, 2010). This dense chromatin organization results in reduced DNA accessibility. Depletion of either one of the listed histones leads to the derepression of silent BESs. For instance, the depletion of H1 results in a higher transcription rate of the promoter region of silent BES, as H1 inhibits Pol I transcription (Pena et al., 2014). Depletion of H3 leads to upregulated Pol I promoter activity (Alsford and Horn, 2012). Simultaneous knockout of the histone variants H3V and H4V induces recombination based switching of *VSG* expression due to increased DNA accessibility at silent BESs (Müller et al., 2018). Histone-related factors like the histone chaperone 'anti-silencing factor 1A' (ASF1A) and histone deacetylases also play vital roles in VSG expression regulation (Alsford and Horn, 2012, Wang et al., 2010). The histone chaperone complex named 'facilitates chromatin transcription' (FACT) regulates nucleosome assembly and is enriched at promoter regions of silent BES (Denninger and Rudenko, 2014). The active BES is further enriched with the 'Trypanosome DNA binding protein 1' (TDP1), which is essential for maintaining its open chromatin status. Depletion of TDP1 results in histone enrichment at the active BES (Narayanan and Rudenko, 2013, Aresta-Branco et al., 2016). Additionally, chromatin remodeling protein TbISWI, 'bromodomain

factors' 2 and 3 (BDF2, BDF3) and the methyltransferase 'disruptor of telomeric silencing 1b' (TbDOT1b) are further chromatin associated factors involved in silent BES repression, thereby maintaining monoallelic expression (Hughes et al., 2007, Figueiredo et al., 2008, Schulz et al., 2015). Depletion of TbISWI results in increased transcription initiation at promoters, TbDOT1b depletion leads to VSG derepression and BDF inhibition decreases BSF specific transcripts and reduces virulence of trypanosomes in mouse models.

Other important factors involved in *VSG* expression site regulation are the telomeres and 'telomere-associated proteins' (TelAPs) which will be further discussed in the following section.

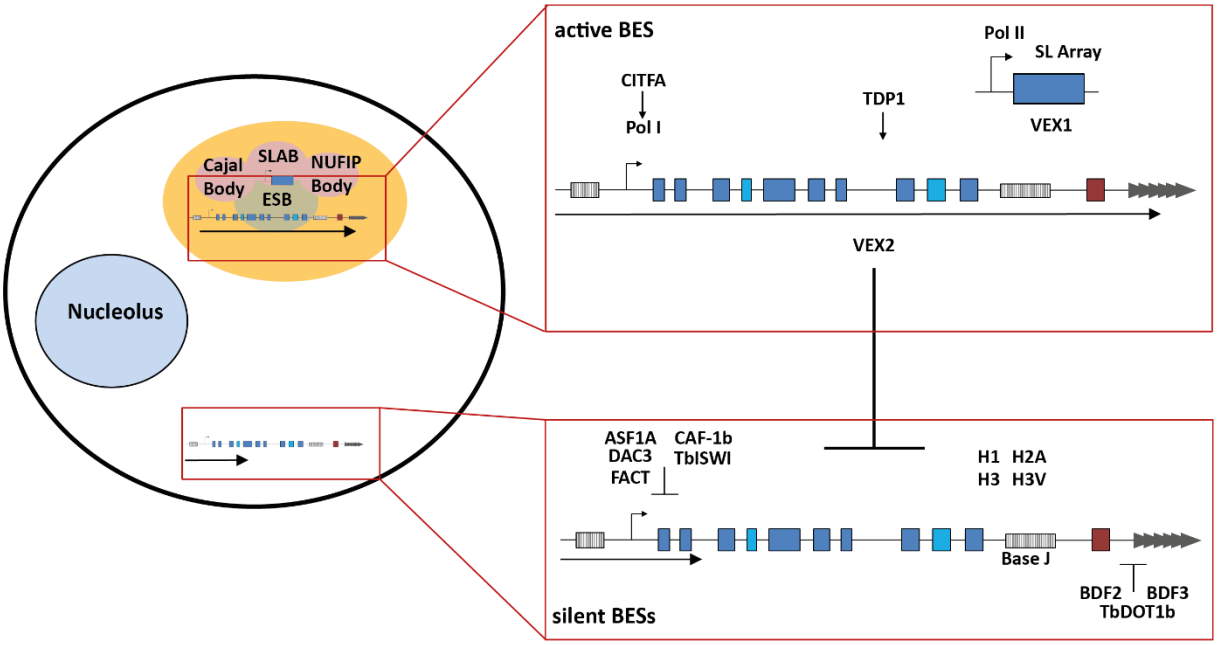

Figure 6: Factors involved in monoallelic VSG expression. The active BES is associated with four nuclear bodies inside the nucleus (black circle), the expression site body which is enriched in Pol I foci (green), the cajal body, the spliced leader array body and the splicing factor body NUFIP (orange). The monoallelic expression of the active bloodstream form expression site depends on an open chromatin status assured by TDP1, Pol I recruitment and transcription initiation influenced by SUMOylated proteins and CITFA, allelic exclusion and the interaction with the splice leader array ministrated by the VEX complex. The silencing of the other bloodstream form expression sites relies on a nucleosome rich structure, enrichment of the Base J, the inhibition of the transcription initiation by several histone chaperones (ASF1A, CAF-1b, FACT), histone modifying factors (DAC3) and chromatin remodelers (TbISWI) as well as telomeric silencing mediated by TbDOT1b, BDF2 and 3 and telomeric proteins (not shown here). Figure adapted from (Budzak et al., 2022, Faria et al., 2019, Cestari and Stuart, 2018).

Telomeres

The primary role of telomeres, located at the end of linear chromosomes, is to safeguard the chromosomal ends from degradations and inappropriate DNA repair by false recognition as DNA breakage sites. This section provides an overview of the telomeric structure and the associated proteins in mammals, yeast and kinetoplastids.

Telomeric structure and function in mammals and yeast

Mammals

Telomeres in mammalian cells consist of a repetitive TTAGGG sequence region, where shelterin, a dynamic multiprotein complex highly specific for telomeric repeats in mammals, is localized (De Lange, 2005) (Figure 7). Together, they form a ˈtelomeric loopˈ (T-loop) structure with the 3'-TTAGGG overhang. This structure prevents the fusion of the telomeric ends and limits the access of nucleases and telomerases (De Lange, 2004). Furthermore, the complex is proposed to be involved in the assembly of the ˈdisplacement loopˈ (D-loop), a loop containing both ˈsingle-strandˈ DNA (ssDNA) and ˈdouble-strandˈ DNA (dsDNA) at the base of the T-loop (Yang et al., 2005).

The shelterin complex consists of six proteins. Among them, the ˈTTAGGG repeat binding factorˈ (TRF) 1 and 2 each contain one Myb-domain and bind the dsDNA repeats directly (Van Steensel and De Lange, 1997, Bilaud et al., 1997). Both form homodimers and interact with ˈTRF1-interacting nuclear factor 2ˈ (TIN2), whereas TRF1 binds TIN2 20-fold tighter than TRF2 (Kim et al., 1999, Li et al., 2000, Chen et al., 2008). TIN2 binds to an adrenocortical dysplasia protein homologue (ACD/TPP1; also known as TINT1, PTOP, PIP1) which associates with the single-stranded TTAGGG repeat binding protein ˈprotector of telomeres 1ˈ (POT1) (Baumann and Cech, 2001, Houghtaling et al., 2004). POT1 consist of two OB-fold domains, an oligonucleotide binding structural motif responsible for the ssDNA binding (Lei et al., 2004). It represses ˈAtaxia telangiectasia and Rad3-relatedˈ (ATR) signaling, usually a response to DSBs by the formation of ssDNA (Denchi and de Lange, 2007). TRF2 additionally interacts with the ˈrepressor/activator protein 1ˈ (RAP1) (Li et al., 2000). In conjunction with TRF2, RAP1 is involved in the inhibition of DNA double-strand break repairs through NHEJ. TRF2 additionally prevents ˈataxia-telangiectasia mutatedˈ (ATM) dependent DNA damage signaling (Denchi and de Lange, 2007, Rai et al., 2016). Another interesting factor interacting with TRF2, which is not part of the shelterin complex is the Ku70-Ku80 heterodimer (Ribes-Zamora et al., 2013). This dimer normally promotes NHEJ and is paradoxically enriched at the telomeres, where it protects telomeres from homologous recombination (Celli et al., 2006). As soon as the function of the shelterin complex is impaired, telomeric ends become shortened and the telomere damage response is initiated (De Lange, 2005). Although this complex is often described as consisting of six different proteins, this is only true for about 5% of the shelterin complex (Lim and Cech, 2021). A complex consisting only of TRF2, RAP1, TIN2, POT1 and TPP1 can be purified, and the complex exhibits a high diversity through post-translational modifications and isoforms of the proteins (Bhanot and Smith, 2012, Grill et al., 2019).

To maintain the telomere length after DNA replication, a ribonucleoprotein enzyme complex named telomerase synthesizes the telomeric repeats *de novo*. This process relies on a non-coding-RNA molecule called TERC (ˈTelomerase RNA componentˈ, hTR in humans) serving as a template (Collins and Mitchell, 2002, Chan and Blackburn, 2002) (Figure 7). The catalytic component called ˈTelomerase reverse transcriptaseˈ (TERT) forms a complex with TERC and various other proteins. The telomerase is recruited by TPP1 which interacts with TERT during S phase (Jády et al., 2006). The shelterin complex also plays a role in enhancing telomerase processivity (Wang et al., 2007). Another factor involved in telomerase activity regulation is a non-coding, ˈtelomeric repeat-containing RNAˈ (TERRA). TERRA is transcribed from subtelomeric promoters and localizes to telomeres (Azzalin et al., 2007, Redon et al., 2010).

TERRA and the telomeric DNA can form a DNA:RNA hybrid structure called R-loop involved in telomere maintenance regulation (Toubiana and Selig, 2018).

In single-cell eukaryotes, the replication of the chromosomal ends by telomerase activity is generally sufficient. However, as age in mammals progresses, the telomerase activity cannot compensate for the telomere shortening in somatic cells anymore. This restricted expression arises from the silencing of TERT, leading to an insufficient quantity of telomerase for maintenance (Gomes et al., 2011). The absence of telomerase results in telomere shortening with a rate of 50-100 bps per doubling, ultimately leading to senescence or apoptosis (Harley et al., 1990, Herbig et al., 2004). In contrast, telomerase expression is upregulated in cancer cells, suggesting that telomere shortening and senescence serves as a mechanism to prevent tumorigenesis by p53 response (Greider and Blackburn, 1996, Jacobs and de Lange, 2004). If cells evade senescence, telomere crisis takes place, leading to genome instability and cell death by autophagy but can also result in the activation of telomerase and the formation of cancer cells (Roake and Artandi, 2020).

Another mechanism to maintain telomere length is called 'alternative lengthening of telomeres' (ALT) (Bryan et al., 1997). This mechanism is based on HR and independent of the telomerase activity. It occurs in 10-15% of tumor cells.

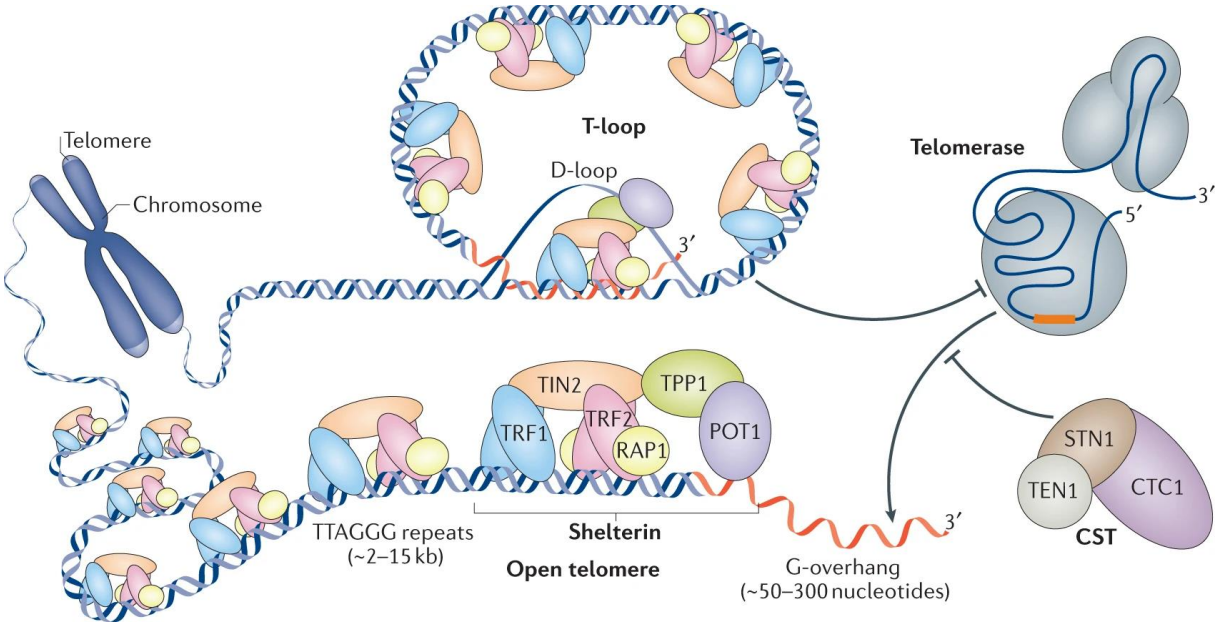

Figure 7: Telomeric region and associated protein complexes. The telomeres consist of multiprotein complexes involved with and bound to the repetitive TTAGGG repeat region at the end of linear chromosomes. The shelterin complex is composed of TTAGGG repeat binding factors 1 and 2 (TRF1, TRF2), TRF1-interacting nuclear factor 2 (TIN2), repressor/activator protein 1 (RAP1), TPP1 and protection of telomeres (POT1). Together with the 3'overhang, they form a displacement loop (D-loop) or telomere-loop (T-loop) structure and regulate telomerase activity. The telomerase is a ribonucleoprotein complex responsible for *de novo* synthesis of telomeric repeats during the open formation of the telomere during cell cycle. The CST complex consists of suppressor of CDC thirteen 1 (STN1), TEN1 and conserved telomere capping protein 1 (CTC1) proteins which bind to the G-overhang and regulate telomerase activity. Figure modified from (Lim and Cech, 2021).

Another protein complex involved in the termination of telomere length extension by the telomerase is called the ˈConserved Telomere Capping Protein 1ˈ(CTC1)-ˈSuppressor of CDC thirteen 1ˈ (STN1)-TEN1 (CST) complex, a ˈreplication protein Aˈ (RPA) like complex (Miyake et al., 2009) (Figure 7). Initially identified in yeast, the CST complex is proposed to bind to ssDNA in a sequence-independent manner through its putative OB-fold domains (Gao et al., 2007). This complex recruits a DNA polymerase α-primase for telomeric C-strand fill-in which if impaired otherwise results in G-overhang lengthening (Casteel et al., 2009, Surovtseva et al., 2009). Overall impairment of CST leads to genome instability not just through overhang lengthening but also due to replication fork stalling and improper DNA damage repair (Wang and Chai, 2018).Chromatin architecture also influences telomere accessibility. Telomeric chromatin consists of highly organized nucleosomes (Nikitina and Woodcock, 2004). It is enriched in histone H3 trimethylated at Lys9 (H3K9me3) and is heterochromatic (Blasco, 2007). This leads to the phenomenon known as ˈtelomere position effectˈ (TPE), a reversible silencing of genes near the telomeres (Arnoult et al., 2012). High H3K9me3 density and the ˈheterochromatin protein 1ˈ (HP1α) mediate the repression of TERRA during telomere elongation.

Yeast

In both *Schizosaccharomyces pombe,* the fission yeast, and *Saccharomyces cerevisiae,* the budding yeast, the primary sequence of the telomeric repeat region is variable and heterogenous ($TTACAG_{2\text{-}8}$ for *S. pombe*, $TG_{2\text{-}3}(TG)_{1\text{-}6}$ for *S. cerevisiae*) (Červenák et al., 2021). *S. pombe* exhibits a variation of the shelterin complex with orthologues for TRF1 (Taz1), Pot1 and Rap1. Similar to humans, Rap1 does not directly bind the telomeric DNA, and Taz1 binds to the telomeres as a homodimer due to having only one Myb domain (Kanoh and Ishikawa, 2001, Tomaska et al., 2004). In contrast, *S. cerevisiae* lacks most orthologues of the shelterin complex. It possesses the CST complex and a complex formed by Rap1 and the ˈRap1 interacting factorsˈ Rif1 and Rif2 (Kupiec, 2014). In this context, Rap1 binds to the duplex telomeric DNA with its two Myb domains and functions as a negative regulator of telomere length. It has a dual role in protecting the telomeres and functions as a general transcription regulator (Azad and Tomar, 2016). Rif1 and Rif2 act as negative regulators of telomeric elongation by repressing the telomerase activity. Rif2 together with Rap1 regulates nuclease access and NHEJ. Additionally, Rap1 interacts with the Sir-complex 2-4 as part of its role in transcriptional repression due to the TPE (Ellahi et al., 2015). Sir proteins interact with histones H3 and H4 and result in transcriptional repression through heterochromatin formation (Luo et al., 2002). The CST complex of *S. cerevisiae* binds the 3’overhang and shares structural similarities to the RPA complex (Gao et al., 2007).

Telomeres have been extensively studied in yeast and mammalians, and the application of cutting-edge methods over the last years provided significant insights to their structure, associated complexes and their functions. For instance, in 2018, the structure of the human telomerase was investigated using cryo-EM studies, shedding light on telomerase-related disease mutations (Nguyen et al., 2018). However, many questions regarding cancer- or genetic disorder treatments remain unanswered. The details of telomere assembly and molecular features of telomere components are still elusive and require further studies. As a result, this field of research is one of the most promising ones for the future.

Telomeric structure and function in kinetoplastids

The TTAGGG repeat region of the telomeres is highly conserved. Even though kinetoplastids branched away early during evolution, this sequence is also found in *T. brucei* and *Leishmania* (Blackburn and Challoner, 1984). Telomere length varies, with a median of 3000 bp (470-24711 bp measured in *T. b. brucei* Lister 427 BSF, (Poláková et al., 2021)). Telomeres typically grow 6-12 bp per cell division, although transcriptionally active telomeres grow faster (Dreesen and Cross, 2008). Notably, the single stranded 3'overhang necessary for forming the T-loop structure is relatively short in *T. brucei* (12 nt compared to 150-400 nt in mammalians) (Sandhu and Li, 2017). Another distinctive feature of Trypanosomatid telomeres is the presence of the previously mentioned Base J, located at the telomeric repeat region and in inactive BES of *T. brucei* BSFs (Borst and Sabatini, 2008). This modified thymine base can also be found in other kinetoplastids like *L. major* and *T. cruzi*, where it is present in both life cycle stages (Genest et al., 2007, Ekanayake et al., 2007).

Unicellular eukaryotic pathogens like kinetoplastids require constant telomerase activity to prevent DNA shortening after cell division. The core component of the telomerase, TERT, is very conserved and is also found in *T. brucei* (TbTERT) and in *Leishmania amazonensis* (LaTERT) (Davis and Chakrabarti, 2022).

TbTERT depletion results in telomere shortening at a rate of 3-6 bp per population doubling, highlighting the role of TERT in telomere maintenance (Dreesen et al., 2005). Telomerase RNA (TbTR) depletion also results in progressive telomere shortening, indicating that TbTR provides the telomere template for TbTERT (Sandhu et al., 2013). Similar to mammalians, another feature to regulate telomere length in *T. brucei* and *L. major* is TERRA (Damasceno et al., 2017). TERRA forms R-loops, which can cause DSB accumulations and therefore increased VSG switching rates in *T. brucei (Saha et al., 2020)*.

Telomeric proteins in Trypanosoma brucei

As described in detail before, the virulent VSG genes are located at the subtelomeric areas. Consequently, the role of telomeres and telomere-associated proteins in trypanosomes is not only restricted to genome stability; they are also involved in the regulation of antigenic variation, crucial for maintaining an infection. To date, three homologues of the shelterin complex of mammalians have been described and further proteins enriched at the telomeric region could be identified and characterized (Figure 8). *Tb*TRF, a homolog of TRF2, was the first protein identified in silico (Li et al., 2005). It self-dimerizes and has a C-terminal Myb domain responsible to bind the TTAGGG repeats in a sequence specific manner. The *Tb*TRF Myb domain is 33-38% identical to the TRF Myb domain of mammals. Depletion of *Tb*TRF via RNAi leads to an increased switching rate through gene conversion due to increased DNA damage, highlighting its role in maintaining telomeric integrity (Jehi et al., 2014a). *Tb*TRF also binds TERRA and its depletion results in an increased TERRA amount (Saha et al., 2021). Soon after, *Tb*RAP1, a RAP1 homolog and a *Tb*TRF interacting factor, was identified via 'co-immunoprecipitation' (co-IP) (Yang et al., 2009). The depletion of *Tb*RAP1 causes a severe phenotype as silent VSGs are derepressed and monocistronic expression is impaired. This leads to the expression of multiple VSGs and the formation of multiple Pol I foci. Additionally, *Tb*RAP1 depletion results in increased TERRA transcription (Nanavaty et al., 2017).

*Tb*TIF2, a homolog of TIN2, interacts with *Tb*TRF (Jehi et al., 2014b). The depletion of *Tb*TIF2 leads to increased subtelomeric DSBs and increased VSG switching. *Tb*TIF2 also stabilizes

protein levels of *Tb*TRF (Jehi et al., 2016). These telomere proteins of *T. brucei* play an important role to balance genome stability but also allow VSG switching events to ensure the survival of the pathogen.

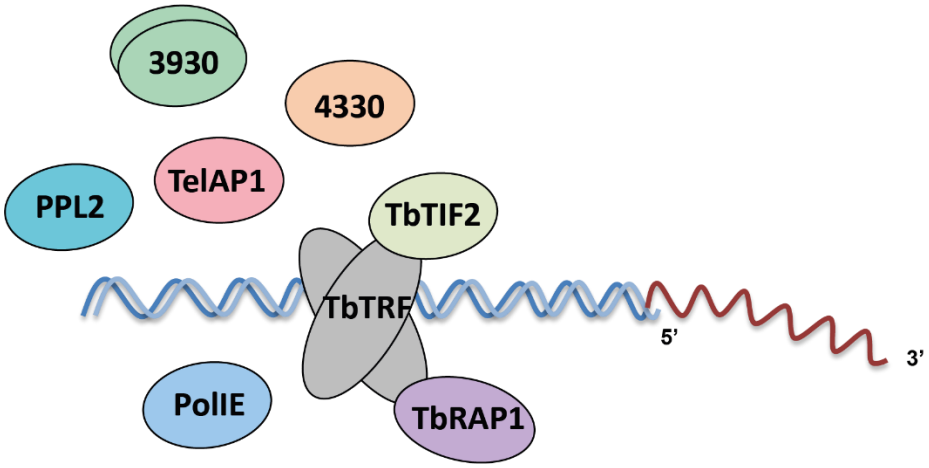

Figure 8: The telomere complex and telomere-associated proteins in *T. brucei*. The three functional homologues of the shelterin complex proteins TRF2 (*TbTRF*), TIN2 (*Tb*TIF2) and RAP1 (*Tb*RAP1) as well as the telomere-associated proteins 'telomere associated protein' 1 (TelAP1), PolIE, PPL2, Tb927.6.4330 and Tb927.9.3930/4000 are represented. DNA double strands are displayed in blue and gray, DNA single strand shown in red.

By performing affinity purification with the telomeric repeat sequence and co-IP with *Tb*TRF, Reis *et al*. co-purified four potential telomere-associated proteins that interact with *Tb*TRF (Reis et al., 2018). The further characterized 'telomere-associated protein' 1 (TelAP1) colocalizes with *Tb*TRF, is upregulated in BSFs, and influences transcriptional BES silencing kinetics. Co-IP of TelAP1 interacting candidates resulted in the enrichment of *Tb*TRF, *Tb*TIF2 and *Tb*RAP1, confirming the interaction of TelAP1 with the telomere complex. It also led to the enrichment of PolIE, PPL2, Tb927.6.4330 and Tb927.9.3930/4000 (Figure 8). The putative translesion polymerase PolIE has also been characterized further and shown to be involved in antigenic variation regulation (Leal et al., 2020). Translesion polymerases replace regular polymerases after DNA damages and fill the lesion by 'translesion synthesis' (TLS) to facilitate further elongation (Sale, 2013). Depletion of PolIE results in DNA damage accumulation, chromosome segregation defects, and derepression of silent VSG genes. The translesion synthesis polymerase 'PrimPol-like protein' 2 (PPL2) is involved in repairing post replicational DNA damage (Rudd et al., 2013). Tb927.6.4330, previously identified via an RNAi library screen for defects in telomere-exclusive expression, has been shown to be a TTAGGG repeat-associated factor involved in VSG derepression and colocalizes with *Tb*TRF (Glover et al., 2016). The protein Tb927.9.3930/4000 has not been further described yet and is only present in four species of *Trypanosoma* (*T. b. gambiense, T. b. brucei, T. evansi* and *T. equiperdum*) (Poláková et al., 2021).

Aims of this study

Telomeres and their underlying processes are crucial for understanding the mechanisms of aging and cancer in humans. Furthermore, in the unicellular pathogen *T. brucei*, telomeric proteins influence the expression of the subtelomeric VSG genes, which are essential for establishing and maintaining parasitemia in the mammalian host. However, their precise involvement in regulation remains unclear, with only three functional homologues of the shelterin complex identified thus far. The questions I aimed to address were as follows:

- Are there other proteins that constitute the telomere complex?
- Are the putative telomere-associated proteins involved in VSG expression regulation?
- Are there distinct telomere-associated protein complexes?
- Does the composition of the telomere complex vary between the PCF and BSF trypanosome stages?
- Is the composition of the telomere complex subject to dynamic changes?
- How do the telomeric proteins interact with each other?

Hence, the objective of my study was to characterize 22 previously identified putative TelAPs and assess their impact on VSG expression site regulation. To achieve this, candidates were depleted using RNA interference (RNAi), allowing for the investigation of potential changes in VSG composition and other regulatory shifts through mass spectrometry analysis. Furthermore, by combining biochemical techniques such as reciprocal affinity purification of the four candidates PolIE, PPL2, Tb927.6.4330 (named TelAP2) and Tb927.9.3930/4000 (named TelAP3), which were previously found to be enriched at the telomeres and interact with *Tb*TRF and/or TelAP1, along with co-IP in RNAi cells, EMSA and immunofluorescence, the composition of the telomere complex was further elucidated.

MATERIALS AND METHODS

Trypanosome culture methods

T. brucei strains

Table 1. Parental *T. brucei* cell lines generated and used in this study.

Name	Genotype	Constructs	Selection	Reference
MITat1.2	BSF Lister 427, MITat1.2, clone 221a	-	-	G. Cross
427	PCF Lister 427	-	-	S. Kramer
2T1	BSF Lister 427, MITat1.2, clone 221a, *TUB::TETR BLE* *RRNA::hygΔstart PAC*	pHD1313, ph3Ep	Phleo, Puro	(Alsford et al., 2005)
MITat 1.2 Cas9	BSF Lister 427, MITat1.2, clone 221a, *TUB::T7RNAP PAC TETR Cas9*	pJ1339	Puro	N. Weisert
427 Cas9	PCF Lister 427 *TUB::T7RNAP PAC TETR Cas9*	pJ1339	Puro	N. Weisert

Abbreviations: MITat1.2 (Molteno institute trypanozoon antigen type 1.2), 2T1 (VSG221 expressing, tagged, clone1), *TUB* (tubulin), *RRNA* (ribosomal RNA locus), *TETR* (tetracycline repressor), *T7RNAP* (T7 RNA polymerase), *Cas9* (CRISPR associated gene 9), *BLE* (bleomycin resistance gene), *PAC* (puromycin N-acetyltransferase gene), *HYG* (hygromycin phosphotransferase gene), Phleo (phleomycin), Puro (puromycin).

Table 2. Transgenic *T. brucei* cell lines generated and used in this study.

Name	Genotype	Construct	Selection	Reference
2T1 MRB1590 RNAi	*TUB::TETR BLE* *RRNA::MRB1590-RNAi^{Ti}HYG*	pHD1313, ph3Ep, pGL2084_MRB1590	Hygro, Phleo	N. Weisert
2T1 NOP89 RNAi	*TUB::TETR BLE* *RRNA::NOP89-RNAi^{Ti}HYG*	pHD1313, ph3Ep, pGL2084_NOP89	Hygro, Phleo	N. Weisert

Name	Genotype	Construct	Selection	Reference
2T1 p33 RNAi	*TUB::TETR BLE RRNA::p33-RNAi^{Ti}HYG*	pHD1313, ph3Ep, pGL2084_p33	Hygro, Phleo	N. Weisert
2T1 p34 RNAi	*TUB::TETR BLE RRNA::p34-RNAi^{Ti}HYG*	pHD1313, ph3Ep, pGL2084_p34	Hygro, Phleo	N. Weisert
2T1 p35 RNAi	*TUB::TETR BLE RRNA::p35-RNAi^{Ti}HYG*	pHD1313, ph3Ep, pGL2084_p35	Hygro, Phleo	N. Weisert
2T1 p38 RNAi	*TUB::TETR BLE RRNA::p38-RNAi^{Ti}HYG*	pHD1313, ph3Ep, pGL2084_p38	Hygro, Phleo	N. Weisert
2T1 p52 RNAi	*TUB::TETR BLE RRNA::p52-RNAi^{Ti}HYG*	pHD1313, ph3Ep, pGL2084_p52	Hygro, Phleo	N. Weisert
2T1 p53 RNAi	*TUB::TETR BLE RRNA::p53-RNAi^{Ti}HYG*	pHD1313, ph3Ep, pGL2084_p53	Hygro, Phleo	N. Weisert
2T1 p68 RNAi	*TUB::TETR BLE RRNA::p68-RNAi^{Ti}HYG*	pHD1313, ph3Ep, pGL2084_p68	Hygro, Phleo	N. Weisert
2T1 p77 RNAi	*TUB::TETR BLE RRNA::p77-RNAi^{Ti}HYG*	pHD1313, ph3Ep, pGL2084_p77	Hygro, Phleo	N. Weisert
2T1 p88 RNAi	*TUB::TETR BLE RRNA::p88-RNAi^{Ti}HYG*	pHD1313, ph3Ep, pGL2084_p88	Hygro, Phleo	N. Weisert
2T1 p105 RNAi	*TUB::TETR BLE RRNA::p105-RNAi^{Ti}HYG*	pHD1313, ph3Ep, pGL2084_p105	Hygro, Phleo	N. Weisert
2T1 PABP2 RNAi	*TUB::TETR BLE RRNA::PABP2-RNAi^{Ti}HYG*	pHD1313, ph3Ep, pGL2084_PABP2	Hygro, Phleo	N. Weisert
2T1 PIF5 RNAi	*TUB::TETR BLE RRNA::PIF5-RNAi^{Ti}HYG*	pHD1313, ph3Ep, pGL2084_PIF5	Hygro, Phleo	N. Weisert

Name	Genotype	Construct	Selection	Reference
2T1 PolIE RNAi	*TUB::TETR BLE* *RRNA::PolIE-RNAi^{Ti}HYG*	pHD1313, ph3Ep, pGL2084_PolIE	Hygro, Phleo	L. Pfaller
2T1 PPL2 RNAi	*TUB::TETR BLE* *RRNA::PPL2-RNAi^{Ti}HYG*	pHD1313, ph3Ep, pGL2084_PPL2	Hygro, Phleo	N. Weisert
2T1 RPA2 RNAi	*TUB::TETR BLE* *RRNA::RPA2-RNAi^{Ti}HYG*	pHD1313, ph3Ep, pGL2084_RPA2	Hygro, Phleo	N. Weisert
2T1 TelAP2 RNAi	*TUB::TETR BLE* *RRNA::TelAP2-RNAi^{Ti}HYG*	pHD1313, ph3Ep, pGL2084_TelAP2	Hygro, Phleo	O. Dyck
2T1 TelAP2 RNAi /*Tb*TRF -/Ty1	*TUB::TETR BLE* *RRNA::TelAP2-RNAi^{Ti}HYG* *TbTRF::Ty1 PAC/ ΔTbTRF::NEO*	pHD1313, ph3Ep, pGL2084_TelAP2, PCR amplified Ty1 from pMOTag2T, PCR amplified *NEO* ORF from pLF-13	Hygro, Phleo, Puro, G418	N. Weisert
2T1 TelAP3 RNAi K1	*TUB::TETR BLE* *RRNA::TelAP3-RNAi^{Ti}HYG*	pHD1313, ph3Ep, pGL2084_TelAP3K1	Hygro, Phleo	L. Pfaller
2T1 TelAP3 RNAi K2	*TUB::TETR BLE* *RRNA::TelAP3-RNAi^{Ti}HYG*	pHD1313, ph3Ep, pGL2084_TelAP3K2	Hygro, Phleo	V. Kreß
2T1 TelAP3 RNAi K3	*TUB::TETR BLE* *RRNA::TelAP3-RNAi^{Ti}HYG*	pHD1313, ph3Ep, pGL2084_TelAP3K3	Hygro, Phleo	N. Weisert
2T1 TelAP3 RNAI K5	*TUB::TETR BLE* *RRNA::TelAP3-RNAi^{Ti}HYG*	pHD1313, ph3Ep, pGL2084_TelAP3K5	Hygro, Phleo	N. Weisert
2T1 UPF1 RNAi	*TUB::TETR BLE* *RRNA::UPF1-RNAi^{Ti}HYG*	pHD1313, ph3Ep	Hygro, Phleo	N. Weisert

Name	Genotype	Construct	Selection	Reference
2T1 XRND RNAi	*TUB::TETR BLE* *RRNA::XRND-RNAi^{Ti}HYG*	pHD1313, ph3Ep	Hygro, Phleo	N. Weisert
MITat1.2 Cas9 PTP:PPL2	*HYG PTP::PPL2 | NEO PTP::PPL2*	PCR-amplified PTP from p2678 *HYG* and p2678 *NEO*	Puro, Hygro, G418	N. Weisert
MITat1.2 Cas9 TelAP2:PTP	*TelAP2::PTP HYG | TelAP2::PTP BLE*	PCR-amplified PTP from p2706 *HYG* and p2706 *BLE*	Puro, Hygro, Phleo	V. Kreß
MITat1.2 Cas9 PTP:TelAP3	*BLE PTP::TelAP3 | HYG PTP::TelAP3*	PCR-amplified PTP from p2678 *BLE* and p2678 *HYG*	Puro, Phleo, Hygro	V. Kreß (V. Kreß, Master thesis, 2020).
MITat1.2 Cas9 TelAP3:PTP	*TelAP3::PTP HYG | TelAP3::PTP BLE*	PCR-amplified PTP from p2706 *HYG* and p2706 *BLE*	Puro, Hygro, Phleo	V. Kreß (V. Kreß, Master thesis, 2020).
SM PTP	*TETR T7RNAP NEO* *RRNA::PTP^{Ti} BLE*	pLEW100v5_PTP	G418, Phleo	N. Eisenhuth
427 Cas9 PTP:PPL2	*NEO PTP::PPL2 | HYG PTP::PPL2*	PCR-amplified PTP from p2678 *NEO* and p2678 *HYG*	Puro, G418, Hygro	N. Weisert
427 Cas9 PTP:PolIE	*NEO PTP::PolIE | HYG PTP::PolIE*	PCR-amplified PTP from p2678 *NEO* and p2678 *HYG*	Puro, G418, Hygro	N. Weisert
427 Cas9 TelAP2:PTP	*TelAP2::PTP NEO | TelAP2::PTP HYG*	PCR-amplified PTP from p2706 and p2706 *BLE*	Puro, G418, Hygro	N. Weisert
29-13 PTP	PCF Lister 427, *TETR T7RNAP NEO HYG* *RRNA::PTP^{Ti} BLE*	pLEW100v5_PTP	G418, Hygro, Phleo	N. Eisenhuth (Eisenhuth et al., 2021)

Abbreviations: Ti (tetracycline inducible), Δ (deletion), *NEO* (aminoglycoside phosphotransferase resistance gene), *PTP (*protein C epitope - tobacco etch virus - protein A epitope), G418 (neomycin), Hygro (hygromycin).

T. brucei growth

Monomorphic ˈbloodstream formˈ (BSF) trypanosomes were cultured in HMI-9 medium (for 10 L: 176.6 g Iscoveˈs modified Dulbeccoˈs medium (IMDM), 30.24 g $NaHCO_3$, 143 µl ß-mercaptoethanol, 100ml penicillin/streptomycin solution (Invitrogen), 282 mg bathocuproine sulfonate, 390 mg thymidine, 1.36 g hypoxanthine, 1.82 g L-cysteine, 1 L heat-inactivated FCS (Sigma), pH 7.5) (Hirumi and Hirumi, 1989). Cells were cultivated in incubators at 37°C, 5% CO_2 and 95% humidity. The maximum cell density of 1 x 10^6 cells/ml was not exceeded to ensure logarithmic growth.

ˈProcyclic formˈ (PCF) trypanosomes were cultured in SDM-79 medium (for 10 L: 20 g $NaHCO_3$, 18.642 g dextrose, 5.134 g L-glutamine, 6.15 g L-proline, 1 g sodium pyruvate, 4.068 g L-threonine, 105 mg sodium acetate, 224.2 mg L-glutamic acid, pH 7.3) (Brun and Schönenberger, 1979). Prior to usage, 900ml of medium was complemented with 7.5 mg/ml hemin, 100 ml heat-inactivated FCS and 10 ml penicillin/streptomycin solution (Invitrogen). Cells were cultivated in incubators at 27°C, 5% CO_2 and 95% humidity. Cell density was kept between 5 x 10^6 and 1 x 10^7 cells/ml to ensure logarithmic growth.

Both media were supplemented with the appropriate amount of drug selection (Table 3) and cells were counted using a Z2 Coulter particle counter (Beckman).

Table 3. Drug selection used for *T. brucei*

Drug	Gene	Stock (mg/ml)	final concentration for BSF (µg/ml)	final concentration for PCF (µg/ml)	Company
G418	*NEO*	10	2	15	AppliChem
Hygromycin	*HYG*	10	3	25	AppliChem
Phleomycin	*BLE*	10	2.5	2.5	InvivoGen
Puromycin	*PAC*	1	0.1	1	AppliChem
Tetracycline	-	10	1	1	AppliChem

Freezing and thawing of *T. brucei*

For the preparation of stabilates 2 x 10^6 BSF cells / 2 x 10^7 PCF cells were harvested by centrifugation (1500 *g*, 4°C, 10 min). The supernatant was discharged, the pellet was resuspended in 500 µl ice-cold freezing medium (HMI-9 for BSF or SDM-79 for PCF supplemented with 10% glycerol) and transferred into cryogenic tubes (Sarstedt). Stabilates were stored at -80°C. For thawing of stabilates, the tubes were shaken in a 37°C water bath and immediately washed with 10 ml pre-warmed medium by centrifugation (1500 *g*, RT, 10 min). The pellet was resuspended with 1 ml medium and transferred into a culture flask containing medium and the appropriate amount of selection drugs.

Transformation of *T. brucei*

For the integration of DNA constructs into genomic loci, a stable transformation by electroporation of *T. brucei* was performed using the Nucleofector II electroporation system (Amaxa Biosystem) (Burkard et al., 2007). 2.5 x 10^7 cells were harvested (1500 *g*, RT, 10 min), washed with pre-warmed TDB (5 mM KCl, 80 mM NaCl, 1 mM $MgSO_4$, 20 mM Na_2PO_4, 2mM NaH_2PO_4, 20 mM glucose, pH 7.4) for BSF or PBS (10 mM Na_2HPO_4, 1.8 mM KH_2PO_4, 140 mM NaCl, 2.7 mM KCl, pH 7.4) for PCF. The pellet was resuspended in 400 µl transfection buffer (90 mM Na_2PO_4, 5 mM KCl,.0.15 mM $CaCl_2$, 50 mM HEPES, pH 7.3) and immediately transferred into a BTX cuvette containing either 10 µg linearized plasmid DNA or 5-10 µg PCR product. If the CRISPR/Cas9 system was used, transfection was carried out by using 7-10 µg of a PCR product and additionally 20 µl of a sgRNA template, amplified via PCR (Beneke et al., 2017). The cuvette was placed into the device and the program ˈX001 free choiceˈ was used for electroporation. Immediately after cells were transferred into a culture flask containing either 30 ml pre-warmed HMI-9 medium for BSF or 10 ml SDM-79 medium for PCF and appropriate parental antibiotic selection. Different dilutions (1:5, 1:10, 1:1,000 and/or 1:1,000) were performed and transferred to a 24-well plate (1ml/well). For PCF, the dilutions were conducted using medium supplemented with 20% FCS. Flasks and well plates were cultivated in incubators at 37°C or 27°C and after 8 h for BSF and 14 h for PCF post transfection respective drugs were added in appropriate concentrations to select for cells, which successfully integrated the transfected constructs.

Growth curve

To determine the doubling time of a cell line, a growth curve was created using the following formula.

$$t_D = \frac{t1 - t0}{ln_2(c1 - c0)}$$

Cells were diluted to 1 x 10^5 cells/ml and 2ml for each triplicate were transferred into a 24-well plate. Measurement of cell density was performed after 24 h and cells were again diluted to 1 x 10^5 cells/ml daily into the next well plate.

Bacterial methods

Bacterial strains

Table 4. *E. coli* strains used in this study.

***E. coli* strain**	**Genotype**	**Application**
TOP10	F-mrcA Δ(mrr-hsdRMS-mcrBC) ϕ80lacZΔM15 ΔlacX74 nupG recA1 ara D139 Δ(ara-leu)7697 galE15 galK16 rpsL (StrR) endA1 λ	Molecular cloning
LOBSTR-BL21(DE3)-RIL	F-ompT $hsdS_B$ (r_B-, m_B-) gal dcm (DE3) λsBamHIo ΔEcoRI-B int::(lacI::PlacUV5::T7 gene1) i21 Δnin5 arnA (H359S, H361S, H592S, H593S) slyD (1-150)	Recombinant protein expression

Bacterial growth

E. coli cells were cultivated in ˈlysogeny brothˈ (LB) medium (0.5% yeast extract, 1% bacto tryptone, 1% NaCl, pH 7.5) or on LB agar plates (LB medium containing 1.5% agar) supplemented with appropriate antibiotics (100 µg/ml ampicillin).

Transformation of E. *coli*

To insert exogenic genetic material into chemical competent *E. coli* TOP10, the transformation technique was used. An appropriate amount of plasmid DNA was added to 100 µl thawed bacteria and incubated on ice for 30 min followed by a heat shock at 42°C for 45 sec. Cells were further incubated on ice for 2 min prior to the adding of 500 µl RT SOC medium (0.5% yeast extract, 2% tryptone, 10 mM NaCl, 2.5 mM KCL, 10 mM $MgCl_2$, 10mM $MgSO_4$, 20 mM glucose). Cells were incubated at 37°C for 1 h shaking at 225 rpm. Afterwards, cells were plated on pre-warmed LB plates containing ampicillin and incubated over night at 37°C.

Isolation of DNA from E. *coli*

Plasmid DNA from over night *E. coli* TOP10 culture was isolated using the *NucleoSpin* Plasmid Miniprep kit or the *NucleoBond PC100* kit (Macherey-Nagel) according to the manufacturer's instructions.

Plasmids used in this study

Table 5. Used and generated plasmids.

Name	Application	Selection in *T. brucei*	Reference
pET-21a(+)	Expression vector for recombinant protein expression in *E. coli,* including a N-terminal T7 tag and a C-terminal 6xHistidin tag.	-	Novagen
pET-21a(+)_TelAP3	Expression vector for recombinant TelAP3-6xHis expression in *E. coli*	-	N. Weisert
pGL2084	Vector for the generation of tetracycline-inducible, stem-loop RNAi cell lines in 2T1 cells. Using the gateway BP clonase II system. After successful integration cells are puromycin sensitive and hygromycin resistant.	Hygro	(Jones et al., 2014)

Name	Application	Selection in *T. brucei*	Reference
pGL2084_p53	*p53* (Tb427.02.6100) fragment (429 bp, 890-1,319 of 1,464 bp ORF) was amplified from genomic DNA using HR104/HR105 containing attB sites for cloning into pGL2084. Linearization with AscI	Hygro	E. Meyer-Nautus
pGL2084_p77	*p77* (Tb427tmp.01.1680) fragment (192 bp, 1,498-1,690 of 2,058 bp ORF) was amplified from genomic DNA using NW120/NW121 containing attB sites for cloning into pGL2084. Linearization with AscI	Hygro	N. Weisert
pGL2084_p97	*p97* (Tb427.10.9780) fragment (424 bp, 163-586 of 2,640 bp ORF) was amplified from genomic DNA using HR82/HR83 containing attB sites for cloning into pGL2084. Linearization with AscI	Hygro	E. Meyer-Nautus
pGL2084_MRB1590	*MRB1590* fragment (421 bp, 187-607 of 2,007 bp ORF) was amplified from genomic DNA using HR98/HR99 containing attB sites for cloning into pGL2084. Linearization with AscI	Hygro	E. Meyer-Nautus
pGL2084_PABP2	*PABP2* fragment (406 bp, 464-870 of 1,668 bp ORF) was amplified from genomic DNA using NW71/NW72 containing attB sites for cloning into pGL2084. Linearization with AscI	Hygro	N. Weisert
pGL2084_RPA2	*RPA2* fragment (406 bp, 19-424 of 768 bp ORF) was amplified from genomic DNA using HR90/91 containing attB sites for cloning into pGL2084. Linearization with AscI	Hygro	E. Meyer-Nautus
pGL2084_TelAP2	*TelAP2* (Tb427_060048400) fragment (456 bp, 136-591 of 642 bp ORF) was amplified from genomic DNA using NW73/NW74 containing attB sites for cloning into pGL2084. Linearization with AscI	Hygro	E. Meyer-Nautus

Name	Application	Selection in *T. brucei*	Reference
pGL2084_TelAP3_K3	*TelAP3* (Tb427_090023800/Tb427_090024100) fragment (200 bp, 785-984 of 1,086 bp ORF) was amplified from genomic DNA using NW229/NW230 containing attB sites for cloning into pGL2084. Linearization with AscI	Hygro	N. Weisert
pGL2084_TelAP3_K5	*TelAP3* (Tb427_090023800/Tb427_090024100) fragment (200 bp, 561-760 of 1,086 bp ORF) was amplified from genomic DNA using NW233/NW234 containing attB sites for cloning into pGL2084. Linearization with AscI	Hygro	N. Weisert
pGL2084_UPF1	*UPF1* fragment (461 bp, 67-527 of 2,529 bp ORF) was amplified from genomic DNA using NW167/NW168 containing attB sites for cloning into pGL2084. Linearization with AscI	Hygro	E. Meyer-Nautus
pJ1339	*Beta tubulin* locus expression vector of *T7RNAP, TETR* and *Cas9* in *T. brucei*. Linearization with HindIII.	Puro	J. Sunter
p2678	Plasmid was cut with NdeI and BstBI to replace the puromycin resistance cassette.	Puro	(Kelly et al., 2007)
p2678_G418	G418mycin resistance cassette was amplified from p2706 using NW92/NW93 containing NdeI and BstBI restriction enzyme sites for cloning into p2678. Plasmid used for CRISPR Cas9-based N-terminal PTP tagging of *GOI.*	G418	N. Weisert
p2678_*HYG*	Hygromycin resistance cassette was amplified from pyrFEKO-*HYG* using NW155/NW156 containing NdeI and BstBI restriction enzyme sites for cloning into p2678. Plasmid used for CRISPR Cas9-based N-terminal PTP tagging of *GOI*.	Hygro	N. Weisert

Name	Application	Selection in *T. brucei*	Reference
p2678_*BLE*	Phleomycin resistance cassette was amplified from pyrFEKO-*BLE* using NW90/NW154 containing NdeI and BstBI restriction enzyme sites for cloning into p2678. Plasmid used for CRISPR Cas9-based N-terminal PTP tagging of *GOI.*	Phleo	N. Weisert
p2706	Plasmid used for CRISPR Cas9-based C-terminal PTP tagging of *GOI*. For molecular cloning, the plasmid was cut with NdeI and BstBI to replace the G418mycin resistance cassette.	G418	(Kelly et al., 2007)
p2706_*HYG*	Hygromycin resistance cassette was amplified from pyrFEKO-*HYG* using NW155/NW156 containing NdeI and BstBI restriction enzyme sites for cloning into p2706. Plasmid used for CRISPR Cas9-based C-terminal PTP tagging of *GOI*.	Hygro	N. Weisert
p2706_*BLE*	Phleomycin resistance cassette was amplified from pyrFEKO-*BLE* using NW90/NW154 containing NdeI and BstBI restriction enzyme sites for cloning into p2706. Plasmid used for CRISPR Cas9-based C-terminal PTP tagging of *GOI*.	Phleo	N. Weisert
pMOTag 2T	Plasmid used for PCR-based C-terminal Ty1 *in situ* tagging of *TbTRF* using NW237/NW238.	Puro	(Oberholzer et al., 2005)
pLF-13	Plasmid used to amplify aminoglycoside phosphotransferase resistance gene for PCR-based gene knockout of *Tb*TRF using NW239/NW240.	G418	(Figueiredo et al., 2008)

DNA methods

Isolation of genomic DNA

Genomic DNA from *T. brucei* was isolated by using the *High Pure PCR Template Preparation Kit* (Roche). Therefore 5 x 10^6 cells were harvested (1500 *g*, RT, 10 min) and the pellet was

resuspended in 200 µl PBS. The following steps were performed according to the manufacturer's instructions.

For the performance of a diagnostic PCR to verify the correct insertion of a transfected construct, the *Phusion Human Specimen Direct PCR Kit* (Thermo Scientific) was used to isolate genomic DNA as a PCR template. 1 x 10^6 cells were harvested (1500 *g*, RT, 10 min), the pellet was resuspended in 20 µl dilution buffer and 0.5 µl DNA release additive was added. After incubation for 5 min at RT and 2 min at 98°C cells were centrifuged (2000 *g*, RT, 5 min) and 1 µl of the supernatant was used as a template for PCR.

Polymerase Chain Reaction

In vitro method used for DNA amplification. PCR reactions contained 1x HF buffer, 200 µM dNTPs, 0.5 µM of each fw and rv primers, 3%DMSO in case of required optimization for improved amplification and 0.02 U/µl of *Phusion™ High-Fidelity DNA Polymerase* (Thermo Fisher). 50 ng of genomic DNA or 10 ng of plasmid DNA was used as a template. If a diagnostic PCR was performed, 1 µl of genomic DNA isolated with the *Phusion Human Specimen Direct PCR Kit* (see: Isolation of genomic DNA) was used. Primers are listed in Table 6 and Table 7 (synthesized by Sigma-Aldrich). Primers for the amplification of a RNAi target sequence for the integration into pGL2084 were generated using the TrypanoFAN RNAi program from ˈdag.compbio.dundee.ac.uk/RNAitˈ to exclude off-target effects (Redmond et al., 2003). Homologous regions of *GOI*s for primers used for tagging by utilizing the CRISPR/Cas9 method as well as primers for sgRNA template generation were designed by using ˈLeishGEdit.netˈ(Beneke et al., 2017).

PCR reactions were carried out in the T100™ thermal cycler (BIO-RAD) with the following cycling parameters. The optimal annealing temperature for primer pairs was determined by using the Tm calculator (Thermo Fisher)(Allawi and SantaLucia, 1997).

98°C (2 min) – [98°C (10 sec) – X°C (30 sec) – 72°C (30 sec/kb)]25-35 cycles – 72°C (10 min) – 4°C (∞)

For sgRNA template amplification, the cycling parameters vary as followed (Beneke et al., 2017).

98°C (30 sec) – [98°C (10 sec) – 60°C (30 sec) – 72°C (15 sec)]35 cycles – 4°C (∞)

Table 6. Oligonucleotides used for PCR.

Name	Description	Application	Sequence
HR82	*p97* fw attB1	Amplification of *p97* RNAi target sequence for pGL2084 integration	GGGGACAAGTTTGTACAAAAAAGCAGGCT GTCGAGGAAATAGCAGCAGG
HR83	*p97* rv attB2		GGGGACCACTTTGTACAAGAAAGCTGGGT GAAGCACCTCTTCCTGAACG

Name	Description	Application	Sequence
HR90	*RPA2* fw attB1	Amplification of *RPA2* RNAi target sequence for pGL2084 integration	GGGGACAAGTTTGTACAAAAAAGCAGGCT AACTTCTTTACTGGTGCCGC
HR91	*RPA2* fw attB2		GGGGACCACTTTGTACAAGAAAGCTGGGT TACAGTCTGACACAAGCCGC
HR98	*MRB1590* fw attB1	Amplification of *MRB1590* RNAi target sequence for pGL2084 integration	GGGGACAAGTTTGTACAAAAAAGCAGGCT GGACGCAATTACGGTGAACT
HR99	*MRB1590* rv attB2		GGGGACCACTTTGTACAAGAAAGCTGGGT CATCAATACGTCGACCATGC
HR104	*p53* fw attB1	Amplification of *p53* RNAi target sequence for pGL2084 integration	GGGGACAAGTTTGTACAAAAAAGCAGGCT AATAGCGCCTGTTGTTGAGG
HR105	*p53* rv attB2		GGGGACCACTTTGTACAAGAAAGCTGGGT AACGGAACGACGGGAATATCA
NW71	*PABP2* fw attB1	Amplification of *PABP2* RNAi target sequence for pGL2084 integration	GGGGACAAGTTTGTACAAAAAAGCAGGCT GTTGAATGGGGTTTCCATTG
NW72	*PABP2* rv attB2		GGGGACCACTTTGTACAAGAAAGCTGGGT CAGGTTCGGGTATTTGCTGT
NW73	*TelAP2* fw attB1	Amplification of *TelAP2* RNAi target sequence for pGL2084 integration	GGGGACAAGTTTGTACAAAAAAGCAGGCT GTATCATTTCCTGTCGAACC
NW74	*TelAP2* rv attB2		GGGGACCACTTTGTACAAGAAAGCTGGGT CCGTAAAGTTATGAGCGTCC
NW120	*p77* fw attB1	Amplification of *p77* RNAi target sequence for pGL2084 integration	GGGGACAAGTTTGTACAAAAAAGCAGGCT TTTTTGCTGGCAAACAGTTG
NW121	*p77* rv attB2		GGGGACCACTTTGTACAAGAAAGCTGGGT CTTGGATCTTGGCCTTTACG
NW167	*UPF1* fw attB1	Amplification of *UPF1* RNAi target sequence for pGL2084 integration	GGGGACAAGTTTGTACAAAAAAGCAGGCT CGACAACGAACACGCTGTTT
NW168	*UPF1* fw attB2		GGGGACCACTTTGTACAAGAAAGCTGGGT TACGTGACTGTGCAACTCCC

Name	Description	Application	Sequence
NW229	*TelAP3* K3 fw attB1	Amplification of *TelAP3* K3 RNAi target sequence for pGL2084 integration	GGGGACAAGTTTGTACAAAAAAGCAGGCT ACTCCGCACCATCAACTTCC
NW230	*TelAP3* K3 rv attB2		GGGGACCACTTTGTACAAGAAAGCTGGGT GGCAAGCCGTGTATACAACG
NW233	*TelAP3* K5 fw attB1	Amplification of *TelAP3* K5 RNAi target sequence for pGL2084 integration	GGGGACAAGTTTGTACAAAAAAGCAGGCT AACTGGTGGAACGTGTACGA
NW234	*TelAP3* K5 rv attB2		GGGGACCACTTTGTACAAGAAAGCTGGGT TTTCTCCAGTGTCCATGGGC
NW90	*BLE* NdeI fw	Amplification of *BLE* from pyrFEKO *BLE* for p2678/p2706 integration	gggaattcCATATG ATGGCCAAGTTGACCAGT
NW154	*BLE* BstBI rv		ggaattcTTCGAA CTAGTCCTGCTCCTCGGCCA
NW92	*NEO* NdeI fw	Amplification of *NEO* from p2706 for p2678 integration	gggaattcCATATG ATGATTGAACAAGATGGATTGC
NW93	*NEO* BstBI rv		ggaattcTTCGAA TTCGAATCAGAAGAACTCGTCA
NW155	*HYG* NdeI fw	Amplification of *HYG* from pyrFEKO *HYG* for p2678/p2706 integration	gggaattcCATATG ATGAAAAAGCCTGAACTCAC
NW156	*HYG* BstBI rv		ggaattcTTCGAA CTCTATTCCTTTGCCCTCG
NW183	*PTP PPL2* fw	Amplification of *PTP* from p2678 with homologous regions of *PPL2* 5'UTR for recombination-based integration	CACTAGGTGCCGCGCAAGAGGTATTTACCG cctaaagtcgaggaggttgact
NW184	*PTP PPL2* rv		GTCGCGCCTCCTGAGTTTTCGGACCCAT ggtggcggaagcttgaga

Name	Description	Application	Sequence
NW136	*PPL2* 5'sgRNA	5'sgRNA primer including T7 promoter sequence, *PPL2* target sequence and sgRNA scaffold sequence	gaaattaatacgactcactataggAGGCGCAAAGAACGATGGTA gttttagagctagaaatagc
NW185	*TelAP2 PTP* fw	Amplification of *PTP* from p2706 containing homologous regions of *TelAP2* 3'UTR for recombination-based integration	TTTGTAGCGTCTGAAACTGAATCTACCACTcggccgctggaagatca
NW186	*TelAP2 PTP* rv		CACACGGGAGAGCAACTGTCAAATCAGCCTtgttgttgttagtggtgct
NW133	*TelAP2* 3'sgRNA	3'sgRNA primer including T7 promoter sequence, *TelAP2* target sequence and sgRNA scaffold sequence	gaaattaatacgactcactataggGTAACGCAAGTTCTTGCTGCgttttagagct agaaatagc
NW189	*PTP PolIE* fw	Amplification of *PTP* from p2678 with homologous regions of *PolIE* 5'UTR for recombination-based integration	CGAGAATATACTCGCTTGTTGTTGTAATAA cctaaagtcgaggaggttgact
NW190	*PTP PolIE* rv		TCTTGCGGAGAAGATTGAAAGATTTTTCAT ggtggcggaagcttgaga
NW142	*PolIE* 5'sgRNA	5'sgRNA primer including T7 promoter sequence, *PolIE* target sequence and sgRNA scaffold sequence	gaaattaatacgactcactataggACTGTTTCTTGCCAGTTGCGgttttagagcta gaaatagc
G00	-	sgRNA scaffold primer	aaaagcaccgactcggtgccacttttttcaagttgataacggactagccttattttaacttgc tatttctagctctaaaac

Name	Description	Application	Sequence
NW237	*TbTRF Ty1* fw	Amplification of *Ty1* from pMOTag 2T for PCR-based C-terminal *in situ* tagging of *TbTRF*	TACAACAACAAGGATACAGGGGAAAGAACAGCGTCGCCGCACG CTCTCCCGAGAAAGCCTCCAATATGGAGAATAACGAGggtaccgggccc cccctcgag
NW238	*TbTRF Ty1* rv		AACAGACAACGGAGTACGACACGCTAGCACAGTGAAGACGCTACCT TTACCCAAGTTCCTCAATGTTTCAACAAACTCAT*tggcggccgctctagaa ctagtggat*
NW239	*TbTRF* KO *NEO* fw	Amplification *NEO* for PCR-based gene knockout of *TbTRF*	ACTTCAGTATACAACATCAAAATTTGGTTGTTCTTTTATATTTTTCTCA TATACTTTGTTGACGTAATTCCAGGGGGGCA cgcgtttccttacatatttctc
NW240	*TbTRF* KO *NEO* rv		AACAGACAACGGAGTACGACACGCTAGCACAGTGAAGACGCTACCT TC CCAAGTTCCTCAATGTTTCAACAAACTCAT ctcgaatccccccatttt

Abbreviations: HR (Helena Reis), NW (Nadine Weisert), fw (forward), rv (reverse).

Table 7. Oligonucleotides used for diagnostic PCR.

Name	Application	Sequence
NW102	ORF of *T7RNAP* fw	CGCTGCATCGAGATGCT
NW103	ORF of *T7RNAP* rv	TTACGCGAACGCGAAGTC
NW104	ORF of *Cas9* fw	TCACCGACGAGTACAAGG
NW105	ORF of *Cas9* rv	TTCTTTTTTGCCTGGCCG
VK1	5'UTR of *TelAP2*	CAGGTATGAAGAGGACGAAG
VK2	3'UTR of *TelAP2*	AGAGAGAGGAGGAGAAGG
NW150	5'UTR of *PPL2*	AGATCATTTTTGCGGTGC
NW151	3'UTR of *PPL2*	ACTTCCCTTTATTACTGCCT
NW226	5'UTR of *PolIE*	CTTCTTTTTCTGCTCCGC
NW227	3'UTR of *PolIE*	CTCTCTTCCACTATTTTACCCA
MM29	5'UTR of *TbTRF*	GCGCGCTGTTAATACACAAGAC
MM30	3'UTR of *TbTRF*	GTGTCAAACAGACAACAGAGTACG
Neo fw	ORF of *NEO*	CCGCTTCCTCGTGCTTTAC

Name	Application	Sequence
Phleo fw	ORF of *BLE*	CAAGTTGACCAGTGCCGTTC
NW86	ORF of *HYG* fw	tccCCCGGG ATGAAAAAGCCTGAACTCAC
NW87	ORF of *HYG* rv	cgcGGATCC CTATTCCTTTGCCCTCGG

Abbreviation: VK (Verena Kreß), MM (Margaux Michel).

Agarose gel electrophoresis

Method used for the separation of DNA fragments according to their size. Agarose gels were poured using 1 x TAE buffer (40 mM Tris-HCl, 20 mM acetic acid, 1 mM EDTA, pH 8) adding agarose (0.5%-2%) and *SYBR™ Safe DNA Gel Stain* (1:50,000) (Thermo Fisher). 6 x DNA loading dye (Thermo Fisher) was added to the DNA samples and the mixture was loaded into the gel chambers. The *GeneRuler DNA Ladder Mix* or the *GeneRuler 1kb DNA ladder* (Thermo Fisher) were used for DNA size estimation and approximate quantification. Electrophoresis was performed under continuous electrical flow in 1 x TAE buffer at 110 V for an appropriate amount of time considering the gel percentage and estimated size of the DNA and monitored by the migration of the tracking dye. Visualization and documentation were performed by using the *iBright™ Imaging System* (Thermo Fisher). In case of purification of the DNA after agarose gel electrophoresis, DNA fragments of the desired size were visualized with the blue light screen, cut with a razor blade, and transferred into a reaction tube.

Purification of DNA

PCR products and cut out DNA fragments from agarose gel were purified using the *NucleoSpin™ Gel and PCR Clean-u*p kit (Macherey-Nagel) according to the manufacturer's instructions.

PCR products and linearized DNA for transfection were purified with isopropanol precipitation. One volume of isopropanol and 0.1 volume of 3 M NaAc pH 5.2 were added to one volume of DNA/PCR product and mixed. The mixture was incubated for >2 h at -20°C and centrifuged (20,000 *g*, 4°C, 30 min). After two wash steps with 500 µl ice-cold ethanol (20,000 *g*, 4°C, 10 min), the pellet was air-dried under sterile conditions in a laminar flow hood. The pellet was precipitated with 15 µl of sterile dH_2O.

Restriction digest

DNA was digested using restriction enzymes according to the manufacturer's instructions (Thermo Fisher).

Ligation

Ligation reactions of vector and insert DNA was carried out in 20 µl volume mixed with T4 ligase buffer and T4 ligase (Thermo Fisher) incubated for 2 h at RT. Different molar ratios of vector to insert DNA can be of advantage, commonly 1:3, 1:5 and 1:7 ratios were used. 10 µl of the reactions were used for *E. coli* transformation.

Quantification of DNA concentration

Quantification of DNA was conducted using the Infinite M200 (Tecan) by measuring the absorption at 260 nm and 280 nm. The ratio of OD_{260} and OD_{280} determines the purity degree of DNA and should be between 1.8 and 1.9.

DNA sequencing

Sequencing of plasmid DNA was carried out by Eurofins genomics according to the company's guidelines. Sequencing results were analyzed by using the CLC main workbench 7 software (CLC bio, Qiagen. Aarhus, Denmark).

Table 8. Oligonucleotides used for sequencing analysis.

Name	Application	Sequence
MBS33	Sequencing of pGL2084	TAAAAGTAGCGCTTACGG
MBS34	Sequencing of pGL2084	TGCCTGCACTAACACTAC
Phleo up2	Sequencing of p2678 *BLE*/ p2706 *BLE*	CAAGTTGACCAGTGCCGTTC
Neo fw	Sequencing of p2678 *NEO*	CCGCTTCCTCGTGCTTTAC
NW14-Hygro	Sequencing of p2678 *HYG*/p2706 *HYG*	CTCGTGCTTTCAGCTTC

Abbreviations: MBS (Majeed Bakari Soale).

Protein methods

Immunofluorescence analysis

1 x 10^6 cells per sample were harvested (1500 x *g*, RT, 10 min) and resuspended in 0.5 ml medium (HMI-9 for BSF, SDM-79 for PCF). 1 ml of Voorheis' modified PBS (vPBS; PBS supplemented with 10 mM glucose, 46 mM sucrose, *1x cOmplete™ EDTA-free Protease Inhibitor Cocktail* (Roche)) was added, cells were centrifuged (750 x *g*, RT, 2 min) and washed twice with 1 ml vPBS under the same centrifugation conditions. Cells were resuspended in 1 ml vPBS containing 4% PFA solution and incubated for 20 min at RT to fix cells. Afterwards, cells were centrifuged again and carefully resuspended in 500 µl RT PBS. The cells were added to a poly-L-lysin coated coverslip inside a 24-well plate and centrifuged (750 x *g*, RT, 1 min). To permeabilize the cells, 0.5 ml 0.25% Triton X-100 in PBS was added to the coverslip and incubated for 5 min at RT. Two wash steps with 1 ml PBS followed. To block unspecific bindings of the antibodies, cells were incubated with 1 ml 3% BSA in PBS for 30 min at RT on a rocking platform. The solution was removed and the primary antibodies (Table 9) diluted in PBS in a total volume of 70 µl per coverslip were added and incubated inside a humidified chamber for 1 h at RT. The coverslips were washed three times with 1 ml PBS for 5 min inside the well plate and secondary antibodies (Table 9) were added applying the same conditions as for the primary antibodies but covered from light. After three washing steps, the coverslip was rinsed with dH_2O and carefully dried on a tissue. One drop of *Vectashield Antifade Mounting Medium with DAPI* (Vector Laboratories) was placed on top of glass slides and the coverslip was placed

onto the Vectashield to embed the cells. The coverslip was sealed using nail polish or glue. Images were captured by using the Leica DMI 6000B microscope and processed with the Fiji software (Fiji-ImageJ2.3.0; Wyne Rasband, National Institute of Health, USA).

Table 9. Primary and secondary antibodies used for immunofluorescence analysis.

Name	Isotype	Clonality	Dilution	Reference
Anti-*Tb*TRF 6F5	Rat	Monoclonal	1:2	E. Kremmer
Anti-TelAP1 2E6	Mouse	Monoclonal	1:2	E. Kremmer
Anti-TelAP2	Rabbit	Polyclonal	1:200	Pineda
Anti-TelAP3	Guinea pig	Polyclonal	1:200	Moravian Biotech
Alexa Fluor 488 anti-rat	Goat	Polyclonal	1:2,000	Thermo Fisher Scientific
Alexa Fluor 594 anti-mouse	Goat	Polyclonal	1:2,000	Thermo Fisher Scientific
Alexa Fluor 594 anti-rabbit	Goat	Polyclonal	1:2,000	Thermo Fisher Scientific
CF^{TM}568 anti-guinea pig	Donkey	Polyclonal	1:500	Sigma-Aldrich

Preparation of whole cell lysates for SDS-PAGE

T. brucei cells were harvested by centrifugation (1500 *g*, 4°C, 10 min) and washed with 1 ml ice-cold TDB or PBS buffer. The cell pellet was resuspended in an appropriate amount of 1 x SDS loading buffer (126 mM Tris-HCl pH 6.8, 20% Glycerol, 4% SDS, 60 mM DTT, 0.02% bromophenol blue) to reach a final concentration of 2-5 x 10^5 cells/µl. The suspension was boiled for 10 min at 95°C and stored at -20°C.

SDS polyacrylamide gel electrophoresis

The separation of proteins according to their molecular mass was conducted by using ˈSodium Dodecyl Sulfateˈ SDS gel electrophoresis. Therefore, polyacrylamide gels were poured with a certain concentration of acrylamide/bisacrylamid for the optimal separation of the 'protein of interest' (POI) (separation gels between 8-15%). Gels were placed into the *Mini-PROTEAN Tetra Vertical Electrophoresis Cell* (BIO-RAD). Total protein extracts with a final density of 2 x10^6 cells were loaded onto the gels and a prestained protein marker (Thermo Fisher) was used for size estimation. Proteins were concentrated in stacking gels (5% acrylamide/bisacrylamid (37.5:1), 500mM Tris-HCl pH 6.8, 0.4% SDS) and separated in separation gels (X% acrylamide/bisacrylamid (37.5:1), 1.5 M Tris-HCl pH 8.8, 0.4% SDS) by running the gels in SDS-running buffer (192 mM glycine, 25 mM Tris, 0.1% SDS) at 100-170 V

using the EV265 electrophoresis power supply (Consort). Separated proteins were further analyzed by Coomassie staining or western blot.

Coomassie staining

After the separation of proteins by SDS PAGE, the gels were transferred into plastic boxes containing water and boiled in a microwave oven. The water was discharged, and the gels were stained using a Coomassie solution (either 0.02% *Coomassie Brilliant Blue G-250* (SERVA), 10% EtOH, 5% aluminiumsulfate-(14-18)-hydrate, 2% orthophosphoric acid or 0.05% Coomassie Brilliant Blue R-250 (AppliChem), 10% isopropanol, 5% acetic acid) and incubated over night at RT shaking. The destaining of the gels was performed by either using water or destain solution (10% isopropanol, 5% acetic acid).

Western blot

Separated proteins were transferred onto ˈPolyvinylidene fluorideˈ PVDF membranes (Merck Millipore) using either the semi-dry or wet blotting technique. In both cases, the membrane was activated prior to usage by placing the membrane in 100% methanol for 15 sec.

If the semi-dry technique was used, the blot assembled as followed from bottom to top in the *Trans-blot SD Semi-Dry Transfer Cell* (BIO-RAD). Two 1.5 mm thick Whatman paper soaked in anode buffer (25 mM Tris-HCl pH 7.6, 20% MeOH), the activated PVDF membrane, the gel, two 1.5 mm thick Whatman paper soaked in cathode buffer (300 mM Tris-NaOH pH 10.4, 20% MeOH, 40 mM ε-aminocaproic acid). The transfer occurred for 1.5-2 h depending on protein size with 0.8 mA/cm^2 per gel using the EV265 electrophoresis power supply (Consort).

If the wet technique was used, the *Mini Trans-Blot Cell* system (BIO-RAD) was used. The black side of the color-coded *Mini Gel Holder Cassette* is placed down, and the blot assembled as followed from bottom to top. A foam pad, one sheet of x mm thick Whatman paper, the gel, the activated PVDF membrane, one sheet of X mm thick Whatman paper, a foam pad. The cassette was closed and inserted into the *Mini Trans-Blot Central Core*, which was placed together with a cold pack into the transfer cell. The transfer occurred for 2 h at 300 mA using the EV265 electrophoresis power supply (Consort).

After the transfer, the membrane was placed into a 50 ml reaction tube and incubated with a 10 ml solution of 5% milk in PBS over night at 4°C to block unspecific bindings of the antibodies. The membrane was then incubated with primary antibodies (Table 10) in a 5 ml solution of 0.1% Tween/PBS for 1 h at RT rotating.

Three washing steps with 10 ml of 0.2% Tween/PBS for 10 min followed. The membrane was incubated with secondary antibodies (Table 10) in a 10 ml solution of 0.1% Tween/PBS supplemented with 0.02% SDS for 1 h at RT rotating and protected from light. After three washing steps carried out as before, the membrane was dried between two Whatman paper sheets and the blots were analyzed using the Odyssey CLx imaging system (LI-COR) and signals were quantified with the ImageStudio software (LI-COR).

Table 10. Primary and secondary antibodies used for western blot analysis.

Name	Isotype	Clonality	Dilution	Reference
Anti-H3	Rabbit	Polyclonal	1:50,000	Pineda

Name	Isotype	Clonality	Dilution	Reference
Anti-PFR L13D6	Mouse	Monoclonal	1:200	K. Gull
Anti-TelAP1 2E6	Mouse	Monoclonal	1:5	E. Kremmer
Anti-*Tb*TRF 6F5	Rat	Monoclonal	1:200	E. Kremmer
Anti-Ty1 BB2	mouse	Monoclonal	1:500	K. Gull
Anti-Protein C	Rabbit	Polyclonal	1:5000	Genescript
IRDye 680LT anti-rabbit IgG	Goat	Polyclonal	1:20,000	LI-COR Bioscience
IRDye 680LT anti-mouse IgG	Goat	Polyclonal	1:20,000	LI-COR Bioscience
IRDye 800CW anti-rabbit IgG	Goat	Polyclonal	1:20,000	LI-COR Bioscience
IRDye 800CW anti-rat IgG	Goat	Polyclonal	1:20,000	LI-COR Bioscience

Abbreviation: H3 (Histone H3), PFR (Paraflagellar rod), IgG (Immunoglobulin G).

Affinity purification

Affinity purification using *IgG Sepharose 6 Fast Flow* beads (GE Healthcare) was conducted to purify interaction partners of PTP-tagged candidates and carried out in quadruplicates with minor changes as described (Schimanski et al., 2005b). Per replica, 1-2 x 10^8 cells were harvested (1500 x *g*, 4°C, 10 min), washed with 10 ml ice-cold wash solution (20 mM Tris HCl pH 7.7, 100 mM NaCl, 3 mM $MgCl_2$, 1 mM EDTA) followed by a second wash step with 10 ml ice cold extraction buffer (150 mM sucrose, 150 mM KCl, 3 mM $MgCl_2$, 20 mM HEPES-KOH, 0.1% Tween 20, 1 mM DTT, 10 µg/ml TLCK, *1x cOmplete™ EDTA-free Protease Inhibitor Cocktail* (Roche)) under the same conditions. The cell pellet was resuspended in 1 ml extraction buffer and lysed by three freeze-thaw cycles in liquid nitrogen and sonicated with two cycles of 30 sec high-power pulse and 30 sec pause using the *Bioruptor Plus sonication device* (Diagenode).

Cells were harvested by centrifugation (20,000 x *g*, 4°C, 20 min) and the supernatant was transferred to a new reaction tube. Per replica, 20 µl of the beads were equilibrated by washing them once with 1 ml ice-cold TST buffer (50 mM Tris pH 7, 150 mM NaCl, 0.05% Tween 20) and twice with 1 ml ice-cold PA-150 buffer (150 mM KCl, 20 mM Tris-HCl pH 7.7, 3 mM $MgCl_2$, 0.1% Tween 20, 0.5 mM DTT, 10 µg/ml TLCK, *1x cOmplete™ EDTA-free Protease Inhibitor Cocktail* (Roche)) (500 x *g* , 4°C, 5 min). The equilibrated beads were added to the lysate and proteins were bound by incubation for 2 h at 4°C under constant rotation. After centrifugation (500 x *g*, 4°C, 5 min) the supernatant was discharged and the beads were washed twice with 1 ml PA-150 buffer (10 min incubation followed by centrifugation (500 x *g*, 4°C, 5 min)). In case the samples were treated with DNase I to investigate, if the interactions

were DNA dependent, the beads were incubated with DNase I in PA-150 buffer for 10 min at 37°C prior to the washing steps. The control samples were also incubated in PA-150 buffer without DNase. Elution of proteins was conducted by adding 65 µl of 1 x *NuPAGE™ LDS-Sample buffer* (Thermo Fisher) supplemented with 100 mM DTT to the beads and boiled for 10 min at 70°C. After centrifugation (1000 x *g*, RT, 1 min), the supernatant was transferred to a new reaction tube using a Hamilton syringe (Hartenstein) and stored at -20°C prior to analyzation by mass spectrometry (F. Butter, Mainz).

Co-Immunoprecipitation

Per co-IP, 30 µl of *Protein G Sepharose™ 4 Fast Flow* bead slurry (GE Healthcare) were used. The bead slurry was washed once with 1 ml PBS and twice with 1 ml 1%BSA in PBS. Afterwards beads were incubated with 1%BSA in PBS for 1 h at 4°C under constant rotation to block unspecific binding. Beads were centrifuged (500 x *g*, 4°C, 1 min), the supernatant was removed, and the antibody was added to the beads and incubated over night at 4°C under constant rotation (1.5 ml monoclonal anti-Ty1 BB2 mouse antibody / 2 ml monoclonal anti-TelAP1 2E6 mouse antibody). Beads were washed three times with 1 ml 0.1% BSA in PBS (500 x *g*, 4°C, 1 min) and resuspended in 100 µl 0.1% BSA in PBS. The beads were stored at 4°C and for longer storage supplemented with sodium azide (0.02% final concentration). Prior to usage beads were equilibrated by washing them 1 ml ice-cold IP buffer (150 mM NaCl, 20 mM Tris HCl pH 8, 10 mM $MgCl_2$, 0.5% NP-40, 10 µg/ml TLCK, *1x cOmplete™ EDTA-free Protease Inhibitor Cocktail* (Roche)) and were resuspended in 100 µl IP buffer.

Per replica, 2 x 10^8 cells were harvested (1500 x *g*, 4°C, 10 min) and washed with 10 ml ice-cold TDB. The pellet was resuspended in 1 ml IP buffer and transferred into a fresh falcon tube. Cells were incubated for 20 min on ice and sonicated with three cycles of 30 sec high-power pulse and 30 sec pause using the *Bioruptor Plus sonication device* (Diagenode). Lysates were centrifuged (10,000 x *g*, 4°C, 10 min) and the supernatant was transferred to a new reaction tube. The previously prepared antibody- bead conjugates in 100 µl IP buffer were added to the supernatant and incubated over night at 4°C under constant rotation. Beads were washed three times with 500 µl IP buffer (500 x *g*, 4°C, 1 min), resuspended in 65 µl 1 x *NuPAGE™ LDS-Sample buffer* (Thermo Fisher) supplemented with 100 mM DTT and boiled for 10 min at 70°C. After centrifugation (1000 x *g*, RT, 1 min), the supernatant was transferred to a new reaction tube using a Hamilton syringe (Hartenstein) and stored at -20°C prior to analyzation by mass spectrometry (F. Butter, Mainz). The co-IP was performed in quadruplicates.

Isolation of soluble VSGs for mass spectrometry analysis

For the isolation of soluble VSGs (Cross, 1984) 4 x 10^7 cells were pre-cooled on ice for 10 min prior to centrifugation (1500 *g*, 4°C, 10 min). After a wash step with TDB the cell pellet was resuspended in 45 µl sodium phosphate buffer (10 mM Na_2HPO_4 and NaH_2PO_4 (20:1) pH 8, 10 µg/ml TLCK, *1x cOmplete™ EDTA-free Protease Inhibitor Cocktail* (Roche)). The suspension was incubated at 37°C for 5 min and cooled down on ice for 2 min. By centrifugation (14.000 *g*, 4°C, 5 min) VSGs were sheared off and the supernatant was transferred into a new reaction tube containing 15 µl 4 x *NuPAGE™ LDS-Sample Buffer* (Thermo Fisher) supplemented with 400 mM DTT. Samples were boiled at 70°C for 10 min and stored at -20°C prior to analyzation by mass spectrometry (F. Butter, Mainz). The isolation was performed in quadruplicates.

Preparation of whole cell lysates for mass spectrometry analysis

For whole proteome analysis of proteins of interest, the preparation of whole cell lysates for mass spectrometry was conducted. 2 x 10^6 cells were harvested (1500 *g*, 4°C, 10 min), washed with 1 min TDB buffer and the cell pellet was resuspended in 60 µl 1 x *NuPAGE™ LDS-Sample buffer* (Thermo Fisher) supplemented with 100 mM DTT. Samples were boiled at 70°C for 10 min and stored at -20°C prior to analyzation by mass spectrometry (F. Butter, Mainz). The preparation was performed in quadruplicates.

Mass spectrometry

The cooperating laboratory of Dr. Falk Butter (IMB, Mainz) performed mass spectrometry and data analysis. To separate the samples, a Novex Bis-Tris 4-12% gradient gel (Thermo Fisher) run in 3-(N-morpholino)propanesulfonic acid (MOPS) for 10 min at 180 V was used and stained with Coomassie brilliant blue G-250 dye (Biozym). Each gel lane was cut into pieces, minced and destained in 50 % EtOH/water. Gels were dehydrated using acetone, reduced by incubation with 10 mM DTT (Sigma Aldrich) and alkylated with 55 mM iodoacetamide protected from light. The dried gel pieces were digested using 1 µM trypsin at 37° C ON. Afterwards, peptides were desalted and stored on StageTips until measurement (Rappsilber et al., 2007). Peptides were separated through a 90-240 min gradient using the EasyLC 1000 UHPLC system under use of a C18 reverse phase column. The column was packed in-house with Reprosil C18 (Dr. Maisch GmbH) previously. The column was enclosed into a column oven (Sonation) and peptides were sprayed into a Q Exactive Plus mass spectrometer (Thermo), which was operating in a data-dependent acquisition mode using a top10 method. Spray voltage was set to approximately 2.4 kilovolt (kV). The acquired raw data files were processed using MaxQuant (version 1.5.8.2) (Cox and Mann, 2008) using the TriTrypDB. Contaminants, protein groups that were only identified by site, protein groups with less than two peptides and reverse hits were removed prior to bioinformatic analysis. Data was used to generate volcano plots by calculating the median and p-value (Welch t-test) and visualized using ggplot2 package of R.

Electromobility shift assay (EMSA)

To obtain if proteins bind DNA *in vitro*, EMSA was performed with recombinant proteins. Complementary oligonucleotides (HR45+HR46 for telomeric DNA, HR47+HR48 for negative control (Table 11)) were annealed by mixing them at a 1:1 molar ratio with a final concentration of 1 µM of each oligonucleotide in 100 µl volume supplemented with 1x ligase buffer (Thermo Fisher) and incubating them at 95°C for 5 min.

To 12µl of EB1 buffer (10 mM Tris-HCl pH 7.6, 5 mM DTT, 1 mM EDTA pH 8.0, 5% glycerin) 50 ng of the annealed oligonucleotides and 0.5-6 µg recombinant protein were added. EB2 buffer (20 mM HEPES/KOH pH 7.6, 1 mM DTT) was added to a final volume of 20 µl and incubated on ice for 30 min. A 5% native acrylamide gel (5% acrylamide/bisacrylamid (37.5:1), TAE buffer) was pre-ran in 1xTAE buffer for 1 h 40 min at 70 V at 4°C. Reactions were loaded into the gel chambers and a 100 bp generuler (Thermo Fisher) was used for DNA size estimation. The gel was run for 90 min at 4°C at 70 V and stained in 50 ml TAE buffer containing *SYBR™ Safe DNA Gel Stain* (1:10,000) (Thermo Fisher). Visualization and documentation were performed by using the *iBright™ Imaging System* (Thermo Fisher).

Table 11. Oligonucleotides used for EMSA.

Name	Application	Sequence
HR45	$(TTAGGG)_{10}$ fw	TTAGGGTTAGGGTTAGGGTTAGGGTTAGGGTTAGGGTTAGGGTTA GGGTTAGGGTTAGGG
HR46	$(TTAGGG)_{10}$ rv	AACCCTAACCCTAACCCTAACCCTAACCCTAACCCTAACCCTAACCCT AACCCTAACCCT
HR47	$(GTGAGT)_{10}$ fw	TTGACAGTGAGTGTGAGTGTGAGTGTGAGTGTGAGTGTGAGTGTG AGTGTGAGTGTGAGT
HR48	$(GTGAGT)_{10}$ rv	AAACTCACACTCACACTCACACTCACACTCACACTCACACTCACACTC ACACTCACTGTC

Recombinant protein expression

Recombinant N-terminal His_6-MBP TelAP2 proteins was obtained from Falk Butter (Mainz) and expressed by using the pCoofy expression system (Scholz et al., 2013). The full length TelAP2 coding sequence (Tb427_ Tb427_060048400) was amplified via PCR using genomic DNA and cloned into the pCoofy4 vector.

To express recombinant C-terminal His_6 TelAP3 protein, the pET21a(+) expression system was used. The full length TelAP3 coding sequence (Tb427_090023800/ Tb427_090024100) was amplified via PCR using genomic DNA as a template and cloned into the pET21a(+) expression vector. The vector was transformed into LOBSTR-BL21(DE3)-RIL *E. coli* cells and a single colony from the selective LB agar plate was used to inoculate 30 ml of selective LB medium over night at 37°C shaking at 180 rpm. The culture was diluted to an OD_{600} of 0.1 in 400 ml LB medium supplemented with 1% glucose and ampicillin. The culture was grown at 37°C shaking at 180 rpm until an OD_{600} of 0.8 was reached. Protein expression was induced with 1 µM IPTG over night at RT shaking at 180 rpm. Cells were harvested (2000 x *g*, 4°C, 20 min) and resuspended on ice with 4 ml ice-cold lysis buffer (50 mM NaH_2PO_4 pH 8, 300 mM NaCl, 10 mM imidazole, 1% Triton X-100, 5 mM beta mercaptoethanol, *1x cOmplete™ EDTA-free Protease Inhibitor Cocktail* (Roche)). Cells were sonicated with 10 cycles of 30 sec high-power pulse and 30 sec pause using the *Bioruptor Plus sonication device* (Diagenode) and centrifuged (10,000 x *g*, 4°C, 10 min) afterwards.

The supernatant was transferred to a new falcon tube, diluted 1:2 with equilibration buffer (50 mM NaH_2PO_4 pH 8, 300 mM NaCl, 10 mM imidazole, 2 mM beta mercaptoethanol) and stored on ice. 400 µl of *HisPur™ Ni-NTA Resin* (Thermo Fisher) were equilibrated by washing once with dH_2O and twice with 4 ml equilibration buffer (1000 x *g*, 4°C, 2 min). The equilibrated resin was added to the lysate and incubated for 1h at 4°C rotating end over end. After centrifugation (1000 x *g*, 4°C, 2 min) the supernatant was discharged and the beads were washed twice with 4 ml wash buffer (50 mM NaH_2PO_4 pH 8, 300 mM NaCl, 20 mM imidazole, 2 mM beta mercaptoethanol) using the same centrifugation settings. Beads were incubated with elution buffer (50 mM NaH_2PO_4 pH 8, 300 mM NaCl, 20 mM imidazole) for 40 min at 4°C rotating end over end and centrifuged afterwards (1000 x *g*, 4°C, 2 min). The purified protein was transferred to a fresh reaction tube using a Hamilton syringe (Hartenstein).

Antibody production and purification

Recombinant His_6-MBP TbTelAP2 and recombinant His_6 TelAP3 proteins were used for the immunization of animals for antibody production. For polyclonal anti-TelAP2 antibody generation, rabbits were immunized, and the antibody was generated by the Company Pineda (Berlin, Germany). For polyclonal anti-TelAP3 antibody generation, one guinea pig was immunized, and the antibody was generated by the company Moravian Biotech (Brno-Židenice, Czech Republic). Sera were tested by Coomassie, western blotting and immunofluorescence for their specificity and purified using the *SulfoLink Immobilization Kit for Peptides* (Thermo Fisher) according to the manufacturer's instructions. Briefly, 0.5-1 mg of recombinant protein was bound to 1 ml of crosslinked beaded agarose in a column and 5-10 ml of serum was purified.

Yeast two-hybrid

The cooperating laboratory of Dr. Falk Butter and Dr. Helle Ulrich (IMB, Mainz) performed yeast two-hybrid screen and data analysis. Yeast two-hybrid interaction screens were performed in the PJ69-4α yeast strain as described before (James, P., Halladay, J. & Craig, E. A. Genomic libraries and a host strain designed for highly efficient two-hybrid selection in yeast. *Genetics* **144**, 1425–1436 (1996).

Table 12. Yeast strain used in this study.

Yeast strain	**Genotype**
PJ69-4α	MATa trp1-901 leu2-3,112 ura3-52 his3-200 gal4Δ gal80Δ LYS2::GAL1-HIS3 GAL2-ADE2 met2::GAL7-lacZ

Co-transformation, the Gal4 activation and DNA-binding domain plasmid into PJ69-4α was followed by resuspension of five transformants per combination in ddH_2O. The suspensions were spotted on SC Trp-Leu-, SC Trp-Leu-His-, SC Trp-Leu-His-Ade- plates and incubated at 30°C for 48-72h. Colony formation was imaged using an Epson Scanner (Perfection V700 Photo, Software 3.81).

RESULTS

Further characterization of telomere-associated proteins in *Trypanosoma brucei*

In a previous study, a list of novel telomere-associated proteins (TelAPs) was generated using two complementary biochemical experimental approaches. First, affinity chromatography using oligonucleotides composed of telomeric repeat sequences identified proteins enriched at the telomeric DNA sites. For the second approach, interacting proteins of the known telomere protein *Tb*TRF were identified by co-IP. As a proof of principal, two of the candidates identified in both screening processes were characterized further and named TelAP1 and PolIE (Reis et al., 2018, Leal et al., 2020). How the other 22 identified proteins (Table 13) are involved with the telomere complex and if they influence VSG expression are mostly still elusive. To refine our understanding of the telomere complex and involved TelAPs, it is necessary to identify additional components and outline their functions.

To specify if the 'proteins of interest' (POI) are genuinely telomere-associated, one can use several sources to verify their localization. TrypTag is a collection of proteins tagged with mNG in PCF cells. According to TrypTag, eleven proteins show a nuclear localization in PCF cells and seven proteins have a positive 'nuclear enrichment score' (NES) supporting their potential involvement in nuclear functions (Dean et al., 2017, Goos et al., 2017)(Table 13). A GO component analysis using TriTrypDB indicated that eleven proteins are at least partially localized in the nucleus, seven in the nucleoplasm, and four in the nucleolus, whereas proteins may be assigned to multiple GO components (Figure 9A, Table S1). These proteins are more likely to be truly associated with the telomeric repeats and the telomere complex. A majority of the proteins have unknown biological processes according to GO process analysis, while five proteins are implicated in RNA processing (Figure 9B, Table S1). 14 proteins are proposed to bind DNA, five bind RNA and three possess a helicase activity based on their GO functions analysis (Figure 9C, Table S1). To improve our understanding of their functions, a preliminary step involves the depletion of these proteins to evaluate their influence on VSG expression site regulation. Additionally, quantitative proteomic analysis can monitor alterations in other protein expression levels within the knockdown cell line.

Table 13. List of POI.

Gene ID	Name	Protein Description (TriTrypDB)	Localization in PCF (TrypTag; N/C terminal tagged)	NES (Goos et al., 2017)	Reference
Tb927.2.6100; Tb427_020032100	p53	hypothetical protein, putative	mitochondrion/ cytoplasm (points)	NA	
Tb927.3.1590; Tb427_030015600	MRB1590	mitochondrial RNA binding complex 1 subunit	cytoplasm/ cytoplasm	-0.16	(Shaw et al., 2015)
Tb927.3.2140; Tb427_030021100	p105	PHD finger domain protein 4	nucleoplasm, cytoplasm	NA	
Tb927.3.5150; Tb427_030055000	p33	exonuclease	cytoplasm/ cytoplasm	-1.29	

Gene ID	Name	Protein Description (TriTrypDB)	Localization in PCF (TrypTag; N/C terminal tagged)	NES (Goos et al., 2017)	Reference
Tb927.5.1700; Tb427_050022800	RPA2	replication factor A 28 kDa subunit, putative	nucleoplasm/ nucleoplasm	-1.09	(Glover et al., 2019)
Tb927.5.2140; Tb427_050027800	UPF1	regulator of nonsense transcripts 1	cytoplasm	-0.92	(Delhi et al., 2011)
Tb927.6.1190; Tb427_060015500	p35	Plus-3 domain/Zinc finger, C3HC4 type (RING finger), putative	endocytic, cytoplasm/ cell tip(posterior), basal body, pro-basal body, cytoplasm	NA	
Tb927.6.4330; Tb427_060048400	TelAP2	telomere-associated protein	nucleoplasm/ nucleus	6.07	(Glover et al., 2016)
Tb927.8.3560; Tb427_080040700	PIF5	DNA repair and recombination helicase protein	nucleolus, cytoplasm, nucleoplasm	-2.04	(Liu et al., 2009)
Tb927.9.10770; Tb427_090061600	PABP2	polyadenylate-binding protein 2	cytoplasm, nucleus	-0.6	(Kramer et al., 2013)
Tb927.9.3930/4000; Tb427_090023800/24100	TelAP3	hypothetical protein, conserved	nucleus, cytoplasm/ nuclear lumen	6.58	
Tb927.9.5020; Tb427_090028700	p52	HMG-box domain containing protein, putative	cytoplasm/ kinetoplast	NA	
Tb927.9.8740; Tb427_090049100	DRBD3	Double RNA binding domain 3	cytoplasm, nucleoplasm/ nucleoplasm, cytoplasm	0.54	(Estevez, 2008)
Tb927.10.1900; Tb427_100022200	p88	DNA topoisomerase IA, putative	cytoplasm/ mitochondrion, antipodal sites	-2.17	
Tb927.10.2200; Tb427_100026200	p38	hypothetical protein, putative	cytoplasm/ mitochondrion, kinetoplast	-3.19	
Tb927.10.2520; Tb427_100029500	PPL2	PrimPol-like protein 2	nucleoplasm/ nucleoplasm, cytoplasm	5.54	(Rudd et al., 2013)
Tb927.10.4220; Tb427_100046500	p34	hypothetical protein, putative	cytoplasm	-3.04	
Tb927.10.6220; Tb427_070054600	XRND	5'-3' exoribonuclease D	nucleolus/ nucleolus, nucleoplasm	3.31	(Li et al., 2006)

Gene ID	Name	Protein Description (TriTrypDB)	Localization in PCF (TrypTag; N/C terminal tagged)	NES (Goos et al., 2017)	Reference
Tb927.10.9780; Tb427_100104600	p97	ATP-dependent DEAD/H RNA helicase, putative	nucleolus/ nucleolus	1.74	
Tb927.11.16120; Tb427_110180600	p68	hypothetical protein, putative	endocytic, cytoplasm/ kinetoplast	NA	
Tb927.11.6790; Tb427_110073000	NOP89	Nucleolar protein 89	nucleolus/ nucleolus	2.99	(Zhou et al., 2018)
Tb927.11.9920; Tb427_110107600	p77	polyubiquitin, putative	cytoplasm, flagellar cytoplasm, nuclear lumen, flagella connector, endocytic/ cytoplasm	-1.55	

List of potential telomere-associated proteins (Reis, 2017). Gene IDs of TREU927 and Lister427 sequences (Berriman et al., 2005, Müller et al., 2018). Protein description according to TriTrypDB, localization in PCF cells according to TrypTag (Aslett et al., 2010, Dean et al., 2017). A positive nuclear enrichment score (NES) indicates a localization in the nucleus (Goos et al., 2017) .Candidates with a nuclear localization according to TrypTag are highlighted in blue.

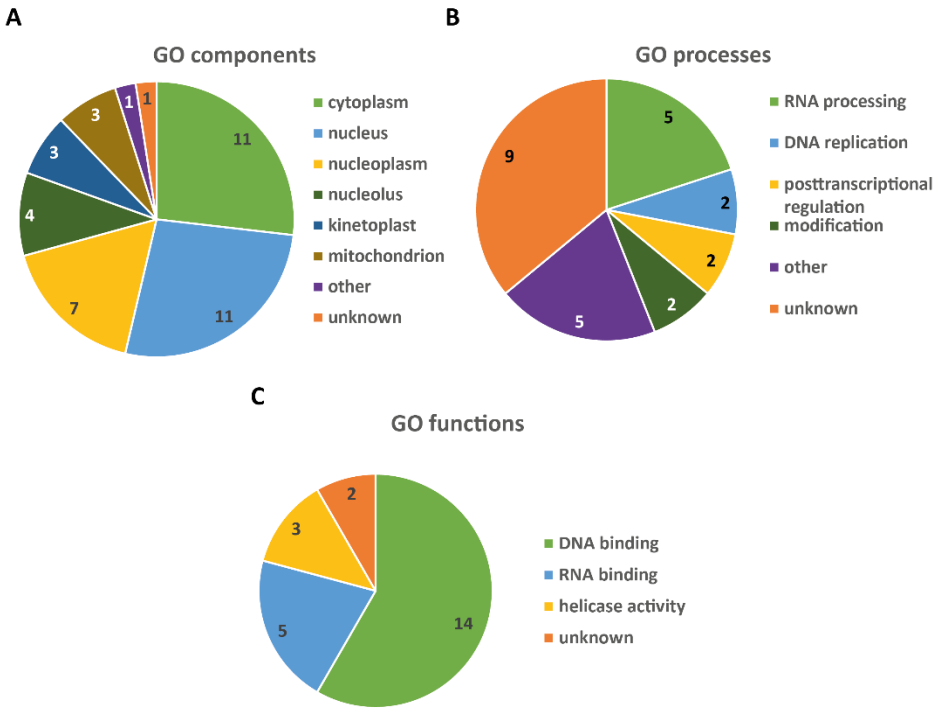

Figure 9: Pie charts of GO terms. (A) Cellular components (GO components), **(B)** biological processes (GO processes) and **(C)** functions (GO functions) of the proteins of interest (POI) according to TriTrypDB. Proteins can be assigned to multiple GO components, GO processes or GO function.

Depletion of proteins using RNAi

To address the question, if the proteins are essential for the organism's viability and to provide a tool for further experiments, the first step was to generate inducible RNAi cell lines in the BSF stage to deplete the POIs. RNAi target sequences, ranging approximately from 200-600 bp were identified using the TrypanoFAN RNAi program and integrated into the pGL2084 vector (Jones et al., 2014). Each linearized plasmid was transfected into 2T1 parental cell lines and RNAi was induced by adding 1 µg/ml tetracycline. It was possible to generate RNAi cell lines for 21 of the 22 candidates. To validate the impact of the protein depletion on cell growth, a growth curve of each cell line was conducted by monitoring the RNAi influence over a period of 96 h. Cell growth was compared to the uninduced cell line and the WT cell line (Figure 10). Among the 21 RNAi cell lines tested, 9 displayed a growth phenotype following protein depletion of a POI (p35, p53, p77, p97, PABP2, PPL2, RPA2, TelAP2, XRND). This outcome indicates that these proteins are essential for the viability of the cell. These findings also confirmed the previously published data on the influence of XRND, PABP2, PPL2 and p4330 (now called TelAP2) depletion on cell viability (Li et al., 2006, Kramer et al., 2013, Rudd et al., 2013, Glover et al., 2016).

In another approach, the absence of the protein on cell viability or cell growth during the differentiation process of BSF to PCF was evaluated. Therefore, the cell lines were monitored during the early stages of the developmental transition while inducing protein depletion. Only RNAi cell lines, that did not exhibit a growth phenotype in BSF cells after protein depletion were selected for this analysis. None of the 12 tested candidates showed a difference in cell growth during differentiation compared to uninduced RNAi cell lines or the WT cell line (data not shown, partially in N. Weisert, Master thesis 2018 and M. Mitnacht, Bachelor thesis 2020).

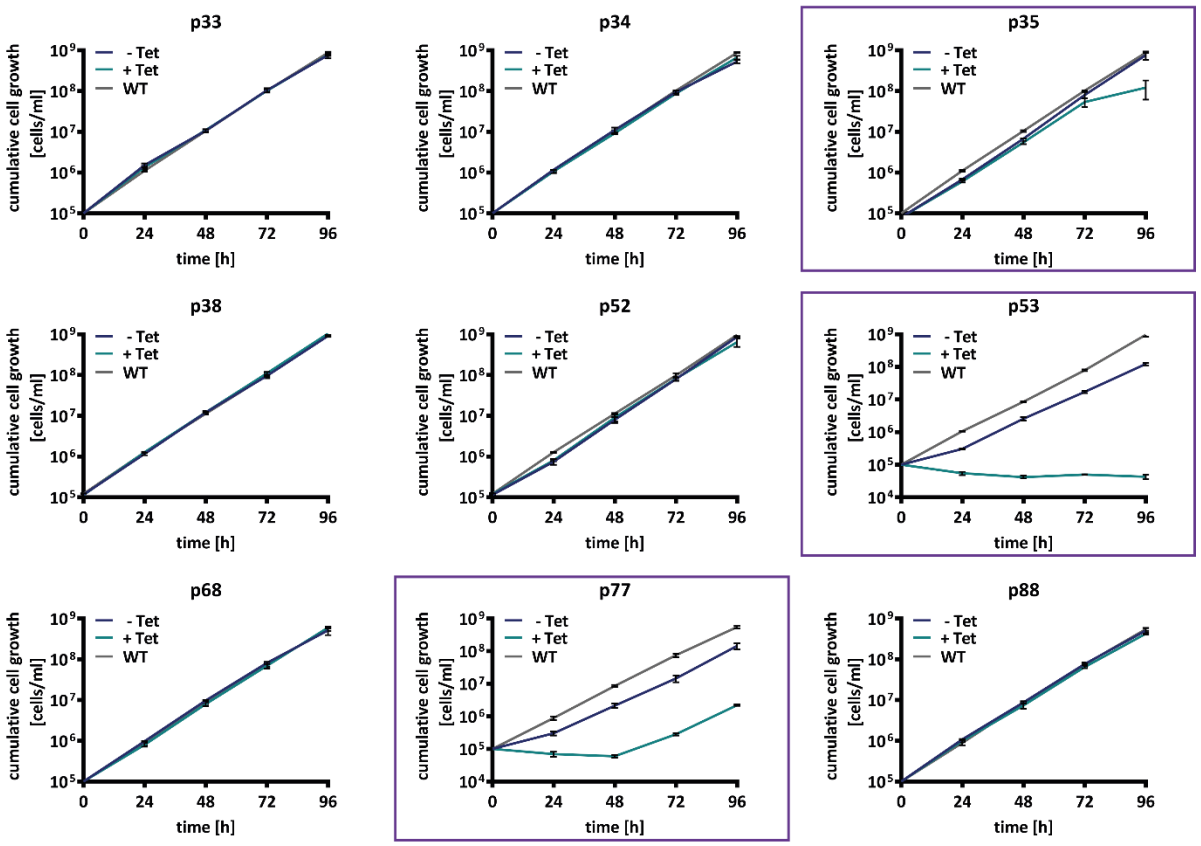

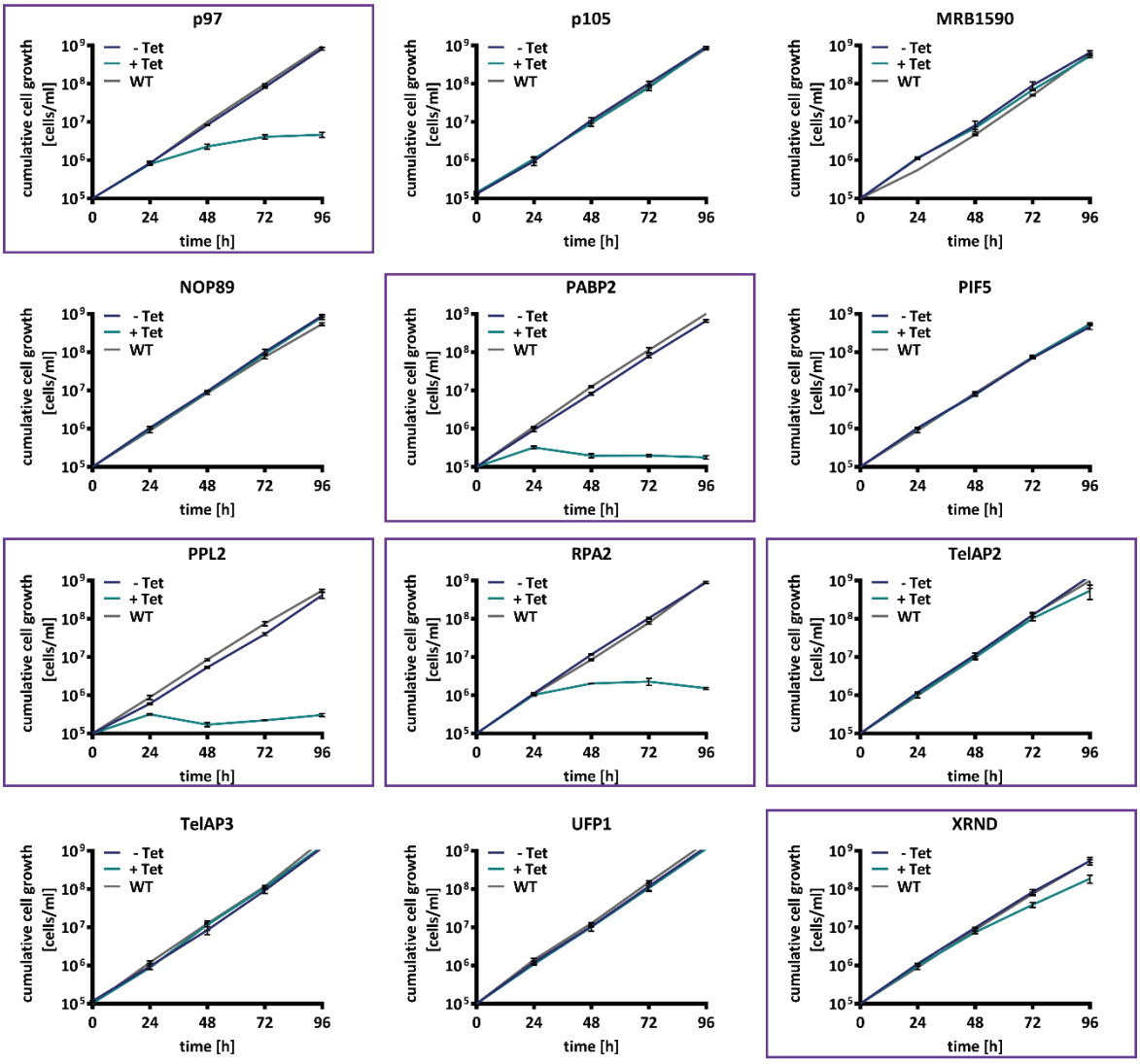

Figure 10: Depletion of potential TelAPs via RNAi in BSF. Measurement of cumulated growth of non induced RNAi cells (- Tet), cells after RNAi induction (+ Tet) using tetracycline (Tet) and wild type cells (WT) (n=3). A standard deviation bar (SD) is included. 9 out of 21 cells show a growth phenotype (marked with a purple square) (Weisert et al., 2023; in preparation).

VSG composition analysis after protein depletion

To assess the impact of protein depletion of the POI on the VSG expression pattern, VSGs were sheared off from the cell surface following RNAi induction, and soluble VSGs were analyzed by mass spectrometry (Figure 11). The analysis was conducted in quadruplicates, comparing induced cells, uninduced cells and WT cells. For cell lines, where the protein depletion did not affect cell growth, VSGs were sheard off and analyzed 72 h after RNAi induction. If the depletion of a protein resulted in a growth phenotype for the cell line, the timepoint chosen for the induced cell lines was adjusted, and in some cases multiple timepoints were measured. Only one timepoint is displayed in Figure 11. The already published data on VSG composition changes following *Tb*RAP1 and PolIE depletion were included (Leal et al., 2020). Cell lines displaying a growth phenotype after the depletion of the POI are marked with a line. Among the 21 candidate proteins examined, the depletion of three candidates had a significant

impact on the VSG expression pattern (Figure 11A). Specifically, the depletion of RPA2 and p97 resulted in a 1 % change of the VSG composition, with 99% of the analyzed VSGs remaining VSG-2 (not included in the figure). The depletion of TelAP2 resulted in a notable difference, with approximately 4% of the VSG composition changes compared to the uninduced cell line sample. This change primarily involved the upregulation of silent VSGs associated with the BES (about 2.5 %), mostly VSG-8 and VSG-15 (Figure 11B). In comparison, *Tb*RAP1 and PolIE depletion led to an upregulation of predominantly MES VSGs (Figure 11C). Only a small percentage of derepressed VSGs derives from internal loci (Figure 11D). It is noteworthy that some upregulation was observed in the uninduced cell lines before protein depletion, suggesting leaky expression without tetracycline induction. A list of all VSGs can be found in Table S2 and Table S3. In summary, these results specified the VSG composition changes after TelAP2 depletion.

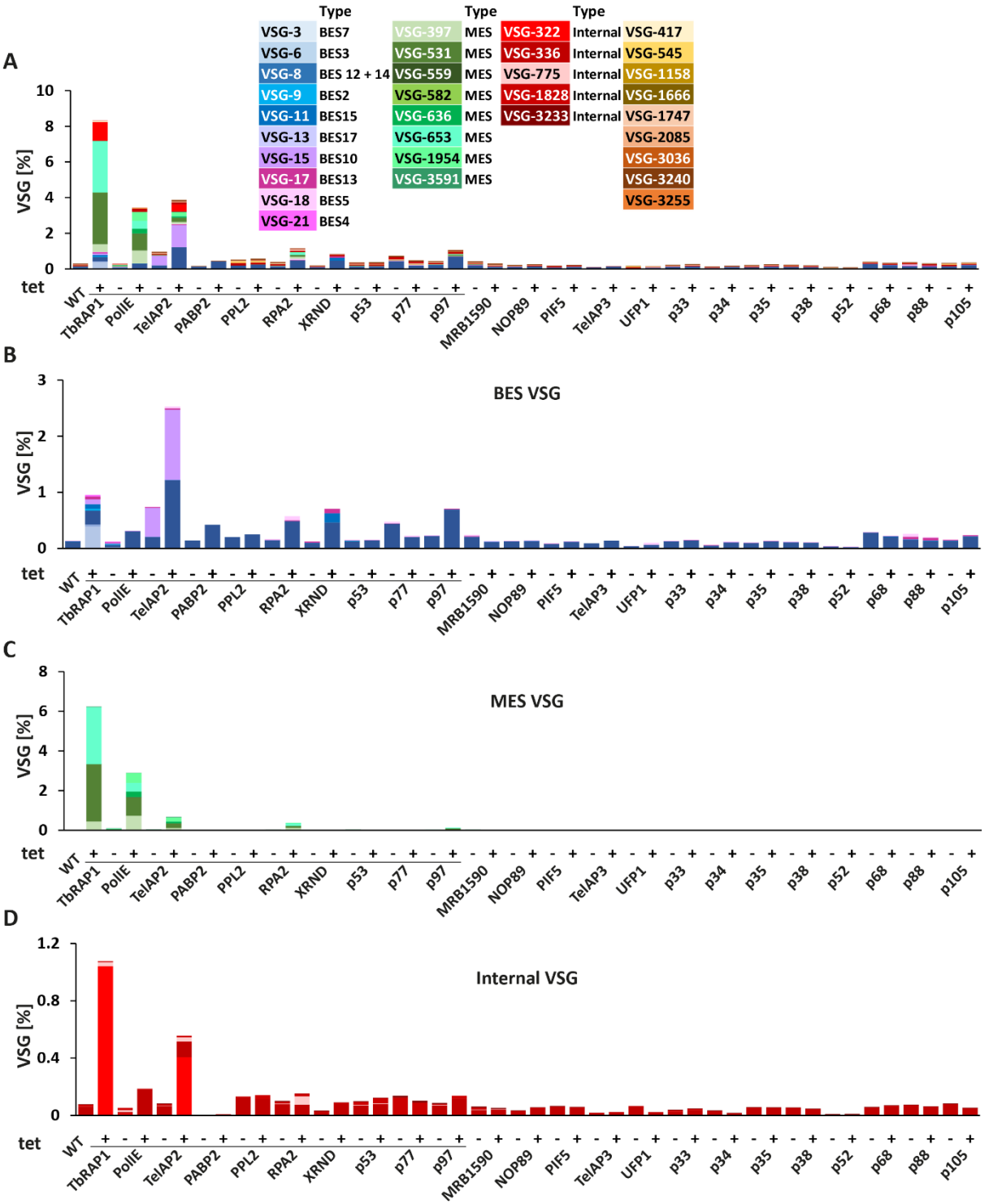

Figure 11: VSG expression pattern changes after depletion of potential TelAPs. VSG analysis of Isolates from quadruplicates of uninduced and induced RNAi cell lines of POIs by mass spectrometry analysis. Expression pattern is displayed in percentage of the LFQ intensities (Y-axis). VSG expression pattern of wildtype cells (WT) served as a control. Previously published data of depleted *Tb*RAP1 and PolIE were included for comparison. VSG-2 expression is not included and has an abundance of 92-99%. All identified VSGs are displayed in a list and are color-coded. Proteins, whose depletions led to a growth phenotype of the cell line, are marked with a black line. There is a deregulation of 4 % of VSGs after TelAP2 depletion, while other POI only showed an expression pattern change up to 1%. **(A)** whole data set. **(B)** BES associated VSGs. **(C)** MES associated VSGs. **(D)** Internal VSGs (Weisert et al., 2023; in preparation).

Whole proteomic analysis of RNAi cell lines

To investigate the effects of POI depletion on a global scale, we performed quantitative proteomics comparing induced and uninduced knockdown strains. This approach allows us to not only assess the impact on telomere-related functions but also unveil any non-telomeric roles played by the POI. The whole proteomic analysis was conducted in quadruplicates for both induced and uninduced RNAi cell lines for 19 candidates (excluding UPF1, p53 and p77 but including PolIE). In cases where protein depletion did not result in a growth phenotype, we selected a 72-hour timepoint after tetracycline induction. However, if protein depletion led to a growth phenotype, we adjusted the timepoint for induced cell lines, and in some instances, multiple timepoints were analyzed. This method also allowed us to determine if RNAi induced depletion of the POI was sufficient to show a significant downregulation of the protein via proteomics.

The summarized findings of the whole proteomic analysis with remarks to the influence of the depletion of the POI to the telomere complex proteins and the potential TelAPs are presented in Table 14.The table includes information on the depleted proteins, the timepoint of RNAi induction using tetracycline, the number of proteins that showed reduced or enriched levels, and additional relevant remarks.The table is further categorized into all proteins, proteins with nuclear localization (nucleus, nuclear lumen, nucleoplasm, nucleolus), proteins specifically located in the nucleus, and proteins within the nucleus who are uniquely reduced or enriched after the depletion of the POI. There was a significant downregulation of PABP2, MRB1590, PIF5, RPA2, XRND, PolIE and TelAP3 after the respective protein depletion. For the other proteins, no significant reduction could be measured. Moreover, the previously observed changes in VSG expression, with several VSGs being upregulated after TelAP2, PolIE, RPA2, and p97 protein depletion, were consistently observed in this analysis.

Of particular interest is the observation that TelAP2 depletion led to a reduction in TbTRF levels 120 hours after RNAi induction. Following TelAP3 depletion, a similar reduction in TbTRF was noted, while PolIE depletion surprisingly resulted in an enrichment of TbTRF. These were the only proteins for which their depletion had a discernible impact on the three telomere complex proteins. Additionally, the depletion of TelAP2, PolIE, XRND, PABP2, p68, p52, p38, and p35 appeared to influence the presence of other potential TelAPs.

Table 14. Summarized numbers of the whole proteomic analysis.

depleted protein	**time-point**	**reduced**				**enriched**				**remarks**
		all	nuclear	nucleus	unique	all	nuclear	nucleus	unique	
TelAP2	**48h**	6	3	2	1	7	1	/	/	TelAP3 reduced
	72h	53	23	11	8	32	8	3	3	TelAP3 reduced
	120h	39	22	15	3	18	5	2	2	*Tb*TRF reduced

depleted protein	time-point	reduced				enriched				remarks
TelAP3		23	15	12	5	16	6	2	1	*Tb*TRF, TelAP3 reduced
PolIE	**48h**	22	8	7	3	211	76	40	22	*Tb*TRF enriched PolIE reduced
	72h	46	20	13	6	419	135	70	24	*Tb*TRF, XRND enriched PolIE reduced
PPL2	**6h**	18	8	3	1	24	14	4	/	
	24h	42	25	19	6	126	51	32	10	
	48h	24	16	11	3	9	4	2	1	
XRND		34	17	11	4	60	18	13	2	XRND, p97 reduced
RPA2	**48h**	41	18	8	3	41	13	8	2	RPA2 reduced
	72h	136	76	38	10	111	31	8	3	RPA2 reduced
PIF5		37	16	7	/	10	3	1	/	PIF5 reduced
NOP89		32	14	7	2	53	18	13	10	
MRB1590		35	16	10	/	13	4	2	/	MRB1590 reduced
PABP2		25	9	6	2	94	43	23	10	TelAP1 enriched PABP2 reduced
p105		21	13	9	2	39	15	7	1	
p97	**48h**	151	82	40	11	35	14	6	4	
	72h	101	53	10	/	88	28	14	4	
p88		77	31	20	3	11	3	0	/	

depleted protein	time-point	reduced				enriched				remarks
p68		31	18	7	/	10	5	3	/	TelAP2, p53 reduced
p52		65	29	14	3	24	7	2	1	TelAP2 reduced
p38		111	60	35	10	39	14	6	2	PolIE enriched
p35		35	12	3	1	47	17	6	1	PolIE reduced
p34		12	7	6	/	58	20	10	5	
p33		13	5	2	2	67	30	18	3	

Candidates located in the nucleus according to TriTrypDB GO component analysis and unique candidates located in the nucleus are highlighted in blue.

This comprehensive proteomic analysis provides valuable insights into the broader implications of POI depletion beyond their telomeric roles and opens new avenues for understanding the complex network of interactions in *Trypanosoma brucei*. These findings, including the VSG composition change analysis and the previous data on potential interactions of the proteins with TelAP1 and *Tb*TRF from Reis et al., 2018 led to the selection of the proteins TelAP2, TelAP3, PPL2 and PolIE for further investigation.

Interaction of telomere-associated proteins in *T. brucei*

Reciprocal affinity purification of four telomere-associated proteins

To identify further telomere-associated proteins in *T. brucei*, four proteins were chosen to be purified with their interacting partners: Tb927.6.4330 (TelAP2); Tb927.9.3930/4000 (TelAP3); Tb927.10.2520 (PPL2) and Tb927.11.5550 (PolIE). TelAP2, TelAP3 and PolIE have previously been significantly co-purified with *Tb*TRF-Ty1 and TelAP1 via co-IP and were enriched at the telomeric repeat oligonucleotides, PPL2 has been co-purified with TelAP1 in BSF (Reis et al., 2018). All of them have a high NES of over 5 (6.07 for TelAP2, 6.58 for TelAP3, 5.74 for PolIE and 5.54 for PPL2). The GO component analysis shows a localization of all four proteins to the nucleus and the nucleoplasm. TelAP2 has been shown to be associated with the telomeric repeat region, colocalizes with *Tb*TRF and its depletion causes VSG derepression (Glover et al., 2016). The depletion of the putative translesion polymerase PolIE also causes VSG composition changes and the expression of previously silent VSGs (Leal et al., 2020). PPL2 is a *Trypanosomal* PrimPol-like translesion polymerase and plays a role in tolerance of DNA damage occurring post replicational (Rudd et al., 2013). If depleted, cells are not vital and arrest in G_2 phase of the cell cycle during replication. Even though protein depletion leads to a loss of cell viability, no VSG expression pattern changes occur. PPL2 is therefore an interesting candidate in comparison to the other translesion polymerase PolIE (Figure 11). TelAP3 is an unknown protein which only occurs in *T. b. gambiense, T. b. brucei, T. evansi* and *T. equiperdum* (Poláková et al., 2021).

Purifications were performed by using the 'tandem affinity purification' (TAP) technique. This method is based on the addition of a PTP tag to the target protein and is proven to be highly efficient to purify low-abundant proteins (Schimanski et al., 2005b).

The tag consists of the human protein C epitope, a ˈtobacco etch virusˈ (TEV) protease cleavage site and protein A epitope from *Staphylococcus aureus*. Protein A and protein C bind IgG and can therefore be used for protein purification using IgG beads. If it is required to purify the protein under native conditions, the cleavage site can be used to cut the protein of interest and its interacting proteins from the beads, which was not required here. To simplify the fusion of the PTP tag to both alleles, a Cas9 expressing cell line in BSF, and PCF cells was established (BSF Cas9, 427 Cas9). These cell lines constitutively express Cas9, a Tet repressor and the T7 RNA polymerase from the tubulin locus. To verify correct integration of the plasmid, diagnostic integration PCR was performed (Figure 12A). To confirm the protein expression of Cas9, whole cell lysates were analyzed via WB using anti-Cas9 polyclonal antibody (Figure 12B). To exclude a growth impairment after constitutively expression of Cas9, growth curves of the cell lines were conducted for 72 h to 96 h (Figure 12C).

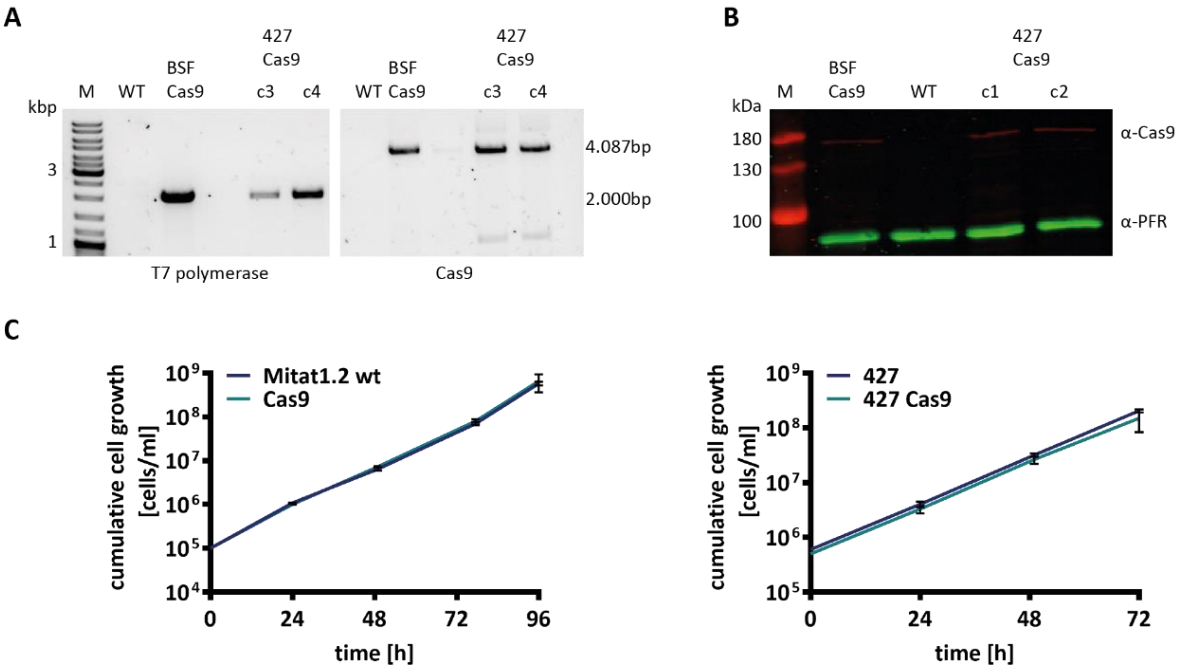

Figure 12: Generation of Cas9 expressing cell lines. (A) Integration PCR using primers binding within the T7 polymerase and Cas9 to confirm construct integration. Genomic DNA of one clone of BSF Cas9 and two clones of PCF Cas9 cells were tested. Wild type (WT) cell DNA served as control. **(B)** Western blot showing Cas9 expression in BSF and PCF cells. WT whole cell lysates served as control, PFR was used as loading control. **(C)** Growth curves in BSF and PCF cells showed no growth influence after Cas9 expression (n=3). WT cells (Mitat1.2 wt and 427) served as control. A standard deviation bar (SD) is included (Weisert et al., 2023; in preparation).

For each POI both alleles were either tagged at the 5'- or 3'-end by PCR transfection of the PTP construct together with a sgRNA template for exact integration using the CRISPR/Cas9 genome editing toolkit (Beneke et al., 2017). As a control, either protein extracts of the WT cell line or protein extracts of cells expressing ectopic PTP were used (Figure 13).

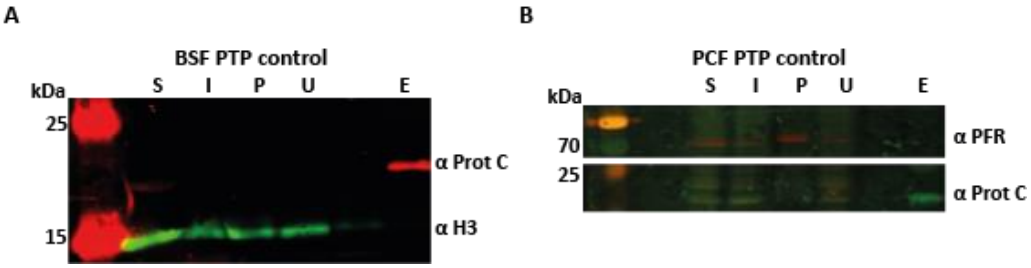

Figure 13: Ectopic PTP expression. Representative western blots of the affinity purifications of ectopic PTP in **(A)** BSF and **(B)** PCF cells. Western blots were incubated with anti-protein C and anti-PFR or anti-H3 antibodies. PFR and H3 signals served as loading control. (S) Start material; whole cell lysate, (I) input material, (P) pellet, (U) unbound material, (E) eluate. 7 (PCF) to. 8 (BSF)-times more eluate material was loaded (Weisert et al., 2023; in preparation).

To validate that the interaction of the POI is DNA-independent, a second AP was performed which combined the AP of two POIs (TelAP2 and PPL2) with DNase I treatment. The DNase I activity was previously tested in the PA-150 buffer using 1µg of plasmid DNA (data not shown). Protein extracts bound to the beads were incubated for 10 min at 37°C prior to the elution of the PTP:POI and their interaction partners .

Affinity purification of PTP tagged PPL2 in BSF and PCF cells

For the generation of PTP tagged PPL2, PTP was added to the n-terminus of the protein in BSF and PCF cells by tagging both alleles at the 5- ‘end. To confirm correct integration, PCR analysis was performed after each transfection (Figure 14A, one exemplary image for BSF cells is displayed) and a growth curve was conducted to confirm unimpaired cell growth after PTP fusion to PPL2 (Figure 14B).

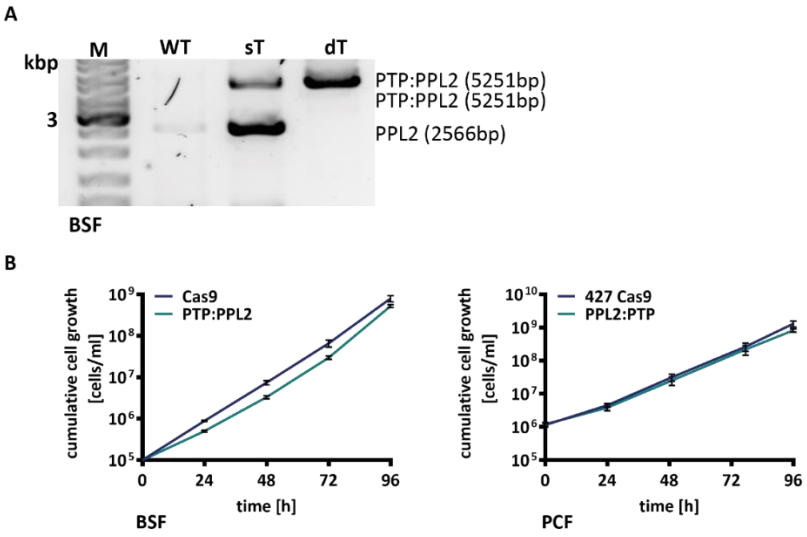

Figure 14: PTP:PPL2 expressing cell lines. (A) Integration PCR using primers binding in the 5’ and 3’UTR region of PPL2. Genomic DNA of single tagged (sT) and double tagged cells (dT) in BSF was tested. Wild type (WT) cell DNA served as control. **(B)** Growth curves of BSF and PCF tagged cells showed no growth phenotype after PTP expression (n=3). Cas9 expressing cells (Cas9 and 427 Cas9) served as control. A standard deviation bar (SD) is included (Weisert et al., 2023; in preparation).

Affinity purifications were performed in quadruplicates, using either protein extracts of cells expressing ectopic PTP (for PCF) or WT cells (for BSF) as control. During the extraction, samples for WB analysis were taken to examine successful purification (Figure 15B) and the eluted material was analyzed via MS (Figure 15A). For BSF cells, $1x10^8$ cells and for PCF cells $2x10^8$ cells were used in total. For the BSF AP, only PolIE was co-enriched with PTP:PPL2. For PCF AP, 61 proteins were enriched, including the telomere complex proteins *Tb*TRF and *Tb*TIF2 as well as the telomere-associated proteins TelAP1, TelAP2, TelAP3 and PolIE. Besides PABP2 no further proteins from Table 13 were found to be enriched. 32 co-enriched proteins have a nuclear localization (nucleus, nuclear lumen, nucleoplasm, nucleolus) based on the curated GO component analysis (TriTrypDB) and 18 of those proteins are localized in the nucleus, like PPL2. 12 proteins have a positive NES. All other proteins are most likely contaminations.

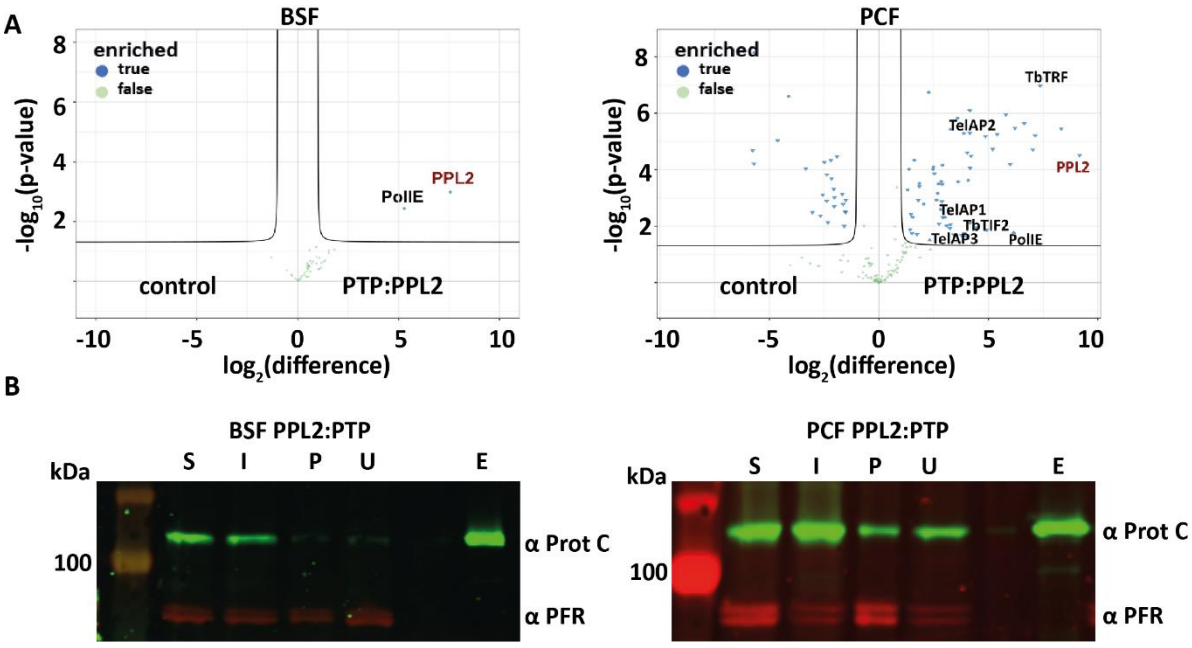

Figure 15: Interaction partners of PPL2. (A) Volcano plots generated from MS data display the co-purified interaction partners of PPL2 in BSF and PCF cells. The Y-axis represents the p-value, the X-axis shows the log_2 fold-changes of detected proteins in control samples (WT/ectopic PTP expressing cells) and PTP:PPL2 samples. Telomere complex proteins and telomere-associated proteins are displayed by name. **(B)** Representative western blots of the affinity purification of PTP:PPL2 in BSF and PCF cells. Western blots were incubated with anti-protein C and anti-PFR antibodies. PFR signal served as loading control. (S) Start material; whole cell lysate, (I) input material, (P) pellet, (U) unbound material, (E) eluate. 7 (PCF) to. 8 (BSF)-times more eluate material was loaded (Weisert et al., 2023; in preparation).

To investigate if the interaction of PPL2 with proteins identified by AP are DNA dependent, a second AP in BSF and PCF cells was performed by adding a DNase I treatment step. The AP was again performed in quadruplicates and protein extracts of untreated PTP:PPL2 cells served as control. Samples were analyzed via MS and WB (Figure 16).

Non of the previously found interactions of PPL2 were lost due to the DNase I treatment as no proteins were enriched in the control samples. This shows that the interactions of PPL2 previously observed are possibly DNA-independent.

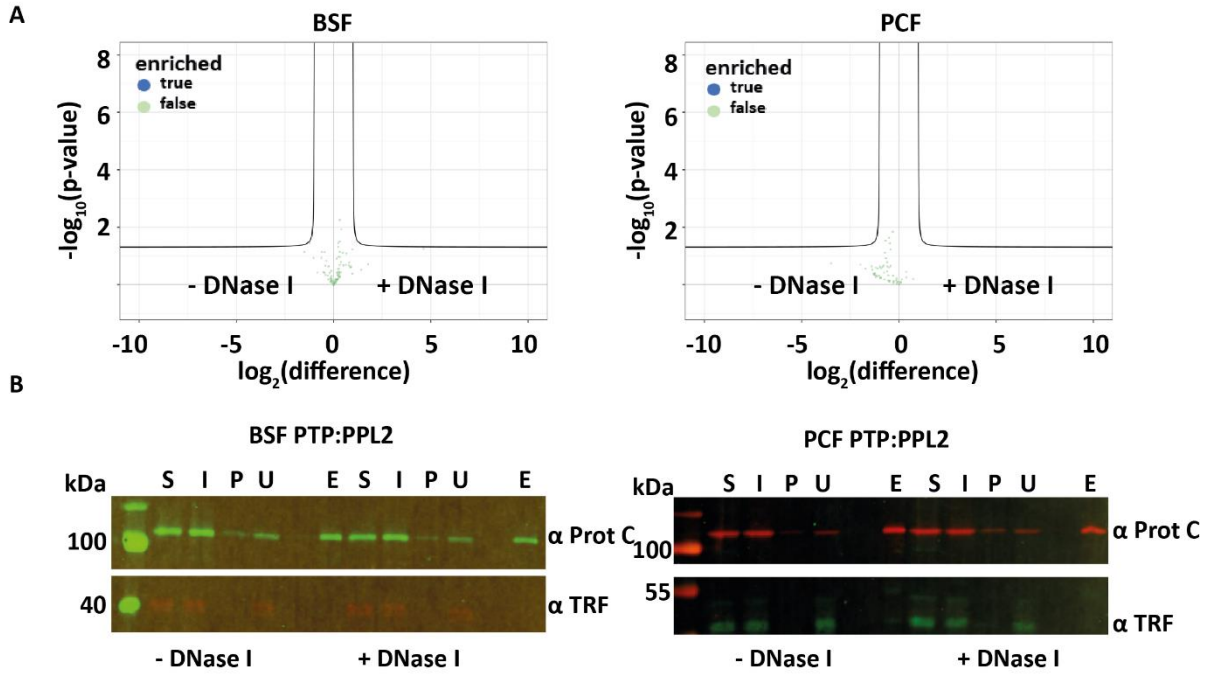

Figure 16: The interaction of PPL2 is not DNA dependent. (A) Volcano plots generated from MS data display the results of the affinity purification of PPL2 in BSF and PCF cells with and without DNase I treatment (- DNase/+ DNase). The Y-axis represents the p-value, the X-axis shows the log_2 fold-changes of detected proteins in both conditions. None of the interaction partners were lost after the DNase I treatment. (**B)** Representative western blots of the affinity purification of PTP:PPL2 with and without DNase I treatment in BSF and PCF cells. Western blots were incubated with anti-protein C and anti-TRF antibodies. (S) Start material; whole cell lysate, (I) input material, (P) pellet, (U) unbound material, (E) eluate. 7-times more eluate material was loaded.

Affinity purification of PTP tagged PolIE in PCF cells

For the generation of PTP tagged PolIE, PTP was added to the n-terminus of the protein in PCF cells by tagging both alleles at the 5- ‘end. To confirm correct integration, PCR analysis was performed after each transfection (Figure 17A) and a growth curve was conducted to confirm unimpaired cell growth after PTP fusion to PolIE (Figure 17B). Unfortunately, it was not possible to generate BSF cell lines with PTP fused to PolIE. Affinity purifications using $2x10^8$ cells per replica were performed in quadruplicates. Protein extracts of cells expressing ectopic PTP were used as control. The eluted material was analyzed via MS (Figure 17C) and samples for WB analysis were taken to examine successful purification (Figure 17D). 86 proteins were enriched, including the telomere complex proteins *Tb*TIF2-*Tb*TRF-*Tb*RAP1 as well as the telomere-associated proteins TelAP1, TelAP2, TelAP3 and PPL2. 55 of the proteins are identical with the co-enriched proteins of PTP:PPL2, including PABP2. 23 of those proteins are localized in the nucleus (TriTrypDB curated GO component analysis) and 14 proteins have a positive NES.

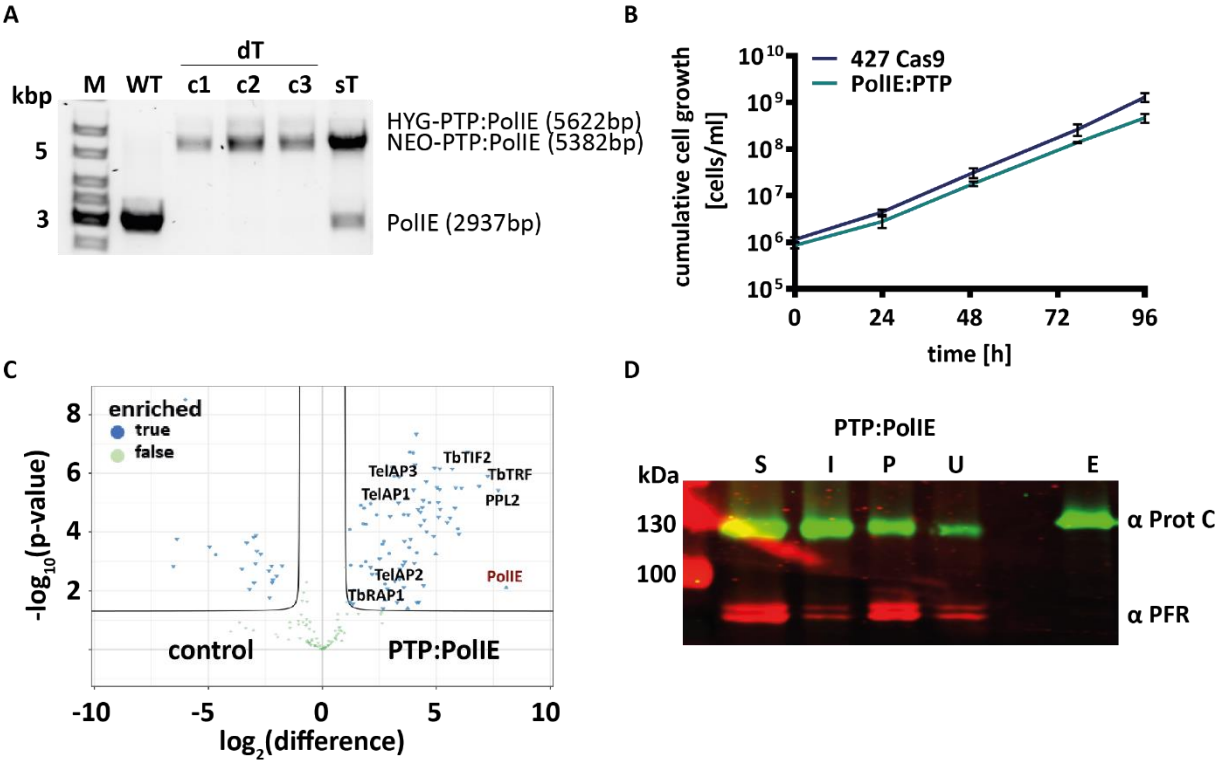

Figure 17: Interaction partners of PolIE. (A) Integration PCR using primers binding in the 5' and 3'UTR region of PolIE. Genomic DNA of single tagged (sT) and three clones of double tagged cells (dT) was tested. Wild type (WT) cell DNA served as control. **(B)** Growth curves of PCF tagged cells showed no growth phenotype after PTP expression (n=3). Cas9 expressing cells (427 Cas9) served as control. A standard deviation bar (SD) is included. **(C)** Volcano plot generated from MS data display the co-purified interaction partners of PolIE in PCF cells. The Y-axis represents the p-value, the X-axis shows the $\log_2$ fold-changes of detected proteins in control samples (ectopic PTP expressing cells) and PTP:PolIE samples. Telomere complex proteins and telomere-associated proteins are displayed by name. (**D)** Representative western blot of the affinity purification of PTP:PolIE in PCF cells. The western blot was incubated with anti-Protein C and anti-PFR antibodies. PFR signal served as loading control. (S) Start material; whole cell lysate, (I) input material, (P) pellet, (U) unbound material, (E) eluate. 7 times more eluate material was loaded (Weisert et al., 2023; in preparation).

Affinity purification of PTP tagged TelAP2 in BSF and PCF cells

For the generation of PTP tagged TelAP2, PTP was added to the C-terminus of the protein in BSF and PCF cells by tagging both alleles at the 3-'end. To confirm correct integration, PCR analysis was performed after each transfection (Figure 18A) and a growth curve was conducted to confirm unimpaired cell growth after PTP fusion (Figure 18B).

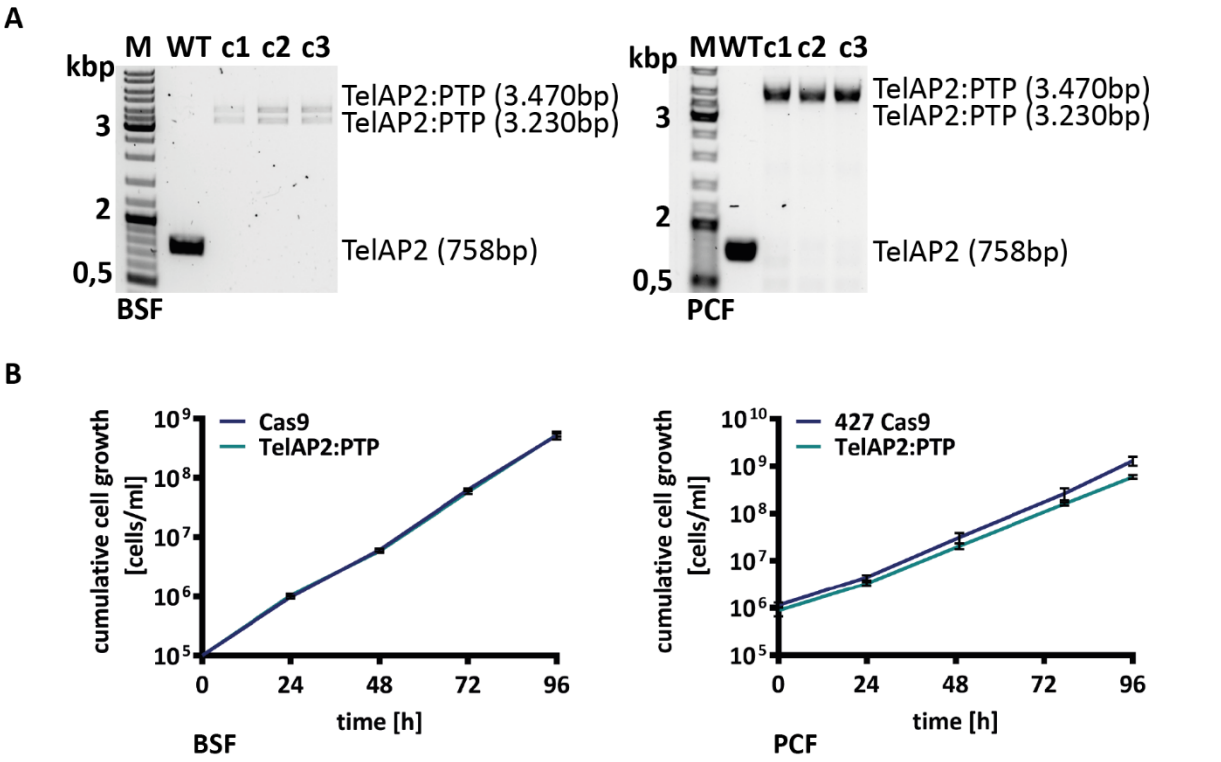

Figure 18: TelAP2:PTP expressing cell lines. (A) Integration PCR using primers binding in the 5' and 3'UTR region of TelAP2. Genomic DNA of three clones in BSF and PCF was tested. Wild type (WT) cell DNA served as control. **(B)** Growth curves of BSF and PCF tagged cells showed no growth phenotype after PTP expression (n=3). Cas9 expressing cells (Cas9 and 427 Cas9) served as control. A standard deviation bar (SD) is included (Weisert et al., 2023; in preparation).

Affinity purifications were performed in quadruplicates, using either protein extracts of cells expressing ectopic PTP (for PCF) or WT cells (for BSF) as control (Figure 19). $2x10^8$ cells in total were used for all approaches. The eluted material was analyzed via MS (Figure 19A) and samples for WB analysis were taken to examine successful purification (Figure 19B). For the BSF AP, only *Tb*TRF, *Tb*TIF2 and TelAP1 could be co-enriched with TelAP2:PTP. For PCF AP, 82 proteins were enriched, including the telomere complex proteins *Tb*TIF2-*Tb*TRF-*Tb*RAP1 as well as the telomere-associated proteins TelAP1, TelAP3, PPL2 and PolIE. 55 of the proteins are identical with the co-enriched proteins of PTP:PPL2 and 73 proteins are identical with the co-enriched proteins of PTP:PolIE. 40 proteins have a nuclear localization (TriTrypDB curated GO component analysis), 20 of those proteins are localized in the nucleus and 14 proteins have a positive NES.

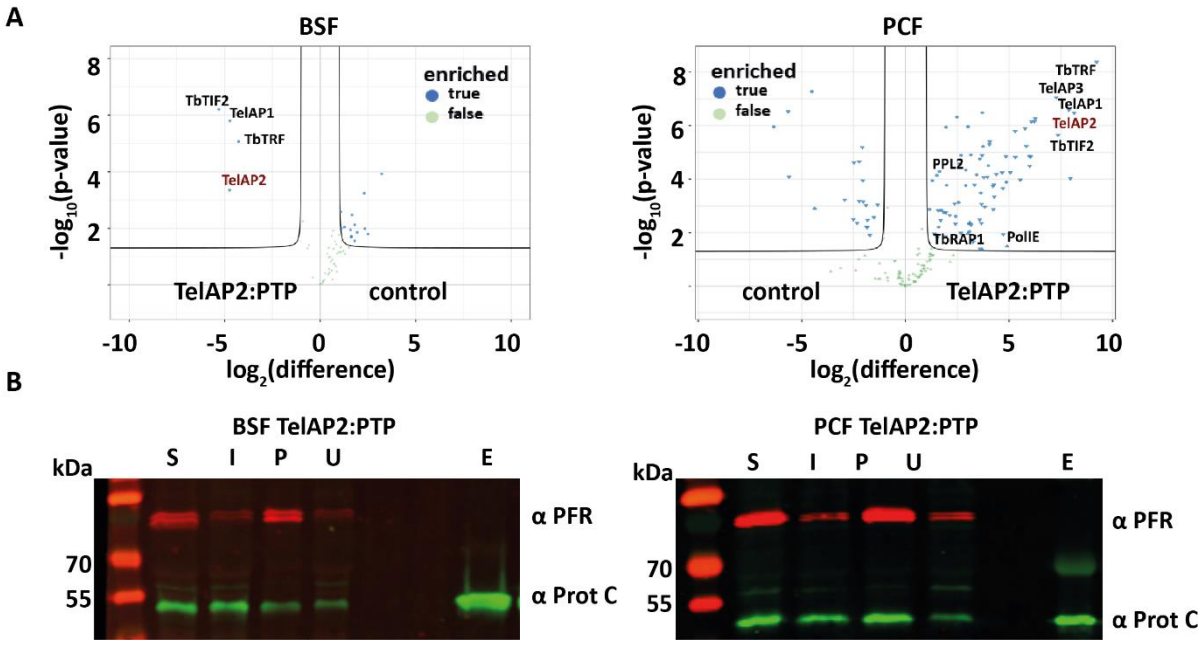

Figure 19: Interaction partners of TelAP2. (A) Volcano plots generated from MS data display the co-purified interaction partners of TelAP2 in BSF and PCF cells. The Y-axis represents the p-value, the X-axis shows the log_2 fold-changes of detected proteins in control samples (WT/ectopic PTP expressing cells) and TelAP2:PTP samples. Telomere complex proteins and telomere-associated proteins are displayed by name. (**B)** Representative western blots of the affinity purification of TelAP2:PTP in BSF and PCF cells. Western blots were incubated with anti-protein C and anti-PFR antibodies. PFR signal served as loading control. (S) Start material; whole cell lysate, (I) input material, (P) pellet, (U) unbound material, (E) eluate 7 (PCF) to. 7.5 (BSF)-times more eluate material was loaded (Weisert et al., 2023; in preparation).

To investigate if the interaction of TelAP2 with proteins identified by AP are DNA dependent, a second AP in BSF and PCF cells was performed adding a DNase I treatment step. The AP was again performed in quadruplicates and protein extracts of untreated TelAP2:PTP cells served as control. Samples were analyzed via WB using Protein C and *Tb*TRF specific antibodies (Figure 20B). MS analysis showed that none of the interactions of TelAP2 were lost in BSF after DNase I treatment but for PCF cells, the interaction of TelAP2 and TelAP1 was dissociated (Figure 20A). This could indicate that the interaction of TelAP1 and TelAP2 is DNA dependent in PCF cells, but DNA is not required for the interaction of TelAP2 with its other interaction partners.

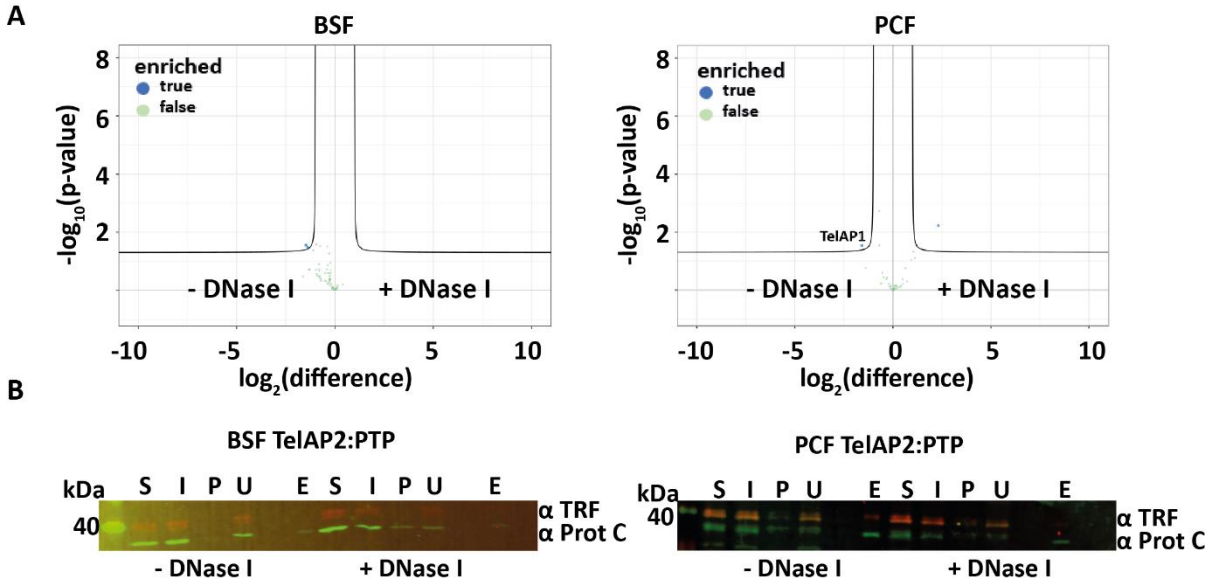

Figure 20: The interaction of TelAP2 could be DNA dependent in PCF. (A) Volcano plots generated from MS data display the results of the affinity purification of TelAP2 in BSF and PCF cells with and without DNase I treatment (- DNase/+ DNase). The Y-axis represents the p-value , the X-axis shows the log_2 fold-changes of detected proteins in both conditions. None of the interaction partners were lost after the DNase I treatment in BSF cells, in PCF cells TelAP1 could not be co-purified with TelAP2 anymore. (**B)** Representative western blots of the affinity purification of TelAP2:PTP with and without DNase I treatment in BSF and PCF cells. Western blots were incubated with anti-protein C and anti-TRF antibodies. (S) Start material; whole cell lysate, (I) input material, (P) pellet, (U) unbound material, (W) wash, (E) eluate. 7-times more eluate material was loaded (Weisert et al., 2023; in preparation).

Affinity purification of PTP tagged TelAP3 in BSF cells

For the generation of TelAP3 tagged cell lines, PTP was added to the C- or N-terminus of the protein in BSF cells by tagging both alleles generating two cell lines. The generation of the cell lines and the affinity purification was performed by V. Kreß and published in her master thesis (V. Kreß, Master thesis, 2020). It was not possible to generate PCF cell lines with PTP fused to TelAP3.

Affinity purifications were performed in quadruplicates, using protein extracts of cells expressing ectopic PTP as control (Figure 21). $2x10^8$ cells in total were used for both approaches. The eluted material was analyzed via MS and samples for WB analysis were taken to examine successful purification (V. Kreß, Master thesis, 2020).

For the AP of the N-terminal tagged TelAP3, only *Tb*TIF2 and the telomere-associated proteins TelAP2 and PolIE could be co-enriched with TelAP3 and 12 proteins in total were significantly enriched. For the AP of the C-terminal tagged TelAP3 also 12 proteins, but different ones were enriched, including the telomere complex proteins *Tb*TIF2 and *Tb*TRF as well as the telomere-associated proteins TelAP1, TelAP2, PPL2 and PolIE. This indicates, that if TelAP3 is N-terminally tagged, the interaction of TelAP3 with TelAP1, *Tb*TRF and PPL2 is impaired. A list of the enriched proteins of both APs is summarized in Table 15. Besides the TelAPs, histone H4, a short-chain dehydrogenase and ADP-ribosylation factor-like protein 3C are the only other proteins with a nuclear localization (TriTrypDB GO term analysis; nucleosome, nuclear envelope, and nuclear lumen). Other proteins can be excluded as contaminations.

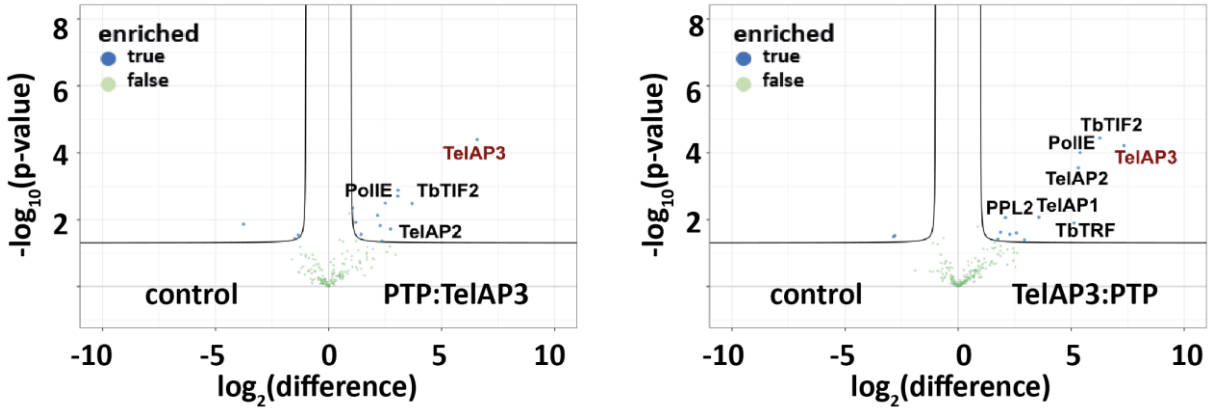

Figure 21: Interaction partners of TelAP3 in BSF. (A) Volcano plots generated from MS data display the co-purified interaction partners of TelAP3 in BSF cells. TelAP3 is either tagged n-terminal (PTP:TelAP3) or c-terminal (TelAP3:PTP). The Y-axis represents the p-value , the X-axis shows the log_2 fold-changes of detected proteins in control samples (cells expressing ectopic PTP) and PTP:TelAP3; TelAP3:PTP samples. Telomere complex proteins and telomere-associated proteins are displayed by name. (V. Kreß, Master thesis, 2020; Weisert et al., 2023; in preparation).

Table 15. Enriched proteins of PTP:TelAP3 and TelAP3:PTP in BSF cells.

TREU927 Gene ID	Name	Protein description	NES	PTP:TelAP3	TelAP3:PTP
Tb927.9.4000; Tb927.3930	**TelAP3**	**hypothetical protein, conserved**	**6.58**	**X**	**X**
Tb927.3.1560	**TIF2**	**TRF-Interacting Factor 2**	**NA**	**X**	**X**
Tb927.11.5550	**PolIE**	**DNA polymerase theta**	**5.74**	**X**	**X**
Tb927.6.4330	**TelAP2**	**telomere-associated protein**	**6.07**	**X**	**X**
Tb927.10.12850	**TRF**	**ttaggg binding factor**	**6.44**		**X**
Tb927.11.9870	**TelAP1**	**telomere-associated protein 1**	**0.96**		**X**
Tb927.5.4260		histone H4, putative	NA		X
Tb927.9.11270	TCP-1-eta	t- complex protein 1 (eta subunit), putative	NA	X	X
Tb927.5.1210		short-chain dehydrogenase, putative	NA		X

TREU927 Gene ID	Name	Protein description	NES	PTP:TelAP3	TelAP3:PTP
Tb927.10.2520	**PPL2**	**PrimPol-like protein 2**	**5.54**		**X**
Tb927.11.13050		calmodulin	NA		X
Tb11.v5.0827		NUP-1 protein, putative		X	X
Tb927.11.15140		bilobe region protein, putative	NA	X	
Tb927.6.3650	ARL3C	ADP-ribosylation factor-like protein 3C, putative	NA	X	
Tb927.10.15390	FAZ7	Flagellum attachment zone protein 7	NA	X	
Tb927.3.1010		hypothetical protein, conserved	NA	X	
Tb927.8.890	Rab1A	Ras-related protein Rab1A	NA	X	
Tb927.9.12630	glk1	glycerol kinase, glycosomal	NA	X	

Telomere complex proteins and telomere-associated proteins are bold. Proteins with a nuclear localization are highlighted blue. Nuclear enrichment score (NES) is displayed. Proteins co-purified with PTP:TelAP3, and/or TelAP3:PTP are marked with an X.

Comparison of the affinity purifications of PPL2 and PolIE with TelAP2 in PCF cells

The enriched proteins of the affinity purifications of PTP:PPL2, PTP:PolIE and TelAP2:PTP in PCF cells with a nuclear localization (also partly) are listed in Table 16.

Table 16. Enriched proteins in PCF cells.

TREU927 Gene ID	Name	Protein description	NES	PPL2	PolIE	TelAP2
Tb927.11.9870	**TelAP1**	**telomere-associated protein 1**	**0.96**	**X**	**X**	**X**
Tb927.10.3200	U2AF35	U2 splicing auxiliary factor, putative	1.45	**X**	**X**	**X**
Tb927.10.2890		enolase	1.52		**X**	**X**
Tb927.11.1900		T-complex protein 1, beta subunit, putative	1.58		**X**	
Tb927.10.13720	RBP29	RNA-binding protein 29, putative	2.56	**X**	**X**	**X**
Tb927.10.2520	**PPL2**	**PrimPol-like protein 2**	**5.54**	**X**	**X**	**X**
Tb927.11.5550	**PolIE**	**DNA polymerase theta**	**5.74**	**X**	**X**	**X**
Tb927.10.12850	***Tb*TRF**	**ttaggg binding factor**	**6.44**	**X**	**X**	**X**
Tb927.9.4000	**TelAP3**	**hypothetical protein, conserved**	**6.58**	**X**	**X**	**X**
Tb927.11.16130	NDPK	nucleoside diphosphate kinase	NA	**X**	**X**	**X**
Tb927.10.2290	J3	chaperone protein DnaJ, putative	NA	**X**	**X**	**X**
Tb927.11.880	CYPA	cyclophilin a	NA	**X**	**X**	**X**
Tb927.11.9590		S-adenosylhomocysteine hydrolase, putative	NA		**X**	**X**
Tb927.11.4700		prostaglandin f synthase	NA		**X**	**X**
Tb927.2.5160	J2	Chaperone protein DnaJ 2	NA	**X**	**X**	**X**

TREU927 Gene ID	Name	Protein description	NES	PPL2	PolIE	TelAP2
Tb927.9.4680	EIF4A1	Eukaryotic initiation factor 4A-1	NA	**X**	**X**	**X**
Tb927.3.1560	***Tb*TIF2**	**TRF-Interacting Factor 2**	NA	**X**	**X**	**X**
Tb927.9.15150	L5	60S ribosomal protein L5, putative	NA		**X**	**X**
Tb927.3.1790		pyruvate dehydrogenase E1 beta subunit, putative	NA		**X**	**X**
Tb927.11.9710	RPL10A	60S ribosomal protein L10a, putative	NA	**X**	**X**	**X**
Tb927.10.6070	UMSBP1	universal minicircle sequence binding protein 1	NA	**X**	**X**	**X**
Tb927.10.4120	RPL30	60S ribosomal protein L30	NA		**X**	
Tb927.9.5320		nucleolar RNA binding protein, putative	NA		**X**	
Tb927.10.5770	VCP	Valosin-containing protein	NA	**X**	**X**	**X**
Tb927.6.4330	**TelAP2**	**telomere-associated protein**	**NA**	**X**	**X**	**X**
Tb927.10.4570		elongation factor 2	NA		**X**	**X**
Tb927.3.1120	RTB2	GTP-binding nuclear protein rtb2, putative	NA	**X**	**X**	**X**
Tb927.8.900	TSR1	splicing factor TSR1	NA		**X**	**X**
Tb927.11.370	***Tb*RAP1**	**repressor activator protein 1**	**NA**		**X**	**X**
Tb927.11.11370	RACK1	receptor for activated C kinase 1	NA	**X**	**X**	**X**
Tb927.11.14000	NRBD1	nuclear RNA binding domain 1	NA		**X**	
Tb927.7.2070		heat shock protein DNAJ, putative	NA		**X**	**X**
Tb927.4.2040	ALBA3	DNA/RNA-binding protein Alba 3	NA		**X**	**X**
Tb927.7.1730		60S ribosomal protein L7, putative	NA		**X**	**X**
Tb927.10.3210		delta-1-pyrroline-5-carboxylate dehydrogenase, putative	NA		**X**	
Tb927.10.14550	HEL67	ATP-dependent RNA helicase HEL67	NA	**X**	**X**	**X**
Tb927.8.3750	NOP56	nucleolar protein 56	NA		**X**	
Tb927.9.11410		60S ribosomal protein L23, putative	NA		**X**	**X**
Tb927.10.5340	RPS18	40S ribosomal protein S18, putative	NA	**X**	**X**	**X**
Tb927.10.8020	POP	prolyl endopeptidase	NA		**X**	
Tb927.9.10770	PABP2	polyadenylate-binding protein 2	NA	**X**	**X**	**X**
Tb927.2.340	RHS4	retrotransposon hot spot protein 4 (RHS4), putative	NA		**X**	
Tb927.9.6070	RPS3	40S ribosomal protein S3, putative	NA		**X**	

Proteins with a nuclear localization based on TriTrypDB GO component analysis. Telomere complex proteins and TelAPs are bold. Nuclear enrichment score (NES) is displayed. Proteins co-purified with PTP:PPL2, PTP:PolIE and/or TelAP2:PTP are marked with an X (Weisert et al., 2023; in preparation).

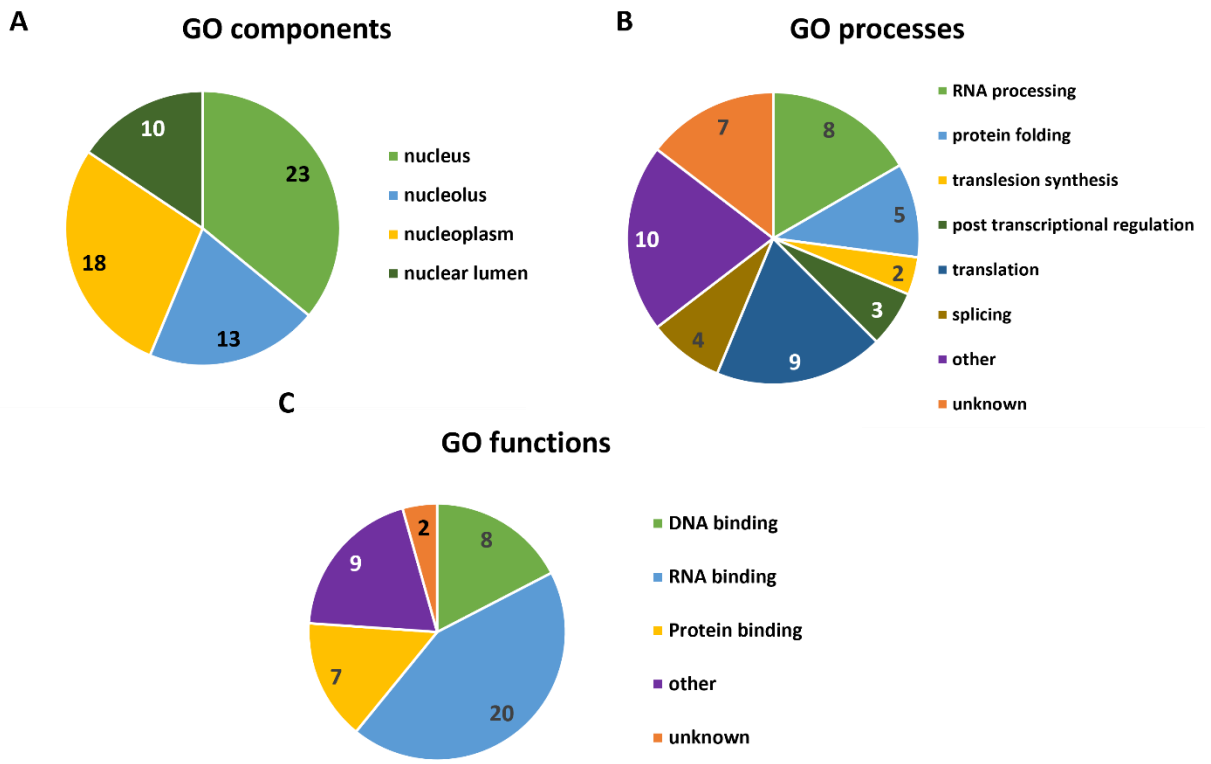

Figure 22: Pie charts of GO terms of the PCF APs. (A) Cellular components (GO components), **(B)** biological processes (GO processes) and **(C)** functions (GO functions) of the enriched proteins with a nuclear localization of **Table 16** according to TriTrypDB. Proteins can be assigned to multiple GO components, GO processes or GO function.

By comparing the affinity purifications of PPL2, PolIE and TelAP2 in PCF with each other, we saw differences regarding the enrichment of TelAPs (Figure 23). When comparing TelAP2 interaction partners to either PolIE or PPL2 interaction partners, *Tb*TRF, *Tb*TIF2, TelAP1 and TelAP3 are significantly enriched with TelAP2 while PolIE and PPL2 are significantly co-enriched with each other (Figure 23A, B). If comparing PPL2 and PolIE purification, the only difference in significant enrichment can be seen regarding *Tb*RAP1, which is co-enriched only with PolIE (Figure 23C). In conclusion, PPL2 and PolIE might be in closer proximity to each other than to the telomere complex proteins or other telomere-associated proteins.

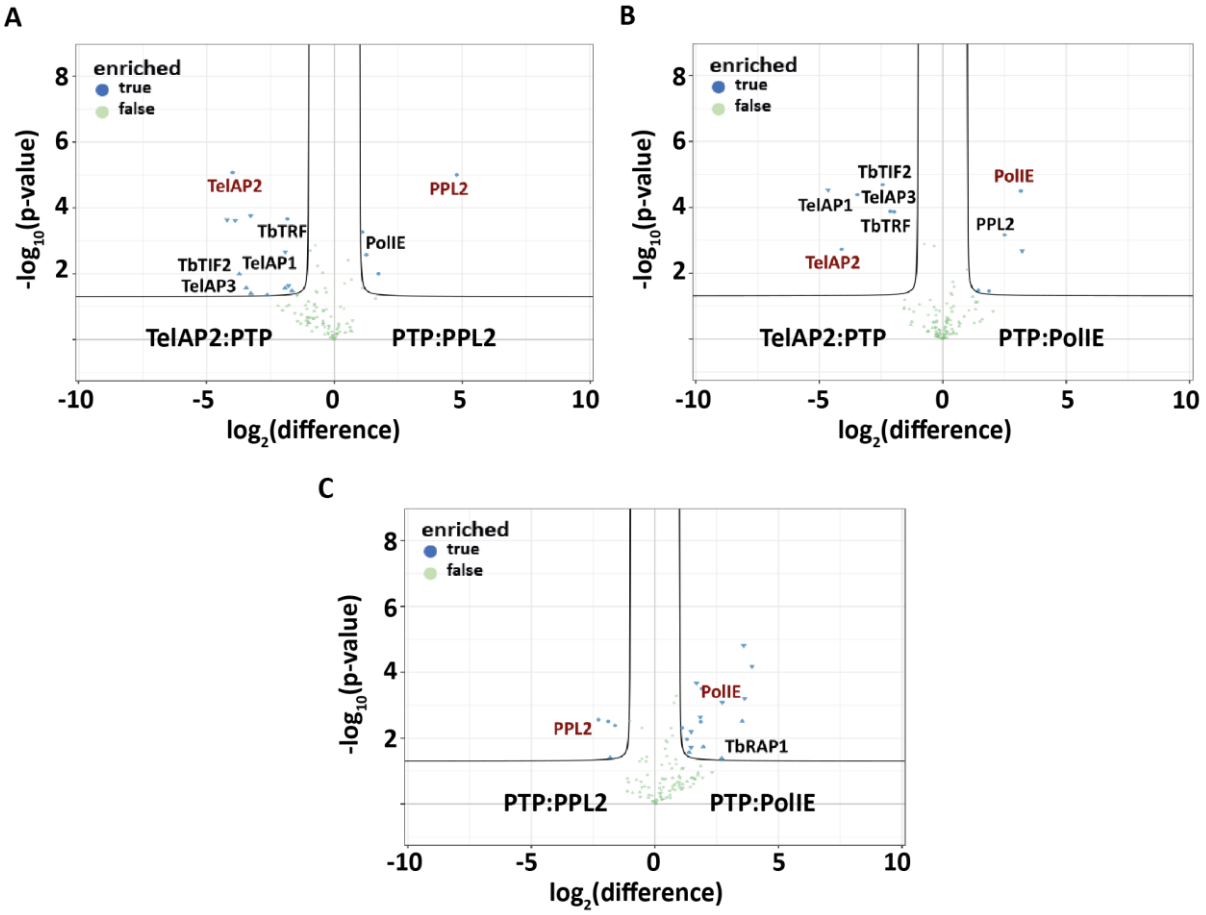

Figure 23: A difference of co-enriched proteins of TelAP2, PPL2 and PolIE. Comparison of the affinity purifications of TelAP2, PPL2 and PolIE in PCF cells. Volcano plots generated from MS data display the co-purified interaction partners in PCF cells. The Y-axis represents the p-value , the X-axis shows the log_2 fold-changes of detected proteins in both samples. Telomere complex proteins and telomere-associated proteins are displayed by name. *Tb*TRF-*Tb*TIF2-TelAP1-TelAP3 is enriched with TelAP2 while PPL2 and PolIE are significantly more enriched with each other than with TelAP2 (**A)** Comparison of TelAP2 and PPL2. **(B)** Comparison of TelAP2 and PolIE. **(C)** Comparison of PPL2 and PolIE (Weisert et al., 2023; in preparation).

The whole dataset of the affinity purifications of the telomere-associated proteins is summarized in Figure 24. Previously published co-IP results of TelAP1 and *Tb*TRF are included for comparison (Reis et al., 2018). As TelAP2 and TelAP3 seem to be in a closer connection to the telomere complex proteins *Tb*TIF2 and *Tb*TRF as well as to TelAP1, the following studies were focused on those two proteins.

	BSF	TRF	TelAP1	TelAP2	TelAP3	PPL2	PolIE	TIF2	RAP1
*	TRF:Ty1		X	X	X		X	X	
*	TelAP1	X		X	X	X	X	X	X
	TelAP2:PTP	X	X					X	
	TelAP3:PTP	X	X	X		X	X	X	
	PTP:TelAP3			X			X	X	
	PTP:PPL2						X		

	PCF	TRF	TelAP1	TelAP2	TelAP3	PPL2	PolIE	TIF2	RAP1
*	TRF:Ty1			X			X	X	
*	TelAP1			X					
	TelAP2:PTP	X	X		X	X	X	X	X
	PTP:PPL2	X	X	X	X		X	X	
	PTP:PolIE	X	X	X	X	X		X	X

Figure 24: Summarized list of co-enriched proteins. Results from (Reis et al., 2018) for *Tb*TRF-Ty1 and TelAP1 co-IP are included and marked with an asterisk (Weisert et al., 2023; in preparation).

TelAP2 and TelAP3 are components of the telomere-associated protein complex

In a previous work, the interaction of TelAP1 with TelAP2 was indicated as the strongest interaction of TelAP1, as it was the only protein that could be co-enriched in PCF using the co-IP approach (Reis, 2017). A direct interaction of TelAP1 and TelAP2 was suggested. The APs of TelAP2 in BSF and PCF cells revealed a strong connection of TelAP2 with the telomere complex proteins *TbTRF* and *Tb*TIF2 and with the telomere-associated proteins TelAP1 and TelAP3. Additionally, TelAP2 depletion influences the VSG expression. To further unravel the role of TelAP2 and TelAP3 in the telomere complex composition, changes of the interaction pattern were investigated via immunofluorescence (IF) and co-IP using the TelAP2 and TelAP3 RNAi cell lines.

Immunofluorescence of TelAP2 in wildtype and TelAP2 depleted cells

The localization of TelAP2 was previously visualized by tagging the protein C-terminal (Glover et al., 2016). In collaboration with Falk Butter, a recombinant HisMBP-TelAP2 protein was produced for further analysis, and a polyclonal antibody was raised in mice. The anti-TelAP2 antibody showed no specificity via western blot (data not shown) but only in immunofluorescence (IF) (Figure 25). The IF assays were performed in BSF and PCF cells and a previously established anti-*Tb*TRF (Reis et al., 2018) was included as a telomere complex marker. The IF confirmed the localization of TelAP2 in the nucleus as already shown at TrypTag for PCF cells, even though the signal only partially colocalize with *Tb*TRF. Successful depletion by RNAi was confirmed as no signal was measured 72 h after depletion (Figure 25C). Interestingly, the distribution of *Tb*TRF changed after TelAP2 depletion and another signal became visible near to the kinetoplast.

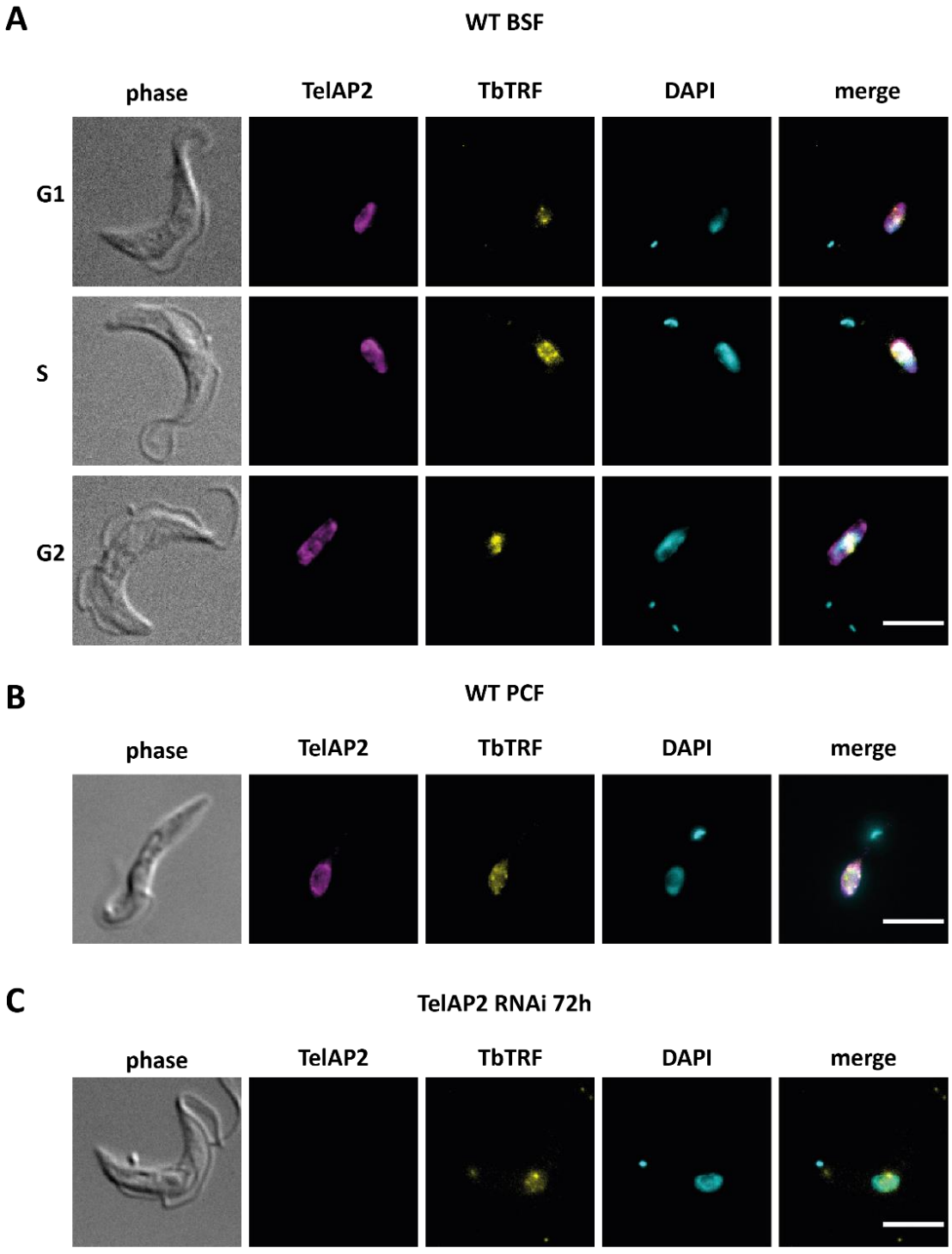

Figure 25: TelAP2 is located in the nucleus in BSF and PCF cells. Indirect immunofluorescence (IF) analysis of TelAP2 (magenta) and *Tb*TRF (yellow). DNA was stained using DAPI (cyan). **(A)** BSF cells in different cell cycle stages (G1, gap1 phase; S, synthesis phase; G2, gap2 phase) were analyzed. **(B)** An exemplary PCF cell is shown. **(C)** TelAP2 depleted cells observed 72 h after RNAi induction using tetracycline. The loss of TelAP2 signal confirmed the specificity of the antibody. Scale bars: 5 µm.

Immunofluorescence of TelAP3 using the TelAP3 antibody in wildtype cells and TelAP3 depleted cells

TelAP3 was enriched by TelAP1 and *Tb*TRF co-IPs in BSF cells as well as via affinity purification of TelAP2 in BSF and PCF cells. To investigate if TelAP3 colocalizes with the telomere complex and to analyze if TelAP3 is cell cycle-regulated, recombinant TelAP3 was generated to produce an anti-TelAP3 antibody. The complete ORF was cloned into the pET21a(+) vector including a c-terminal 6xHis tag and transformed into LOBSTR-BL21(DE3)-RIL *E. coli* cells.

After induction of the expression with IPTG, a TelAP3-His fusion protein was detected at 55-60 kDa (data not shown). The detected molecular weight is higher than the expected weight of approximately 39 kDa. The His-tag is known to alter the running behavior of tagged proteins. Furthermore, this data is in line with the size of TelAP3-PTP protein previously detected via WB by Verena Kreß in her master thesis (V. Kreß, Master thesis, 2020). Polyclonal antibodies against the recombinant His-TelAP3 protein were raised in guinea pig and rabbit. The specificity could not be validated via western blot, as the produced antibodies only recognized the recombinant protein and not the protein in BSF or PCF cell lysates (data not shown).

IF was performed in BSF, PCF and TelAP3 depleted cells using the anti-TelAP3 guinea pig antibody (Figure 26). *Tb*TRF served as a telomere complex marker, DAPI was used to stain the DNA. The IF confirmed that TelAP3 is a nuclear protein, as already proposed by TrypTag and by the nuclear enrichment score of 6.32 (Goos et al., 2017) and was present in all cell cycle stages in the BSF (Figure 26A). The distribution of TelAP3 and *Tb*TRF was identical, both in BSF and PCF cells (Figure 26A,B). When depleted via RNAi, TelAP3 was no longer present in the cell (Figure 26C). Interestingly, the distribution of *Tb*TRF changed upon TelAP3 depletion and another *Tb*TRF signal was visible near to the kinetoplast. The same effect on *Tb*TRF distribution was observed after TelAP2 depletion.

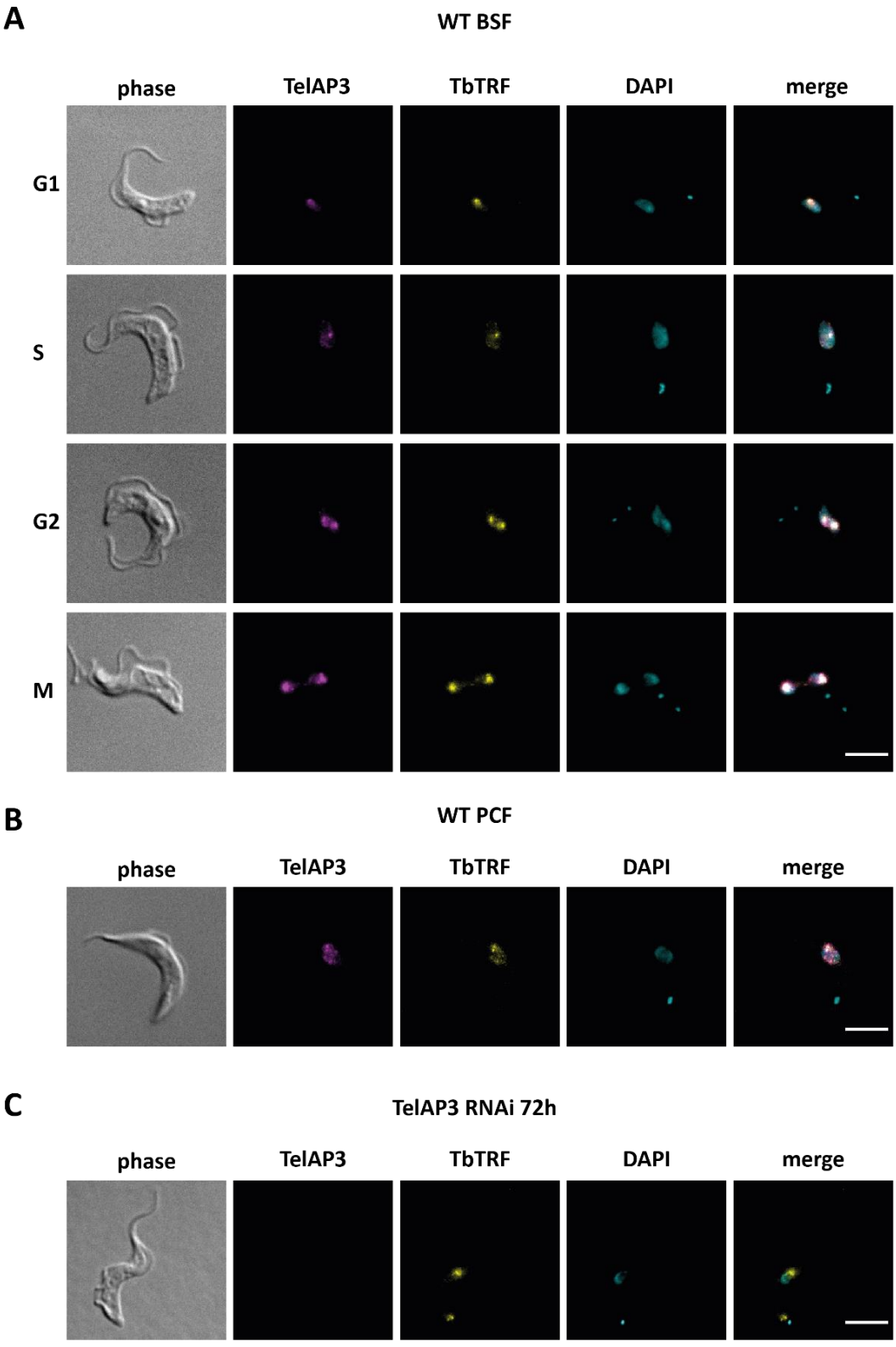

Figure 26: TelAP3 is located in the nucleus and colocalizes with *Tb*TRF. Indirect immunofluorescence (IF) analysis of TelAP3 (magenta) and *Tb*TRF (yellow). DNA was stained using DAPI (cyan). **(A)** BSF cells in different cell cycle stages (G1, gap1 phase; S, synthesis phase; G2, gap2 phase; M, mitosis) were analyzed. **(B)** An exemplary PCF cell is shown. **(C)** TelAP3 depleted cells were observed 72 h after RNAi induction using tetracycline. The loss of TelAP3 signal confirmed the specificity of the antibody. Scale bars: 5 µm.

Recombinant TelAP2 does not interact directly with telomeric DNA

As previously established, TelAP1 does not directly interact with telomeric DNA, prompting the question of whether either TelAP2 or TelAP3 could serve as a linker. To address this question, an electromobility shift assay was performed (Figure 27). Recombinant HisMBP-TelAP2, His-TelAP3 and HisMBP-*Tb*TRF (used as a positive control) were employed. Double-stranded TTAGGG oligonucleotides for telomeric DNA and GTGAGT oligonucleotides for control DNA were applied. The incubation of *Tb*TRF with the telomeric DNA resulted in a noticeable shift, confirming successful DNA binding by the recombinant protein. No shift was observed after denaturation of *Tb*TRF or after incubation of *Tb*TRF with the control DNA.

When using recombinant TelAP2, no shift was observed at all (Figure 27A). Despite varying the amount of recombinant TelAP2, the result remained consistent (data not shown). Therefore, as it has already been shown for TelAP1, the interaction of TelAP2 with the telomeres is most likely established due to protein-protein interactions. Contrary to TelAP2, even small amounts (0.5 µg) of recombinant TelAP3 bound to telomeric DNA and control DNA (Figure 27B). This could imply that TelAP3 binds unspecific to DNA. Denatured protein as well as smaller amounts of TelAP3 did not generate a shift. This could suggest that TelAP3 might be necessary for TelAP1 and/ or TelAP2 interaction with the telomeres.

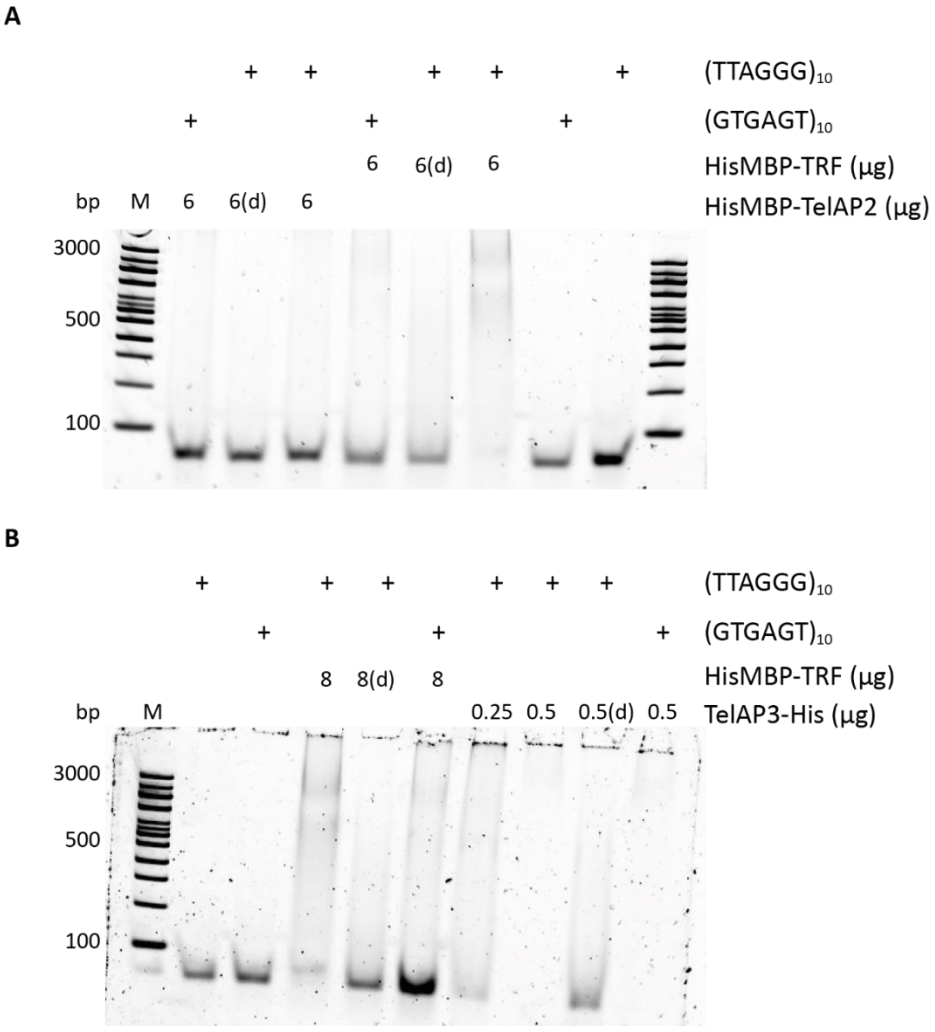

Figure 27: Recombinant HisMBP-TelAP2 does not bind to telomeric DNA. Different amounts of recombinant proteins were either incubated with $(TTAGGG)_{10}$ oligonucleotides or $(GTGAGT)_{10}$ oligonucleotides, serving as telomeric DNA or negative control DNA, respectively. Additionally denatured protein (d) was incubated with telomeric repeats. Samples were separated on a native polyacrylamide gel, stained with SybrSafe. **(A)** EMSA using HisMBP-*Tb*TRF and HisMBP-TelAP2. Only native recombinant *Tb*TRF displays a shift when incubated with $(TTAGGG)_{10}$ oligonucleotides. **(B)** TelAP3 displays a shift when incubated with either $(TTAGGG)_{10}$ oligonucleotides or $(GTGAGT)_{10}$ oligonucleotides (Weisert et al., 2023; in preparation).

TelAP2 influences the interaction of TelAP1 with the telomere complex

Mass spectrometry data of depleted TelAP2 and TelAP3 cell lines revealed a downregulation of other telomere-associated proteins (Table 14). If TelAP2 was depleted via RNAi, a significant downregulation of TelAP3 and *Tb*TRF was observed compared to uninduced whole cell lysate samples. Similarly, when TelAP3 was depleted, *Tb*TRF was also downregulated. Furthermore, affinity purifications of the proteins indicated a potentially stronger interaction among TelAP1, TelAP2, TelAP3, *Tb*TIF2 and *Tb*TRF as opposed to PPL2 and PolIE (Figure 23). Therefore, the interaction pattern changes after the depletion of TelAP2 and TelAP3 were further investigated.

To assess the impact of these changes on TelAP1's interaction pattern, a co-IP using the TelAP1 antibody was conducted. TelAP2 RNAi cell lines at 48h and TelAP3 RNAi cell lines at 72h after

RNAi induction with tetracycline were utilized. A wildtype cell line served as a negative control. Mouse anti-TelAP1 antibodies were immobilized onto protein G sepharose beads and added to cell extracts of four replicates per cell line using $2x10^8$ cells per replica. Samples were collected and analyzed via WB using either anti-TelAP1 antibodies (Figure 28A) or anti-*Tb*TRF and anti-H3 antibodies (Figure 28B). A reduced *Tb*TRF signal in the final eluate sample of the induced TelAP2 RNAi cell line was observed, leading to the suggestion, that the interaction of *Tb*TRF with TelAP1 was compromised.

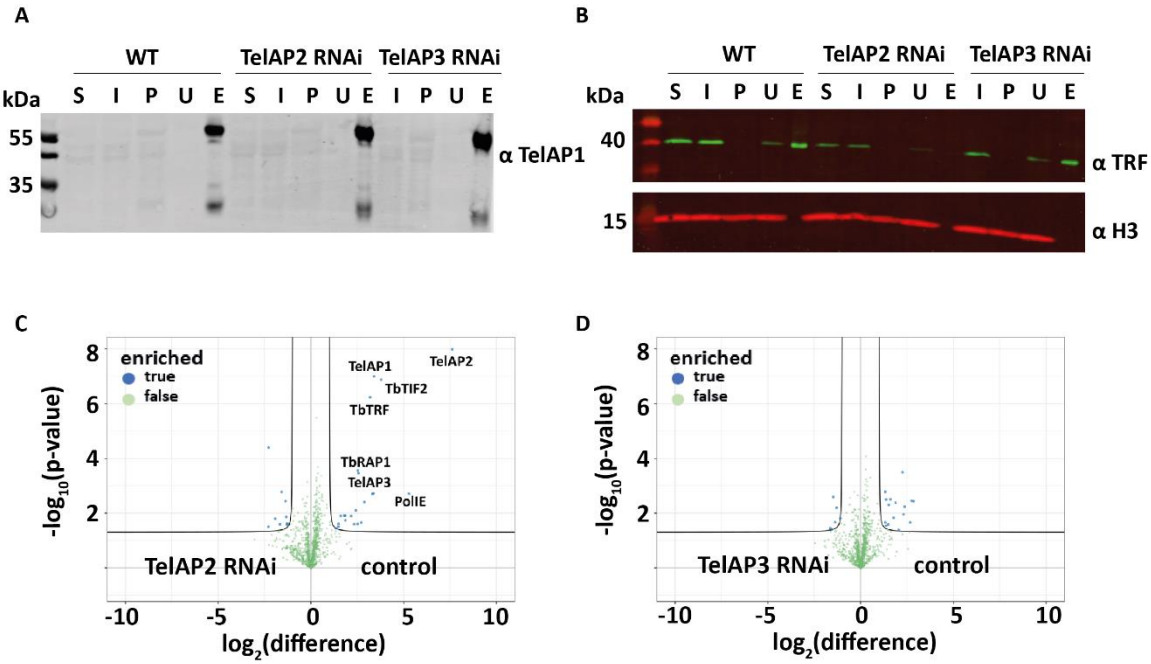

Figure 28: Co-IP of TelAP1 in TelAP2 and TelAP3 depleted cells. Co-IP was performed in wildtype (WT), TelAP2 RNAi, and TelAP3 RNAi cell lines (induced with tetracycline for 48 h/ 72 h prior to the co-IP) using the TelAP1 monoclonal mouse antibody **(A)** Representative western blot of TelAP1 co-IP incubated with anti-TelAP1 mouse antibody. **(B)** Representative western blot of TelAP1 co-IP incubated with anti-TRF and anti-H3 antibodies. The signal of TRF is not present in the TelAP2 RNAi eluate. (S) Start material; whole cell lysate, (I) input material, (P) pellet, (U) unbound material, (E) eluate. 7 times more eluate material was loaded. **(C)** Volcano plots generated from MS data display the co-purified interaction partners of TelAP1 in TelAP2 depleted cells and TelA3 depleted cells compared to the wild type cells. The Y-axis represents the p-value , the x-axis shows the log_2 fold-changes of detected proteins in control samples (wild type cells) and either TelAP2 RNAi or TelAP3 RNAi samples. Telomere complex proteins and telomere-associated proteins are displayed by name. After TelAP2 depletion, none of the previous telomere-associated interaction partners was identified. No interaction changes are detectable after TelAP3 depletion (Weisert et al., 2023; in preparation).

MS analysis of the eluted material showed no difference regarding the enrichment of telomere complex proteins or TelAPs when comparing wildtype samples to TelAP3 depleted cell line material (Figure 28C). 11 of the 16 proteins enriched with TelAP1 in the WT control cell line are ribosomal proteins. If the purified proteins of the TelAP2 depleted cell line material was compared, 22 proteins were enriched in the WT control material, including an enrichment of the previously identified candidates and TelAP1 itself (Figure 28D). Peptide counts of TelAP1 in the TelAP2 depleted cell material revealed a reduced availability of TelAP1.

Most of the other enriched proteins are again ribosomal proteins (13 proteins, 10 are identical to enriched proteins in the TelAP3 RNAi cell line). None of the proteins enriched with TelAP1 in the RNAi cell lines are located in the nucleus.

To investigate the effect of the TelAP2 depletion on the interactions of *Tb*TRF, the existing TelAP2 RNAi cell line was further modified by tagging one allele of *TbTRF* C-terminal with Ty1 and knocking out the second allele. MS data analysis showed an enrichment of TelAP1 and TelAP2 in the control cell line (Figure 29). This confirms the assumption that TelAP2 is vital for the interaction of TelAP1 with the telomere complex. *Tb*TRF was also enriched which suggests a lower abundance of the protein after the depletion of TelAP2. Due to these two datasets, the following investigations focused on the interaction of TelAP1 and TelAP2.

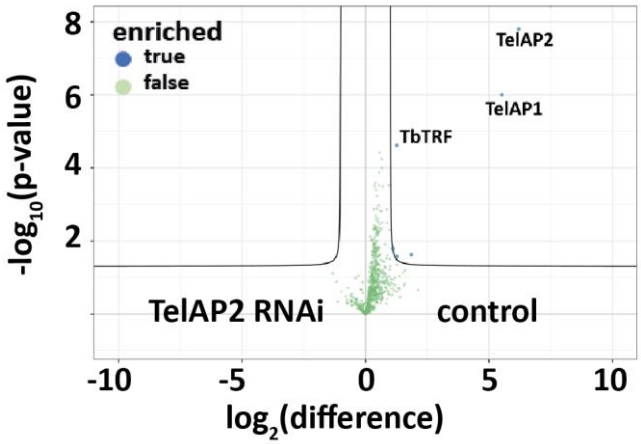

Figure 29: Co-IP of *Tb*TRF in TelAP2 depleted cells. A *Tb*TRF co-IP was performed in an induced and uninduced TelAP2 RNAi/*Tb*TRF-/Ty1 cell line (induced by tetracycline for 48 h prior to the co-IP) using the BB2 anti Ty1 monoclonal mouse antibody. Volcano plot generated from MS data displaying the co-purified interaction partners of *Tb*TRF in TelAP2 depleted cells compared to the wild type cells. The Y-axis represents the p-value , the X-axis shows the $\log_2$ fold-changes of detected proteins in control samples (wild type cells) and TelAP2 RNAi samples. Telomere complex proteins and telomere-associated proteins are displayed by name. After TelAP2 depletion, the interaction of TelAP1 and *Tb*TRF is lost (Weisert et al., 2023; in preparation).

Next, we wanted to confirm these results by immunofluorescence analysis of TelAP2 depleted cells using anti-*Tb*TRF and anti-TelAP1 antibodies. To increase the analyzed time window, IF samples were fixed 0 h, 48 h, 72 h, 96 h and 120 h after induction of the TelAP2 depletion. Anti-TelAP1 mouse and anti-*Tb*TRF rat antibodies were used (Figure 30). TelAP1 and *Tb*TRF signals at 0 h after induction showed the same localization pattern as previously published (Reis et al., 2018). After 48 h the TelAP1 signal intensity significantly decreased and was no longer concentrated in the nucleus. After 72 h, no TelAP1 signal was detectable. The *Tb*TRF signal distribution changed too, as another foci was visible near to the kinetoplast after 48 h. After 96 h even more delocalized signals were visible suggesting even a cytoplasmic localization. Interestingly, *Tb*TRF reverted to nuclear localization 120 hours after induction.

Nevertheless, the signal intensity significantly decreased compared to the 0 h timepoint.

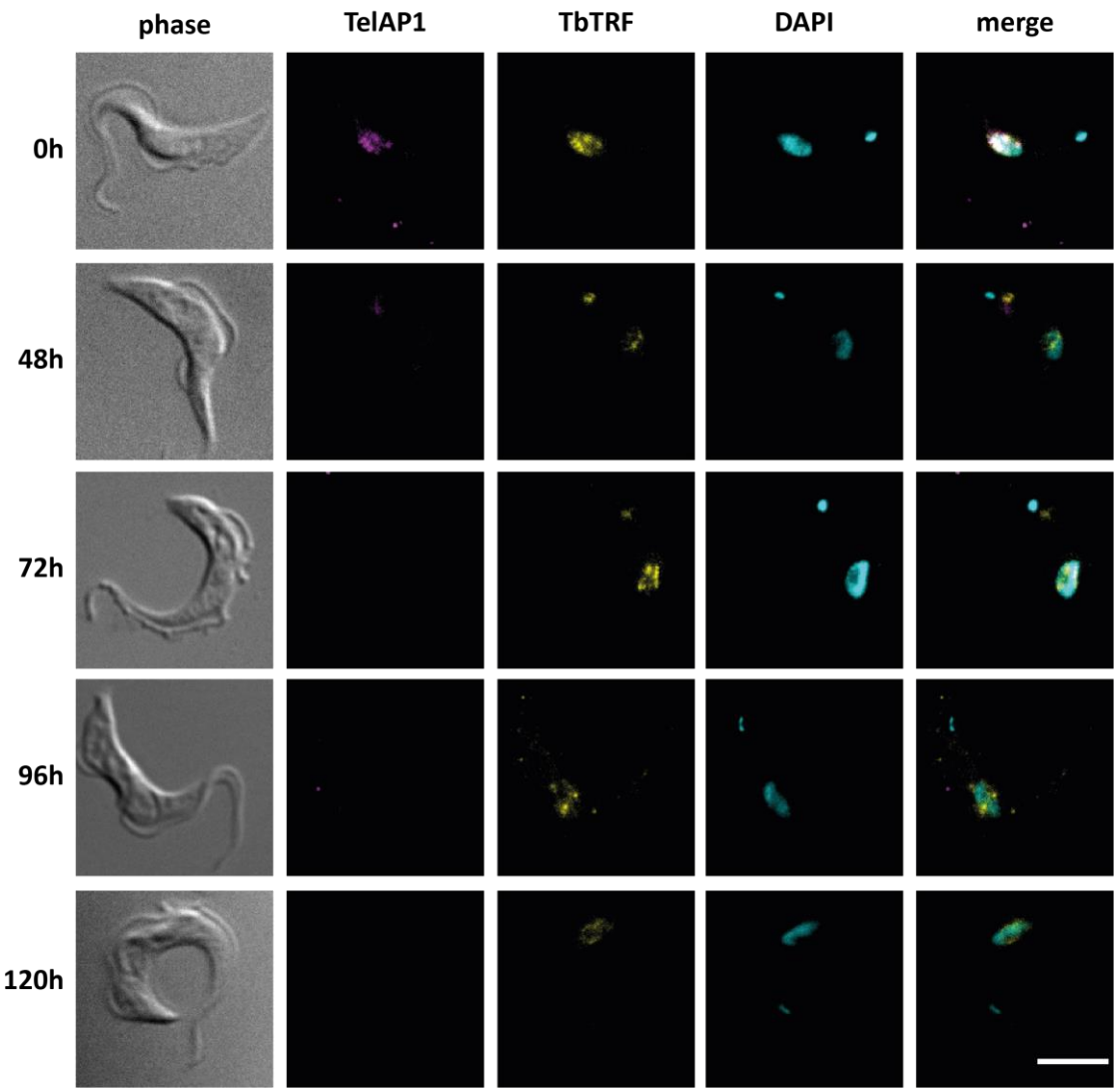

Figure 30: TelAP1 interaction with the telomere complex is TelAP2 dependent. Indirect immunofluorescence analysis of uninduced and induced (48 h, 72 h, 96 h, 120 h) TelAP2 RNAi cells. A monoclonal mouse antibody was used for TelAP1 detection (magenta) and a monoclonal rat antibody for *Tb*TRF (yellow). DNA was stained using DAPI (cyan). Scale bar: 5 µm (Weisert et al., 2023; in preparation)..

Another approach to identify protein-protein interactions is the incorporation of the Yeast-two Hybrid (Y2H) method. Therefore, the protein sequences of PPL2 and PolIE (two fragments each), full-length TelAP1, TelAP2, TelAP3 and *Tb*TRF were cloned in bait and prey vectors and used to transform yeast cells (Figure 31). The interaction of TelAP1 and TelAP2 could be validated by this approach as under high-selective growth conditions, only the combination of TelAP1 and TelAP2 proteins allowed the growth of yeast cells.

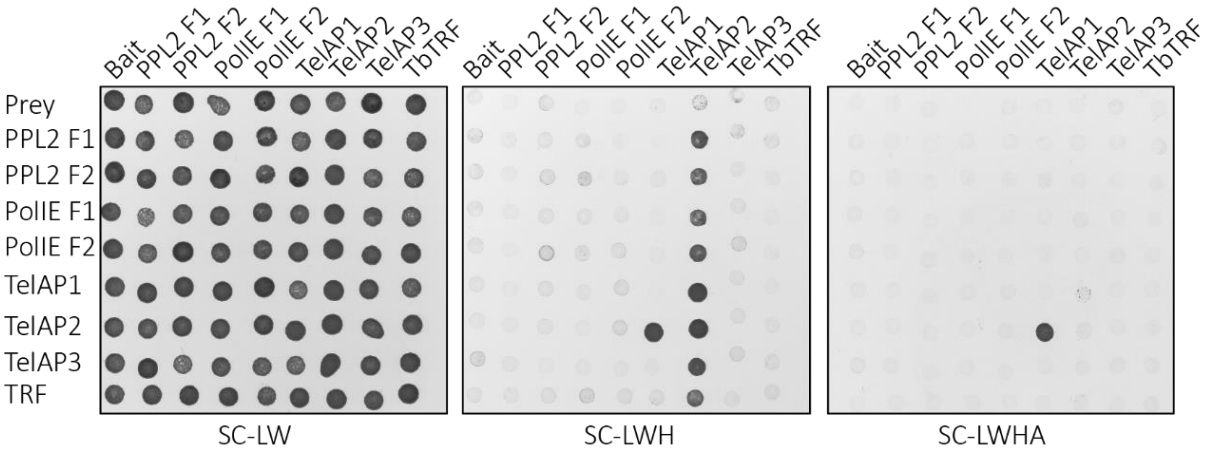

Figure 31: Yeast 2-hybrid assay of telomere-associated proteins. Gene sequences were integrated in the pGBT9 bait vector and in the pGAD424 prey vector and transformed into yeast cells. For PPL2 and PolIE, the genes were split into two fractions (F1 and F2). Yeast cells transformed with empty prey and bait vectors served as controls. SC-LW plate contains non-selective media, SC-LWH plates contain moderately selective media (-histidine) and SC-LWHA plates contain more selective media (-histidine and -adenine). Growth of yeast cells in SC-LWH and SC-LWHA medium indicates an interaction between two proteins. TelAP2 shows an interaction with TelAP1 (Weisert et al., 2023; in preparation).

Taken together, both co-IPs and IF using TelAP2 depleted cells revealed an influence of TelAP2 on the interaction of TelAP1 with the telomere complex. The Y2H assay confirmed the interaction of TelAP1 and TelAP2 seen by AP and IP. Our data concluded that the TelAP1 interaction with the telomere complex and other TelAPs is TelAP2 dependent.

DISCUSSION

Although three functional homologues of the shelterin complex have been identified and characterized, our understanding of the composition of telomeres in *T. brucei* remains incomplete and the roles of previously discovered telomere-associated proteins remains elusive. In this work, I aimed to further characterize a set of potential telomere-associated proteins in *T. brucei* by investigating the impact of protein depletion on VSG expression pattern changes. My findings reveal that only a few of the potential TelAPs have a significant impact on VSG expression. Interestingly, there is no direct correlation between an impaired growth due to the essentiality of the protein and VSG regulation. Furthermore, my investigation of the interaction pattern of four TelAPs suggest a strong association between the translesion polymerases PPL2 and PolIE. The precise nature of this connection and its function within the telomere complex requires further investigations. Additionally, the telomere-associated proteins TelAP1, TelAP2 and TelAP3 are closely connected with the telomere complex proteins TbTRF and TbTIF2. Moreover, the findings of this study provides clear evidence that TelAP2 interacts either directly or through a linker with TelAP1, playing a crucial role in the localization of TelAP1 to the telomeres and influencing its abundance.

The role of the potential TelAPs

Further characterization of the potential TelAPs

To assess whether these TelAPs are genuinely associated with telomeres, the study employed a multifaceted approach. First, subcellular localization analysis of these proteins using Tryptag.org identified a nuclear localization in 11 proteins in PCFs, while seven proteins exhibit a NES (Goos et al., 2017). This localization strongly suggests their potential involvement in nuclear processes. Furthermore, a gene ontology analysis conducted through TriTrypDB reveals that several of these proteins are linked to critical processes such as RNA processing, DNA and RNA binding, and helicase activity - all of which could be relevant for telomere maintenance. To explore the functional significance of these TelAPs, RNAi was employed to generate inducible knockdown cell lines for 21 out of the 22 candidates. The impact of protein depletion on cell growth was assessed, revealing that nine cell lines exhibiting a growth phenotype upon protein depletion (TelAP2, PPL2, PABP2, XRND, RPA2, p97, p35, p77 and p53), indicating their essential roles in cell viability. These findings align with previous data on the importance of further characterized proteins (TelAP2, PPL2, PABP2, XRND) in maintaining cell viability (Glover et al., 2016, Rudd et al., 2013, Li et al., 2006, Kramer et al., 2013). While the other 12 proteins do not display a growth phenotype, they can still be important for telomere maintenance as the deletion of TelAP1 for example also does not result in growth impairment despite its association with the telomere complex proteins. Of these 12 proteins, only MRB1590, UPF1, PIF5 and NOP89 are further characterized (Shaw et al., 2015, Delhi et al., 2011, Liu et al., 2009, Zhou et al., 2018).

TelAP2 was first identified by a screen for defects in telomere-exclusive expression, alongside VEX1 (Glover et al., 2016). Here, VEX1 displayed a substantially stronger phenotype upon depletion and was characterized as a regulator of VSG exclusion. Even though the phenotype upon TelAP2 depletion is less pronounced, it can still play a significant role in VSG silencing by

establishing an uncompromised telomere structure. TelAP3 is an unknown nuclear protein, not further described in the literature yet.

T. brucei relies heavily on post-transcriptional mechanisms to regulate gene expression (Clayton and Shapira, 2007, Figueiredo et al., 2009). ˈPolyadenylate-binding protein 2ˈ (PABP2) emerges as a crucial player in this process, helping to fine-tune gene expression at the post-transcriptional level (Kramer et al., 2013). Functioning as a homolog of the polyadenylate-binding protein (PABP) found in other eukaryotes, PABP2 is a RNA-binding protein that specifically targets the poly-A tail of mRNAs. By binding to this tail, it shields mRNAs from exonucleases, thereby enhancing mRNA stability. Additionally, PABP2 participates in mRNA translation regulation by interacting with translation initiation factors and ribosomes, facilitating efficient protein synthesis. PABP2 is also believed to play a role in responding to environmental stressors, such as changes in temperature or nutrient availability. It may assist the parasite in adapting to varying conditions by regulating mRNA stability and translation in response to stress. The exoribonuclease XRND contributes to the post-transcriptional regulation by engaging in RNA quality control, RNA processing, and post-transcriptional gene regulation (Li et al., 2006). Its exoribonuclease activity enables the degradation of RNA molecules in a 5'-3' direction, contributing to the maintenance of RNA integrity and the regulation of gene expression in the parasite. The protein p33 is a putative exonuclease, located in the cytoplasm in PCFs. Here these two proteins could be located to the telomeres to mediate the resection of the 5’end of telomeres through their exonuclease activity. The ATP-dependent RNA helicase ˈUP-Frameshift 1ˈ (UPF1) is a regulator of nonsense transcripts and therefore involved in mRNA quality control. It interacts with UPF2 and also PABP1 (Delhi et al., 2011). Human UPF1 can localize to the nucleus and interacts with the telomere protein TPP1 and with telomerase while being associated with chromatin for transcription elongation-coupled RNA surveillance, making this protein an interesting candidate in trypanosomes (Chawla et al., 2011, Hong et al., 2019).

PPL2, a PrimPol-like protein, plays an essential role in successful DNA replication (Rudd et al., 2013). RNAi-induced depletion of the protein results in an accumulation of DNA damage, leading to a cell cycle arrest in the G2 phase. Therefore, it is postulated that PPL2, like human PrimPol, contributes to the repair of post-replicative damage through its TLS activity. This process involves replacing the regular polymerase and allowing replication to continue, a mechanism critical for preserving genomic stability (Iyer et al., 2005, García-Gómez et al., 2013). RPA2 is a 28 kDa subunit of the ˈReplication Factor Aˈ (RPA) complex in trypanosomes. In eukaryotic cells, RPA is a highly conserved heterotrimeric ssDNA binding protein complex that plays a crucial role in various DNA metabolic processes, including DNA replication, repair, and recombination (Chen et al., 2013). It is composed of three subunits: RPA1, RPA2, and RPA3 (Wold, 1997) and is involved in stabilizing and protecting ssDNA regions that are generated during DNA replication (Caldwell and Spies, 2020, Dueva and Iliakis, 2020). RPA2 binds to ssDNA with high affinity, preventing it from forming secondary structures and protecting it from degradation (Bastin-Shanower and Brill, 2001). In *Trypanosoma brucei*, RPA foci form in response to induced DSBs, are detectable in all cell cycle stages and associate with silent VSG BES at the nuclear periphery (Glover et al., 2019). The foci forms during the S phase of the cell

cycle and persist. The N terminus of RPA2 seems to be required for RNA Pol I assembly (Daniels et al., 2012). In *T. cruzi* and *Leishmania amazonensis*, RPA1 binds to telomeric ssDNA, which is normally linked to the CST complex in mammalians and *Tc*RPA1 and *Tc*RPA2 form nuclear repair foci (Pavani et al., 2016, Pavani et al., 2018, Fernandes et al., 2020). Recently, an inhibitor of RPA1 in *T. brucei* was identified, impacting only the ssDNA binding activity of TbRPA1 and no other ortholog in humans, *Leishmania* or *T. cruzi*, implementing the opportunity to develop a new therapeutic treatment of African trypanosomiasis (Mukherjee et al., 2023).

The protein p97 is a putative ATP-dependent DEAD/H RNA helicase and possibly playing an important role in mRNA metabolism and ribosome biogenesis function like other DExD/H box helicase proteins (Cristodero and Clayton, 2007, Bakari-Soale et al., 2021). PIF5 is DNA repair and recombination helicase protein (Liu et al., 2009). This helicase could aid with the replication of telomeric DNA. The protein p35 is a putative Plus-3 domain/Zinc finger, C3HC4 type (RING finger) protein. This could also indicate a role in epigenetic gene regulation (Droll et al., 2013, Ceballos-Pérez et al., 2023). The protein p52 is a putative HMG-box domain containing protein, indicating a potential role in DNA-binding (Stros et al., 2007). The protein p88 is a putative DNA topoisomerase IA and could therefore be involved in relaxing supercoiled DNA by introducing breaks in ssDNA (Balaña-Fouce et al., 2014). The protein p105 is a PHD finger domain protein 4. The protein p77 could potentially be involved in polyubiquitination. For p34, p38, p53 and p68 no further information besides their localization in PCFs is available.

Why these proteins are potentially interacting with the telomeric repeat regions needs to be further unraveled, especially because not all of them are localized in the nucleus or have a positive NES. One possibility could be that some are only involved in the regulation and mediation of telomeric DNA replication.

The involvement of TelAPs in VSG expression

From the 21 investigated protein depletions, only the depletion of three candidates (TelAP2, RPA2 and p97) resulted in a significant change in the VSG expression pattern of the cell. Therefore, not every depletion of a potential TelAP that causes a growth phenotype has a significant influence on VSG regulation. For instance, the translesion polymerase PPL2 has no discernible effect on expression site regulation, even though its depletion results in a severe growth phenotype. In contrast, the putative translesion polymerase PolIE appears to play a role in VSG expression regulation. This suggests that even functionally similar proteins enriched at the telomeres can have different effects on VSG regulation, if at all.

While for RPA2 and p97 the changes were minor with only 1% of VSGs changed and 99% of the analyzed VSGs was still VSG-2, TelAP2 displayed a 4% change in VSG composition. Furthermore, the depletion of *Tb*RAP1, PolIE or TelAP2 led to distinct changes in the VSG expression pattern, indicating the involvement of different mechanisms in VSG regulation that might be disrupted. The depletion of *Tb*RAP1 and PolIE mostly result in an upregulation of MES VSG protein expression (Leal et al., 2020). MES only contain metacyclic VSG, important for the cell cycle arrested metacyclic form of trypanosomes, which is the only form capable of

infecting the mammalian host. It expresses a metacyclic VSG protein on its surface as a pre-adaption mechanism (Hajduk and Vickerman, 1981, MacGregor et al., 2012). This VSG variant is therefore not normally expressed in stumpy or slender BSFs and the MES contains no ESAGs. TelAP2 depletion leads to an upregulation of VSG8 and VSG15, both transcribed from previously silent BES. Various mechanisms of VSG switching can occur during the periodic exchange of VSGs on the parasite's surface. One such mechanism, in which an active BES is inactivated, and a previously silent BES is activated, is referred to as an *in situ* switch (Taylor and Rudenko, 2006, Vink et al., 2012). In this context, TelAP2 could potentially play a role in preventing unregulated BES switching of this kind. *In situ* switches are epigenetically regulated and do not result in changes of the DNA sequence through recombination like gene conversion or telomere exchange. Here, the previously active BES is silenced, and a silent BES is transcriptionally activated. This suggests an involvement of TelAP2 in the maintenance of monoallelic VSG expression by inhibiting the expression of silent BES. There could also be an *in vitro* preference for certain VSGs, related to chromatin environment. One has to keep in mind though, that *in situ* switches can also occur between an active BES and a MES, therefore these findings do not exclude a similar mechanism for *Tb*RAP1 and PolIE.

TelAPs can influence the abundance of each other

To gain a global perspective on the impact of TelAP depletion, the study conducts quantitative proteomic analyzes comparing induced and uninduced knockdown strains for 19 candidates. The depletion of some TelAPs (TelAP2, PolIE, XRND, PABP2, p68, p52, p38 and p35) influences the occurrence of other potential TelAPs, indicating the possibility of complex interactions within the telomere complex. The depletion of XRND therefore results in a reduced amount of the putative ATP-dependent DEAD/H RNA helicase p97. The depletion of the unknown protein p38 enriches PolIE while the putative Plus-3 domain/Zinc finger, C3HC4 type (RING finger) protein p35 depletion reduces the PolIE amount. If the proteins p68 and the putative HMG-box domain containing protein p52 are depleted, the amount of TelAP2 is reduced. PABP2 reduction results in enriched TelAP1 amounts. How these proteins influence each other has still to be investigated. An interesting approach would be to tag these TelAPs in the knockdown strains to further investigate if the changes of the amount of protein is visible via IF.

Interestingly, the depletion of TelAP2 and TelAP3 result in a reduced amount of *Tb*TRF. The only orthologues of TelAP3 are present in *Trypanosoma brucei gambiense*, *Trypanosoma brucei brucei, Trypanosoma evansi* and *Trypanosoma equiperdum*. No other homologues are known in other species indicating that TelAP3 is highly conserved among trypanosomes. Previous works assumed that TelAP3 is the previously characterized protein ST-1 (Reis et al., 2018), V. Kreß, Master thesis 2020). ST-1, a protein with a molecular mass of 39kDa, which is the proposed mass of TelAP3, displays a binding affinity to the C-rich strand of the subtelomeric repeat region (Eid and Sollner-Webb, 1995). As no further information other than the localization of TelAP3 and its potential unspecific binding capacity to DNA is accessible, this assumption can neither be confirmed nor denied. Notably, TelAP3 is not essential for cell viability in BSF parasites and also displays no influence on VSG expression regulation. Only proteomic MS analysis displayed an influence on *Tb*TRF upon depletion, as the amount of the telomere complex protein was reduced. Though, this reduction could not be confirmed via IF. What could be seen was the occurrence of other *Tb*TRF foci near the

kinetoplast, also seen after TelAP2 depletion. The only other protein which stabilizes protein levels of *Tb*TRF is *Tb*TIF2 (Jehi et al., 2016). Here, *Tb*TIF2 protects *Tb*TRF from degradation and is essential for maintaining normal *Tb*TRF protein levels. Both proteins suppress VSG switching but contrary to TelAP2 and TelAP3 depletion, which result in a mild growth phenotype (TelAP2) and no growth phenotype (TelAP3), *Tb*TIF2 depletion results in a severe cell growth arrest and an increased amount of subtelomeric DSBs. As the depletion of *Tb*TRF similarly results in a severe growth arrest, one would assume similar results when depleting TelAP2 or TelAP3 if these proteins are really essential to stabilize the protein amount of *Tb*TRF. Here, further investigations have to unravel the possible influence and interaction of TelAP2 and TelAP3 with *Tb*TRF.

In summary, this research contributes valuable insights into the roles of TelAPs for the telomere complex of *Trypanosoma brucei* and their impact on VSG expression. The study's comprehensive approach, combining the knowledge of localization studies, functional assays, and proteomic analyses, provides a foundation for further exploration of these critical components and even potential drug targets for combating African sleeping sickness.

Reciprocal affinity purifications of TelAPs and their limitations to identify interactions

This study used reciprocal affinity purifications combined with quantitative MS analysis to discover new and to confirm estimated interacting proteins of PPL2, PolIE, TelAP2 and TelAP3 in BSF and PCF cells. Here, the core set of previously identified proteins, namely *Tb*TRF, *Tb*TIF2, *Tb*RAP1, TelAP1, TelAP2, TelAP3, PPL2 and PolIE could be enriched and confirmed their potential interactions found by Reis et al in 2018. The APs of TelAP2, PPL2 and TelAP3 in BSF cells resulted in 56 (TelAP2), 40 (PPL2) and 187/166 (TelAP3; either n- or c-terminal tagged) quantified proteins and only 3 (TelAP2), 2 (PPL2) and 11 (TelAP3) proteins were positively enriched with the POI. Notably, the APs in PCF cells led to substantially higher numbers of purified proteins. Here, the APs in PCF resulted in 178 (TelAP2), 165 (PPL2) and 189 (PolIE) quantified proteins with significantly higher numbers in positively enriched proteins: 81 (TelAP2), 60 (PPL2) and 85 (PolIE). Even though tandem affinity purifications (TAPs) have been used before and are a solid technique to identify protein complexes and protein-protein interactions in trypanosomes (Schimanski et al., 2005a, Ouna et al., 2012, Badjatia et al., 2016, Eisenhuth et al., 2021), the applied approach in this study used only the first affinity purification step of the TAP and can therefore lead to false positive results. To further exclude non-specific bindings and false positive results especially in PCF cells, a previously established control cell line expressing ectopic PTP was used (Eisenhuth et al., 2021). Still, only 24-29.5% of the enriched proteins of the PCF APs of PPL2, PolIE and TelAP2 are located in the nucleus even though all three proteins are nuclear. To further minimize the occurrence of non-specific protein enrichments, one should include the second step of the affinity purification. This could already help to minimize the amounts. On the other hand, even by applying an additional step, false positive results cannot be completely excluded and have been observed before (Ouna et al., 2012).

Another weakness of the AP approach is the chance that weak and transient interactions may be overlooked. To address this limitation, ˈproximity-dependent biotin identificationˈ (BioID), another suitable method for investigating protein-protein interactions, could be employed

(Morriswood et al., 2013). For this method, a protein of interest is tagged with a modified form of the 35-kDa bacterial biotin ligase BirA. By biotinylating all nearby proteins of the tagged bait protein in a proximity-dependent manner and employing affinity purification using streptavidin-coated beads, this method enables the purification of potential interaction proteins under native conditions. It also enables the usage of harsher lysis conditions to exclude cytoskeletal proteins and therefore aims the possibility to additionally exclude unspecific bindings and false positive results.

BioID, AP using a PTP tag, as well as co-IPs using a tag as done for *Tb*TRF, have the disadvantage, that the protein is not in its native stage but rather is an artificial fusion protein. This can result in a loss of interaction partners, who could possibly not interact with the side of the tag (Baudouin et al., 2020). Immunoprecipitations using specific antibodies done for TelAP1 have the advantage to target the native protein and not a tagged, modified version. Here the disadvantage is the loss of interaction partners due to the impersistence of itracomplex interactions during washing steps (Morriswood et al., 2013). As all methods to identify interaction partners of a protein of interest have its advantages and disadvantages, the best step would be to incorporate all three methods for further interaction studies and compare the results.

While the APs performed in this study aimed to identify interaction partners of the proteins of interest in both BSF and PCF life cycle stages, it was not possible to tag PolIE in BSF cells and TelAP3 in PCF cells. Therefore, for these two proteins other approaches either using another tag or antibodies for immunoprecipitation would be ideal.

Additionally, these findings do not support nor contradict the prior assumption that the telomere complex composition is stage-specifically regulated or that multiple telomere protein complexes coexist simultaneously, as described in mammals (Reis et al., 2018, Bhanot and Smith, 2012, Grill et al., 2019). Future work should also analyze interactions during the transition of the BSF to the PCF life cycle stage to identify possible stage specific interactions. Another limitation of the AP of this study is the usage of monomorphic trypanosomes as they are adapted to culture. If further differentiation experiments for stage specific interaction studies would be applied, one should use pleomorphic trypanosomes, as they can differentiate in the fly, leading to a more near to *in vivo* study of interactions.

While no new candidates were identified using this approach, this data further supports the existence of a core set of telomeric proteins in both PCF and BSF cells.

The interaction of TelAPs

The translesion polymerases PPL2 and PolIE

Two of the main proteins identified in the APs and previous IPs and the telomeric repeat pulldown are the translesion polymerases PPL2 and PolIE. Translesion polymerases are necessary for the replication of damaged DNA as they can bypass the damage. They lack the 3-5'exonuclease activity, have a low fidelity and a low processivity of DNA synthesis (Vaisman and Woodgate, 2017). The interaction pattern between PPL2 and PolIE suggests a direct interaction between these two polymerases. They exhibited a stronger purification efficiency with each other compared to TelAP1, TelAP2, TelAP3, *Tb*TIF2, and *Tb*TRF.

PolIE, previously further characterized by Leal et al. in 2020 and Rabbani et al. in 2022, consists of a polymerase and a helicase. Usually, the role of the helicases is to utilize the energy derived from nucleoside triphosphate hydrolysis to translocate along nucleic acid strands, unwind the helical structure of double-stranded nucleic acid, and, in some cases, disrupt protein-nucleic acid interactions (Abdelhaleem, 2010). It is suggested that PolIE additionally plays a role in maintaining telomere stability by binding to the telomeric repeats associated with chromatin. After depletion of PolIE, changes in telomere localization have been observed (Leal et al., 2020). Another publication indicated that PolIE suppresses telomerase mediated telomere G strand elongation and additionally ensures a proper telomere C strand synthesis (Rabbani et al., 2022). Here, PolIE is associated with the maintenance of telomere integrity by preventing DNA recombination at the telomeric regions. PPL2, a Prim-Pol (Primase-Polymerase) like protein, is essential for DNA replication by possibly bypassing replication-blocking lesions and fill post replicational gaps. Its depletion prevents the transition from G2/M phase into mitosis, results in cell cycle arrest and the activation of the DNA damage response in trypanosomes (Rudd et al., 2013). Like human PrimPol, PPL2 is located in the nucleus and mitochondrial matrix. Additionally, PPL2 is a protein with telomere-binding activity (Michel, Master thesis 2011).

The potential interaction of PPL2 and PolIE could be a result of their proximity to each other as they both could be involved in telomere maintenance by ensuring telomere C strand synthesis. Interestingly, by implementing a DNase step in the AP of PTP:PPL2 in BSF and PCF cells, the interaction with PolIE was not lost, indicating that the interaction is not DNA dependent. Here, further studies have to be implemented to unravel this potential interaction.

The interaction of TelAP2 and TelAP3 with the telomere complex

The findings presented in this discussion shed light on the intricate interactions and roles of TelAP1, TelAP2, and TelAP3 in the context of the telomere complex in *Trypanosoma brucei*. This study builds upon previous research and employs various techniques, including IF, co-IP, and MS analysis, to elucidate the dynamics of these proteins in different cellular contexts.

Comparing the APs of TelAP2, PPL2 and PolIE in PCF trypanosomes, we observed that TelAP1, TelAP2, TelAP3 and the telomere complex proteins *Tb*TRF and *Tb*TIF2 appear closely connected. By implementing IF using TelAP2 and TelAP3 specific antibodies, I demonstrated their nuclear localization proximate to *Tb*TRF throughout the BSF cell cycle. For BSFs, the co-localization of TelAP2 and *Tb*TRF had previously been reported by Glover et al. in 2016. The localization in PCFs aligns with the localization found by TrypTag.org, placing TelAP3 in the nucleus and the nuclear lumen and TelAP2 in the nucleus and nucleoplasm.

As telomeric proteins bind telomeres either directly or through protein-protein interactions, an important aspect of this study was the exploration of whether TelAP2 and TelAP3 interact directly with telomeric DNA. Electromobility shift assays are based on the principal that DNA oligonucleotides in connection with a protein forming a complex migrate more slowly than the protein or the oligonucleotides alone. This approach revealed that TelAP2 does not directly bind to telomeric DNA, similar to TelAP1 (Reis, 2017). On the other hand, TelAP3 displayed binding to telomeric nucleotides and control oligonucleotides, suggesting potential non-specific DNA-binding capabilities. These results raise questions about the role of TelAP3 within the telomere complex. It is important to note that ESMA has limitations, such as the non-native state of recombinant proteins and the possibility that dissociation during

electrophoresis could prevent the detection of an interaction (Hellman and Fried, 2007). This method can give false positive results due to non-specific binding, and false negative results due to low-affinity binding. An alternative would be to perform chromatin immunoprecipitation, as this technique allows the identification of protein-DNA interactions *in vivo* as was done for *Tb*RAP1 (Yang et al., 2009).

By performing TelAP1 co-IPs in TelAP2 and TelAP3 depleted cells, we saw that the absence of TelAP2 influences the interaction of TelAP1 with the other telomere-associated proteins, as no interaction with previously enriched proteins was possible anymore (Reis et al., 2018). This pattern was confirmed through *Tb*TRF co-IP. Immunofluorescence analysis of TelAP2-depleted cells using the TelAP1 antibody further supported these findings. TelAP1's signal intensity decreased significantly after TelAP2 depletion, and its localization within the nucleus was disrupted. *Tb*TRF also exhibited altered localization patterns. These observations strongly suggest that TelAP2 does indeed interact with TelAP1 and is vital for the interaction of TelAP1 with the telomere complex. TelAP2 depletion led to a reduced interaction between TelAP1 and *Tb*TRF, reinforcing the idea that TelAP2 plays a crucial role in mediating the interaction of TelAP1 with the telomere complex.

Another approach to identify protein-protein interactions is a yeast two-hybrid screen. This method has been successfully used before to confirm or identify interactions in *T. brucei* (López-Farfán et al., 2014, Baudouin et al., 2020). An advantage of this approach is the ability to identify interaction domains by expressing only parts of the bait or prey protein. A disadvantage is the possibility of false negative results due to the lack of posttranslational modifications and the non-native protein state. By using this method, we have another indication that TelAP2 does indeed interact with TelAP1. While this method provides additional evidence of TelAP2's interaction with TelAP1, its limitations necessitate caution in excluding other potential interactions.

The findings of this study clearly show that the interaction of TelAP1 with TelAP2 is crucial for its participation in the telomere complex protein interaction. In the absence of TelAP2, TelAP1 can no longer enrich *Tb*TRF as an interaction partner via IP and looses its nuclear location shown through IF. How the interaction between TelAP1 and TelAP2 is established and how TelAP2 mediates TelAP1 localization to the telomere complex needs to be further unraveled. TelAP1, other than TelAP2 has no influence on VSG expression and even though its protein expression is upregulated in BSF, it is not essential for the viability of BSF or PCF trypanosomes (Reis et al., 2018). Knockout strains revealed that TelAP1 deletion influences VSG silencing early during differentiation of BSF to PCF cells. TelAP2 on the other hand influences VSG expression and its depletion results in silent BES VSG derepression and cells display a growth phenotype 48 h after protein depletion. Both therefore most likely fulfill distinct roles at the telomeres of *T brucei*.

Conclusion

In summary, this study provides valuable insights into the intricate network of interactions within the telomere complex of *Trypanosoma brucei*. It highlights the central role of TelAP2 in possibly mediating the interaction between TelAP1 and the telomere complex, while also raising questions about the functions of TelAP3 and its potential role in DNA binding. Furthermore, our findings suggest that PolIE and PPL2, despite their shared classification as translesion polymerases, occupy distinct roles in proximity to each other at the telomeres (Figure 32). Further research into the precise mechanisms and functions of these proteins is needed to fully understand their contributions to VSG regulation and telomere maintenance in *Trypanosoma brucei*.

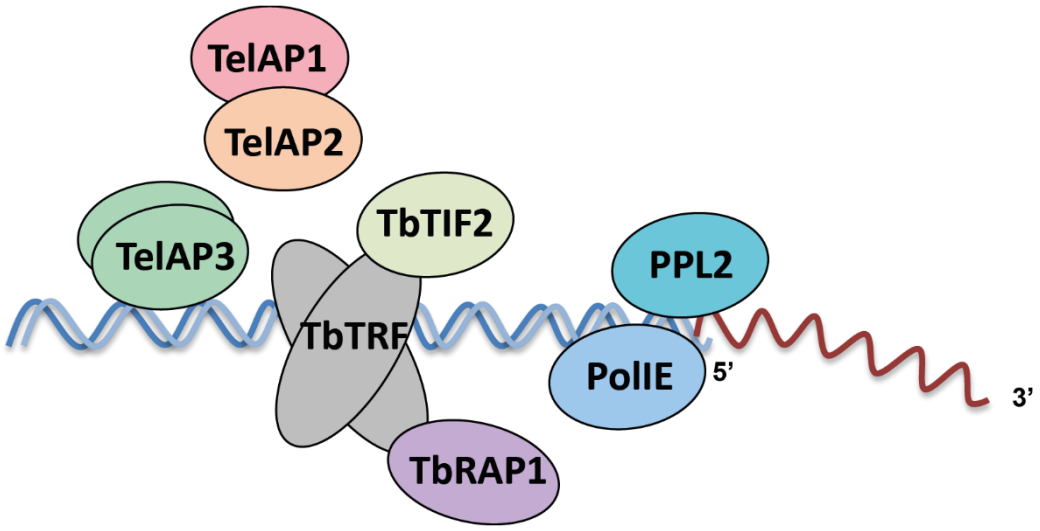

Figure 32: The telomere complex and predicted telomere-associated proteins.

BIBLIOGRAPHY

ABDELHALEEM, M. 2010. Helicases: an overview. *Methods Mol Biol,* 587**,** 1-12.

ADL, S. M., SIMPSON, A. G., LANE, C. E., LUKEŠ, J., BASS, D., BOWSER, S. S., BROWN, M. W., BURKI, F., DUNTHORN, M. & HAMPL, V. 2012. The revised classification of eukaryotes. *Journal of eukaryotic microbiology,* 59**,** 429-514.

ALLAWI, H. T. & SANTALUCIA, J. 1997. Thermodynamics and NMR of internal G⊙ T mismatches in DNA. *Biochemistry,* 36**,** 10581-10594.

ALSFORD, S. & HORN, D. 2012. Cell-cycle-regulated control of VSG expression site silencing by histones and histone chaperones ASF1A and CAF-1b in Trypanosoma brucei. *Nucleic Acids Res,* 40**,** 10150-60.

ALSFORD, S., KAWAHARA, T., GLOVER, L. & HORN, D. 2005. Tagging a T. brucei RRNA locus improves stable transfection efficiency and circumvents inducible expression position effects. *Molecular and biochemical parasitology,* 144**,** 142-148.

ANSORGE, I., STEVERDING, D., MELVILLE, S., HARTMANN, C. & CLAYTON, C. 1999. Transcription of 'inactive'expression sites in African trypanosomes leads to expression of multiple transferrin receptor RNAs in bloodstream forms. *Molecular and biochemical parasitology,* 101**,** 81-94.

ARESTA-BRANCO, F., PIMENTA, S. & FIGUEIREDO, L. M. 2016. A transcription-independent epigenetic mechanism is associated with antigenic switching in Trypanosoma brucei. *Nucleic Acids Res,* 44**,** 3131-46.

ARNOULT, N., VAN BENEDEN, A. & DECOTTIGNIES, A. 2012. Telomere length regulates TERRA levels through increased trimethylation of telomeric H3K9 and HP1α. *Nature structural & molecular biology,* 19**,** 948-956.

ASLETT, M., AURRECOECHEA, C., BERRIMAN, M., BRESTELLI, J., BRUNK, B. P., CARRINGTON, M., DEPLEDGE, D. P., FISCHER, S., GAJRIA, B. & GAO, X. 2010. TriTrypDB: a functional genomic resource for the Trypanosomatidae. *Nucleic acids research,* 38**,** D457-D462.

AZAD, G. K. & TOMAR, R. S. 2016. The multifunctional transcription factor Rap1: a regulator of yeast physiology. *Frontiers in Bioscience-Landmark,* 21**,** 918-930.

AZZALIN, C. M., REICHENBACH, P., KHORIAULI, L., GIULOTTO, E. & LINGNER, J. 2007. Telomeric repeat–containing RNA and RNA surveillance factors at mammalian chromosome ends. *Science,* 318**,** 798-801.

BADJATIA, N., PARK, S. H., AMBROSIO, D. L., KIRKHAM, J. K. & GUNZL, A. 2016. Cyclin-Dependent Kinase CRK9, Required for Spliced Leader trans Splicing of Pre-mRNA in Trypanosomes, Functions in a Complex with a New L-Type Cyclin and a Kinetoplastid-Specific Protein. *PLoS Pathog,* 12**,** e1005498.

BAKARI-SOALE, M., IKENGA, N. J., SCHEIBE, M., BUTTER, F., JONES, N. G., KRAMER, S. & ENGSTLER, M. 2021. The nucleolar DExD/H protein Hel66 is involved in ribosome biogenesis in Trypanosoma brucei. *Sci Rep,* 11**,** 18325.

BALAÑA-FOUCE, R., ALVAREZ-VELILLA, R., FERNÁNDEZ-PRADA, C., GARCÍA-ESTRADA, C. & REGUERA, R. M. 2014. Trypanosomatids topoisomerase re-visited. New structural findings and role in drug discovery. *Int J Parasitol Drugs Drug Resist,* 4**,** 326-37.

BASTIN-SHANOWER, S. A. & BRILL, S. J. 2001. Functional analysis of the four DNA binding domains of replication protein A. The role of RPA2 in ssDNA binding. *J Biol Chem,* 276**,** 36446-53.

BATES, P. A. 2007. Transmission of Leishmania metacyclic promastigotes by phlebotomine sand flies. *International journal for parasitology,* 37**,** 1097-1106.

BATRAM, C., JONES, N. G., JANZEN, C. J., MARKERT, S. M. & ENGSTLER, M. 2014. Expression site attenuation mechanistically links antigenic variation and development in Trypanosoma brucei. *Elife,* 3**,** e02324.

BAUDOUIN, H. C. M., PFEIFFER, L. & OCHSENREITER, T. 2020. A comparison of three approaches for the discovery of novel tripartite attachment complex proteins in Trypanosoma brucei. *PLoS Negl Trop Dis,* 14**,** e0008568.

BAUMANN, P. & CECH, T. R. 2001. Pot1, the putative telomere end-binding protein in fission yeast and humans. *Science,* 292**,** 1171-1175.

BENEKE, T., MADDEN, R., MAKIN, L., VALLI, J., SUNTER, J. & GLUENZ, E. 2017. A CRISPR Cas9 high-throughput genome editing toolkit for kinetoplastids. *Royal Society open science,* 4**,** 170095.

BERRIMAN, M., GHEDIN, E., HERTZ-FOWLER, C., BLANDIN, G., RENAULD, H., BARTHOLOMEU, D. C., LENNARD, N. J., CALER, E., HAMLIN, N. E. & HAAS, B. 2005. The genome of the African trypanosome Trypanosoma brucei. *science,* 309**,** 416-422.

BHANOT, M. & SMITH, S. 2012. TIN2 stability is regulated by the E3 ligase Siah2. *Molecular and cellular biology,* 32**,** 376-384.

BILAUD, T., BRUN, C., ANCELIN, K., KOERING, C. E., LAROCHE, T. & GILSON, E. 1997. Telomeric localization of TRF2, a novel human telobox protein. *Nature genetics,* 17**,** 236-239.

BILLINGTON, K., HALLIDAY, C., MADDEN, R., DYER, P., BARKER, A. R., MOREIRA-LEITE, F. F., CARRINGTON, M., VAUGHAN, S., HERTZ-FOWLER, C., DEAN, S., SUNTER, J. D., WHEELER, R. J. & GULL, K. 2023. Genome-wide subcellular protein map for the flagellate parasite Trypanosoma brucei. *Nat Microbiol,* 8**,** 533-547.

BLACKBURN, E. H. & CHALLONER, P. B. 1984. Identification of a telomeric DNA sequence in Trypanosoma brucei. *Cell,* 36**,** 447-457.

BLASCO, M. A. 2007. The epigenetic regulation of mammalian telomeres. *Nature Reviews Genetics,* 8**,** 299-309.

BORGES, A. R., LINK, F., ENGSTLER, M. & JONES, N. G. 2021. The Glycosylphosphatidylinositol Anchor: A Linchpin for Cell Surface Versatility of Trypanosomatids. *Frontiers in Cell and Developmental Biology***,** 2681.

BORST, P. & SABATINI, R. 2008. Base J: discovery, biosynthesis, and possible functions. *Annu. Rev. Microbiol.,* 62**,** 235-251.

BRUN, R. & BALMER, O. 2006. New developments in human African trypanosomiasis. *Current opinion in infectious diseases,* 19**,** 415-420.

BRUN, R. & SCHÖNENBERGER 1979. Cultivation and in vitro cloning or procyclic culture forms of Trypanosoma brucei in a semi-defined medium. Short communication. *Acta Trop,* 36**,** 289-92.

BRYAN, T. M., ENGLEZOU, A., DALLA-POZZA, L., DUNHAM, M. A. & REDDEL, R. R. 1997. Evidence for an alternative mechanism for maintaining telomere length in human tumors and tumor-derived cell lines. *Nature medicine,* 3**,** 1271-1274.

BUDZAK, J., JONES, R., TSCHUDI, C., KOLEV, N. G. & RUDENKO, G. 2022. An assembly of nuclear bodies associates with the active VSG expression site in African trypanosomes. *Nature Communications,* 13**,** 1-18.

BURKARD, G., FRAGOSO, C. & RODITI, I. 2007. Highly efficient stable transformation of bloodstream forms of Trypanosoma brucei. *Molecular and biochemical parasitology,* 153**,** 220-223.

BURTON, P., MCBRIDE, D. J., WILKES, J. M., BARRY, J. D. & MCCULLOCH, R. 2007. Ku heterodimer-independent end joining in Trypanosoma brucei cell extracts relies upon sequence microhomology. *Eukaryotic cell,* 6**,** 1773-1781.

CALDWELL, C. C. & SPIES, M. 2020. Dynamic elements of replication protein A at the crossroads of DNA replication, recombination, and repair. *Crit Rev Biochem Mol Biol,* 55**,** 482-507.

CASTEEL, D. E., ZHUANG, S., ZENG, Y., PERRINO, F. W., BOSS, G. R., GOULIAN, M. & PILZ, R. B. 2009. A DNA polymerase-α· primase cofactor with homology to replication protein A-32 regulates DNA replication in mammalian cells. *Journal of Biological Chemistry,* 284**,** 5807-5818.

CEBALLOS-PÉREZ, G., RICO-JIMÉNEZ, M., GÓMEZ-LIÑÁN, C. & ESTÉVEZ, A. M. 2023. Role of the RNA-binding protein ZC3H41 in the regulation of ribosomal protein messenger RNAs in trypanosomes. *Parasit Vectors,* 16**,** 118.

CELLI, G. B., DENCHI, E. L. & DE LANGE, T. 2006. Ku70 stimulates fusion of dysfunctional telomeres yet protects chromosome ends from homologous recombination. *Nature cell biology,* 8**,** 885-890.

ČERVENÁK, F., SEPŠIOVÁ, R., NOSEK, J. & TOMÁŠKA, Ľ. 2021. Step-by-step evolution of telomeres: lessons from yeasts. *Genome biology and evolution,* 13**,** evaa268.

CESTARI, I. & STUART, K. 2018. Transcriptional regulation of telomeric expression sites and antigenic variation in trypanosomes. *Current Genomics,* 19**,** 119-132.

CHAN, S. W. & BLACKBURN, E. H. 2002. New ways not to make ends meet: telomerase, DNA damage proteins and heterochromatin. *Oncogene,* 21**,** 553-563.

CHAWLA, R., REDON, S., RAFTOPOULOU, C., WISCHNEWSKI, H., GAGOS, S. & AZZALIN, C. M. 2011. Human UPF1 interacts with TPP1 and telomerase and sustains telomere leading-strand replication. *Embo j,* 30**,** 4047-58.

CHEN, H., LISBY, M. & SYMINGTON, L. S. 2013. RPA coordinates DNA end resection and prevents formation of DNA hairpins. *Mol Cell,* 50**,** 589-600.

CHEN, Y., YANG, Y., VAN OVERBEEK, M., DONIGIAN, J. R., BACIU, P., DE LANGE, T. & LEI, M. 2008. A shared docking motif in TRF1 and TRF2 used for differential recruitment of telomeric proteins. *Science,* 319**,** 1092-1096.

CLAYTON, C. 2013. The regulation of trypanosome gene expression by RNA-binding proteins. *PLoS Pathog,* 9**,** e1003680.

CLAYTON, C. & SHAPIRA, M. 2007. Post-transcriptional regulation of gene expression in trypanosomes and leishmanias. *Molecular and biochemical parasitology,* 156**,** 93-101.

CLAYTON, C. E. 2002. Life without transcriptional control? From fly to man and back again. *EMBO J,* 21**,** 1881-8.

COLLINS, K. & MITCHELL, J. R. 2002. Telomerase in the human organism. *Oncogene,* 21**,** 564-579.

CORDON-OBRAS, C., GOMEZ-LIÑAN, C., TORRES-RUSILLO, S., VIDAL-COBO, I., LOPEZ-FARFAN, D., BARROSO-DEL JESUS, A., ROJAS-BARROS, D., CARRINGTON, M. & NAVARRO, M. 2022. Identification of sequence-specific promoters driving polycistronic transcription initiation by RNA polymerase II in trypanosomes. *Cell reports,* 38**,** 110221.

COX, J. & MANN, M. 2008. MaxQuant enables high peptide identification rates, individualized ppb-range mass accuracies and proteome-wide protein quantification. *Nature biotechnology,* 26**,** 1367-1372.

CRISTODERO, M. & CLAYTON, C. E. 2007. Trypanosome MTR4 is involved in rRNA processing. *Nucleic Acids Res,* 35**,** 7023-30.

CROSS, G. A. 1975. Identification, purification and properties of clone-specific glycoprotein antigens constituting the surface coat of Trypanosoma brucei. *Parasitology,* 71**,** 393-417.

CROSS, G. A. 1984. Release and purification of Trypanosoma brucei variant surface glycoprotein. *Journal of cellular biochemistry,* 24**,** 79-90.

CROSS, G. A., KIM, H.-S. & WICKSTEAD, B. 2014. Capturing the variant surface glycoprotein repertoire (the VSGnome) of Trypanosoma brucei Lister 427. *Molecular and biochemical parasitology,* 195**,** 59-73.

DAMASCENO, J. D., SILVA, G. L., TSCHUDI, C. & TOSI, L. R. 2017. Evidence for regulated expression of Telomeric Repeat-containing RNAs (TERRA) in parasitic trypanosomatids. *Memórias do Instituto Oswaldo Cruz,* 112**,** 572-576.

DANIELS, J. P., GULL, K. & WICKSTEAD, B. 2012. The trypanosomatid-specific N terminus of RPA2 is required for RNA polymerase I assembly, localization, and function. *Eukaryot Cell,* 11**,** 662-72.

DAVIS, J. A. & CHAKRABARTI, K. 2022. Telomerase ribonucleoprotein and genome integrity—An emerging connection in protozoan parasites. *Wiley Interdisciplinary Reviews: RNA,* 13**,** e1710.

DE LANGE, T. 2004. T-loops and the origin of telomeres. *Nature reviews Molecular cell biology,* 5**,** 323-329.

DE LANGE, T. 2005. Shelterin: the protein complex that shapes and safeguards human telomeres. *Genes & development,* 19**,** 2100-2110.

DEAN, S., SUNTER, J. D. & WHEELER, R. J. 2017. TrypTag. org: a trypanosome genome-wide protein localisation resource. *Trends in parasitology,* 33**,** 80-82.

DELHI, P., QUEIROZ, R., INCHAUSTEGUI, D., CARRINGTON, M. & CLAYTON, C. 2011. Is there a classical nonsense-mediated decay pathway in trypanosomes? *PloS one,* 6**,** e25112.

DENCHI, E. L. & DE LANGE, T. 2007. Protection of telomeres through independent control of ATM and ATR by TRF2 and POT1. *Nature,* 448**,** 1068-1071.

DENNINGER, V. & RUDENKO, G. 2014. FACT plays a major role in histone dynamics affecting VSG expression site control in Trypanosoma brucei. *Mol Microbiol,* 94**,** 945-62.

DEWAR, C. E., MACGREGOR, P., COOPER, S., GOULD, M. K., MATTHEWS, K. R., SAVILL, N. J. & SCHNAUFER, A. 2018. Mitochondrial DNA is critical for longevity and metabolism of transmission stage Trypanosoma brucei. *PLoS Pathog,* 14**,** e1007195.

DREESEN, O. & CROSS, G. A. 2008. Telomere length in Trypanosoma brucei. *Exp Parasitol,* 118**,** 103-10.

DREESEN, O., LI, B. & CROSS, G. A. 2005. Telomere structure and shortening in telomerase-deficient Trypanosoma brucei. *Nucleic Acids Res,* 33**,** 4536-43.

DROLL, D., MINIA, I., FADDA, A., SINGH, A., STEWART, M., QUEIROZ, R. & CLAYTON, C. 2013. Post-transcriptional regulation of the trypanosome heat shock response by a zinc finger protein. *PLoS Pathog,* 9**,** e1003286.

DUEVA, R. & ILIAKIS, G. 2020. Replication protein A: a multifunctional protein with roles in DNA replication, repair and beyond. *NAR Cancer,* 2**,** zcaa022.

EID, J. E. & SOLLNER-WEBB, B. 1995. ST-1, a 39-kilodalton protein in Trypanosoma brucei, exhibits a dual affinity for the duplex form of the 29-base-pair subtelomeric repeat and its C-rich strand. *Mol Cell Biol,* 15**,** 389-97.

EISENHUTH, N., VELLMER, T., RAUH, E. T., BUTTER, F. & JANZEN, C. J. 2021. A DOT1B/Ribonuclease H2 Protein Complex Is Involved in R-Loop Processing, Genomic Integrity, and Antigenic Variation in Trypanosoma brucei. *mBio,* 12**,** e0135221.

EKANAYAKE, D. K., CIPRIANO, M. J. & SABATINI, R. 2007. Telomeric co-localization of the modified base J and contingency genes in the protozoan parasite Trypanosoma cruzi. *Nucleic acids research,* 35**,** 6367-6377.

ELLAHI, A., THURTLE, D. M. & RINE, J. 2015. The chromatin and transcriptional landscape of native Saccharomyces cerevisiae telomeres and subtelomeric domains. *Genetics,* 200**,** 505-521.

ENGSTLER, M. & BOSHART, M. 2004. Cold shock and regulation of surface protein trafficking convey sensitization to inducers of stage differentiation in Trypanosoma brucei. *Genes & development,* 18**,** 2798-2811.

ENGSTLER, M., PFOHL, T., HERMINGHAUS, S., BOSHART, M., WIEGERTJES, G., HEDDERGOTT, N. & OVERATH, P. 2007. Hydrodynamic flow-mediated protein sorting on the cell surface of trypanosomes. *Cell,* 131**,** 505-15.

ENGSTLER, M., THILO, L., WEISE, F., GRUNFELDER, C. G., SCHWARZ, H., BOSHART, M. & OVERATH, P. 2004. Kinetics of endocytosis and recycling of the GPI-anchored variant surface glycoprotein in Trypanosoma brucei. *J Cell Sci,* 117**,** 1105-15.

ERBEN, E. D., FADDA, A., LUEONG, S., HOHEISEL, J. D. & CLAYTON, C. 2014. A genome-wide tethering screen reveals novel potential post-transcriptional regulators in Trypanosoma brucei. *PLoS Pathog,* 10**,** e1004178.

ESTEVEZ, A. M. 2008. The RNA-binding protein Tb DRBD3 regulates the stability of a specific subset of mRNAs in trypanosomes. *Nucleic acids research,* 36**,** 4573-4586.

FARIA, J., GLOVER, L., HUTCHINSON, S., BOEHM, C., FIELD, M. C. & HORN, D. 2019. Monoallelic expression and epigenetic inheritance sustained by a Trypanosoma brucei variant surface glycoprotein exclusion complex. *Nat Commun,* 10**,** 3023.

FARIA, J., LUZAK, V., MÜLLER, L. S., BRINK, B. G., HUTCHINSON, S., GLOVER, L., HORN, D. & SIEGEL, T. N. 2021. Spatial integration of transcription and splicing in a dedicated compartment sustains monogenic antigen expression in African trypanosomes. *Nature microbiology,* 6**,** 289-300.

FERNANDES, C. A. H., MOREA, E. G. O., DOS SANTOS, G. A., DA SILVA, V. L., VIEIRA, M. R., VIVIESCAS, M. A., CHATAIN, J., VADEL, A., SAINTOMÉ, C., FONTES, M. R. M. & CANO, M. I. N. 2020. A multi-approach analysis highlights the relevance of RPA-1 as a telomere end-binding protein (TEBP) in Leishmania amazonensis. *Biochim Biophys Acta Gen Subj,* 1864**,** 129607.

FIGUEIREDO, L. M. & CROSS, G. A. 2010. Nucleosomes are depleted at the VSG expression site transcribed by RNA polymerase I in African trypanosomes. *Eukaryot Cell,* 9**,** 148-54.

FIGUEIREDO, L. M., CROSS, G. A. & JANZEN, C. J. 2009. Epigenetic regulation in African trypanosomes: a new kid on the block. *Nat Rev Microbiol,* 7**,** 504-13.

FIGUEIREDO, L. M., JANZEN, C. J. & CROSS, G. A. 2008. A histone methyltransferase modulates antigenic variation in African trypanosomes. *PLoS biology,* 6**,** e161.

FRANCO, J. R., SIMARRO, P. P., DIARRA, A. & JANNIN, J. G. 2014. Epidemiology of human African trypanosomiasis. *Clinical epidemiology,* 6**,** 257.

GAO, H., CERVANTES, R. B., MANDELL, E. K., OTERO, J. H. & LUNDBLAD, V. 2007. RPA-like proteins mediate yeast telomere function. *Nature structural & molecular biology,* 14**,** 208-214.

GARCÍA-GÓMEZ, S., REYES, A., MARTÍNEZ-JIMÉNEZ, M. I., CHOCRÓN, E. S., MOURÓN, S., TERRADOS, G., POWELL, C., SALIDO, E., MÉNDEZ, J., HOLT, I. J. & BLANCO, L. 2013. PrimPol, an archaic primase/polymerase operating in human cells. *Mol Cell,* 52**,** 541-53.

GENEST, P.-A., TER RIET, B., CIJSOUW, T., VAN LUENEN, H. G. & BORST, P. 2007. Telomeric localization of the modified DNA base J in the genome of the protozoan parasite Leishmania. *Nucleic acids research,* 35**,** 2116-2124.

GILINGER, G. & BELLOFATTO, V. 2001. Trypanosome spliced leader RNA genes contain the first identified RNA polymerase II gene promoter in these organisms. *Nucleic acids research,* 29**,** 1556-1564.

GLOVER, L., ALSFORD, S. & HORN, D. 2013. DNA break site at fragile subtelomeres determines probability and mechanism of antigenic variation in African trypanosomes. *PLoS Pathog,* 9**,** e1003260.

GLOVER, L., HUTCHINSON, S., ALSFORD, S. & HORN, D. 2016. VEX1 controls the allelic exclusion required for antigenic variation in trypanosomes. *Proc Natl Acad Sci U S A,* 113**,** 7225-30.

GLOVER, L., MARQUES, C. A., SUSKA, O. & HORN, D. 2019. Persistent DNA Damage Foci and DNA Replication with a Broken Chromosome in the African Trypanosome. *mBio,* 10.

GOMES, N. M., RYDER, O. A., HOUCK, M. L., CHARTER, S. J., WALKER, W., FORSYTH, N. R., AUSTAD, S. N., VENDITTI, C., PAGEL, M. & SHAY, J. W. 2011. Comparative biology of mammalian telomeres: hypotheses on ancestral states and the roles of telomeres in longevity determination. *Aging cell,* 10**,** 761-768.

GOOS, C., DEJUNG, M., JANZEN, C. J., BUTTER, F. & KRAMER, S. 2017. The nuclear proteome of Trypanosoma brucei. *PLoS One,* 12**,** e0181884.

GRAHAM, S. V., WYMER, B. & BARRY, J. D. 1998. A trypanosome metacyclic VSG gene promoter with two functionally distinct, life cycle stage-specific activities. *Nucleic acids research,* 26**,** 1985-1990.

GREIDER, C. W. & BLACKBURN, E. H. 1996. Telomeres, telomerase and cancer. *Scientific American,* 274**,** 92-97.

GRILL, S., BISHT, K., TESMER, V. M., SHAMI, A. N., HAMMOUD, S. S. & NANDAKUMAR, J. 2019. Two separation-of-function isoforms of human TPP1 dictate telomerase regulation in somatic and germ cells. *Cell reports,* 27**,** 3511-3521. e7.

GRÜNFELDER, C. G., ENGSTLER, M., WEISE, F., SCHWARZ, H., STIERHOF, Y. D., BOSHART, M. & OVERATH, P. 2002. Accumulation of a GPI‐anchored protein at the cell surface requires sorting at multiple intracellular levels. *Traffic,* 3**,** 547-559.

GÜNZL, A. 2010. The pre-mRNA splicing machinery of trypanosomes: complex or simplified? *Eukaryotic cell,* 9**,** 1159-1170.

HAJDUK, S. & VICKERMAN, K. 1981. Antigenic differentiation of Trypanosoma brucei: studies on metacyclic and first parasitaemia populations. *Trans R Soc Trop Med Hyg,* 75**,** 145-6.

HARLEY, C. B., FUTCHER, A. B. & GREIDER, C. W. 1990. Telomeres shorten during ageing of human fibroblasts. *Nature,* 345**,** 458-460.

HELLMAN, L. M. & FRIED, M. G. 2007. Electrophoretic mobility shift assay (EMSA) for detecting protein-nucleic acid interactions. *Nat Protoc,* 2**,** 1849-61.

HERBIG, U., JOBLING, W. A., CHEN, B. P., CHEN, D. J. & SEDIVY, J. M. 2004. Telomere shortening triggers senescence of human cells through a pathway involving ATM, p53, and p21CIP1, but not p16INK4a. *Molecular cell,* 14**,** 501-513.

HERTZ-FOWLER, C., FIGUEIREDO, L. M., QUAIL, M. A., BECKER, M., JACKSON, A., BASON, N., BROOKS, K., CHURCHER, C., FAHKRO, S., GOODHEAD, I., HEATH, P., KARTVELISHVILI, M., MUNGALL, K., HARRIS, D., HAUSER, H., SANDERS, M., SAUNDERS, D., SEEGER, K., SHARP, S., TAYLOR, J. E., WALKER, D., WHITE, B., YOUNG, R., CROSS, G. A., RUDENKO, G., BARRY, J. D., LOUIS, E. J. & BERRIMAN, M. 2008. Telomeric expression sites are highly conserved in Trypanosoma brucei. *PLoS One,* 3**,** e3527.

HIRUMI, H. & HIRUMI, K. 1989. Continuous cultivation of Trypanosoma brucei blood stream forms in a medium containing a low concentration of serum protein without feeder cell layers. *J Parasitol,* 75**,** 985-9.

HONG, D., PARK, T. & JEONG, S. 2019. Nuclear UPF1 Is Associated with Chromatin for Transcription-Coupled RNA Surveillance. *Mol Cells,* 42**,** 523-529.

HOUGHTALING, B. R., CUTTONARO, L., CHANG, W. & SMITH, S. 2004. A dynamic molecular link between the telomere length regulator TRF1 and the chromosome end protector TRF2. *Current biology,* 14**,** 1621-1631.

HOVEL-MINER, G. A., BOOTHROYD, C. E., MUGNIER, M., DREESEN, O., CROSS, G. A. & PAPAVASILIOU, F. N. 2012. Telomere length affects the frequency and mechanism of antigenic variation in Trypanosoma brucei. *PLoS Pathog,* 8**,** e1002900.

HUANG, J. & VAN DER PLOEG, L. 1991. Requirement of a polypyrimidine tract for trans‐splicing in trypanosomes: discriminating the PARP promoter from the immediately adjacent 3′ splice acceptor site. *The EMBO journal,* 10**,** 3877-3885.

HUGHES, K., WAND, M., FOULSTON, L., YOUNG, R., HARLEY, K., TERRY, S., ERSFELD, K. & RUDENKO, G. 2007. A novel ISWI is involved in VSG expression site downregulation in African trypanosomes. *EMBO J,* 26**,** 2400-10.

HUGHES, L., BORRETT, S., TOWERS, K., STARBORG, T. & VAUGHAN, S. 2017. Patterns of organelle ontogeny through a cell cycle revealed by whole-cell reconstructions using 3D electron microscopy. *Journal of cell science,* 130**,** 637-647.

IYER, L. M., KOONIN, E. V., LEIPE, D. D. & ARAVIND, L. 2005. Origin and evolution of the archaeo-eukaryotic primase superfamily and related palm-domain proteins: structural insights and new members. *Nucleic Acids Res,* 33**,** 3875-96.

JACOBS, J. J. & DE LANGE, T. 2004. Significant role for p16INK4a in p53-independent telomere-directed senescence. *Current Biology,* 14**,** 2302-2308.

JÁDY, B. E., RICHARD, P., BERTRAND, E. & KISS, T. 2006. Cell cycle-dependent recruitment of telomerase RNA and Cajal bodies to human telomeres. *Molecular biology of the cell,* 17**,** 944-954.

JANZ, L. & CLAYTON, C. 1994. The PARP and rRNA promoters of Trypanosoma brucei are composed of dissimilar sequence elements that are functionally interchangeable. *Molecular and Cellular Biology,* 14**,** 5804-5811.

JEHI, S. E., LI, X., SANDHU, R., YE, F., BENMERZOUGA, I., ZHANG, M., ZHAO, Y. & LI, B. 2014a. Suppression of subtelomeric VSG switching by Trypanosoma brucei TRF requires its TTAGGG repeat-binding activity. *Nucleic acids research,* 42**,** 12899-12911.

JEHI, S. E., NANAVATY, V. & LI, B. 2016. Trypanosoma brucei TIF2 and TRF Suppress VSG Switching Using Overlapping and Independent Mechanisms. *PLoS One,* 11**,** e0156746.

JEHI, S. E., WU, F. & LI, B. 2014b. Trypanosoma brucei TIF2 suppresses VSG switching by maintaining subtelomere integrity. *Cell Res,* 24**,** 870-85.

JONES, N. G., THOMAS, E. B., BROWN, E., DICKENS, N. J., HAMMARTON, T. C. & MOTTRAM, J. C. 2014. Regulators of Trypanosoma brucei cell cycle progression and differentiation identified using a kinome-wide RNAi screen. *PLoS pathogens,* 10**,** e1003886.

KANOH, J. & ISHIKAWA, F. 2001. spRap1 and spRif1, recruited to telomeres by Taz1, are essential for telomere function in fission yeast. *Current Biology,* 11**,** 1624-1630.

KASSEM, A., PAYS, E. & VANHAMME, L. 2014. Transcription is initiated on silent variant surface glycoprotein expression sites despite monoallelic expression in Trypanosoma brucei. *Proc Natl Acad Sci U S A,* 111**,** 8943-8.

KELLY, S., REED, J., KRAMER, S., ELLIS, L., WEBB, H., SUNTER, J., SALJE, J., MARINSEK, N., GULL, K. & WICKSTEAD, B. 2007. Functional genomics in Trypanosoma brucei: a collection of vectors for the expression of tagged proteins from endogenous and ectopic gene loci. *Molecular and biochemical parasitology,* 154**,** 103.

KENNEDY, P. G. 2019. Update on human African trypanosomiasis (sleeping sickness). *Journal of neurology,* 266**,** 2334-2337.

KEVRIC, I., CAPPEL, M. A. & KEELING, J. H. 2015. New world and old world Leishmania infections: a practical review. *Dermatologic clinics,* 33**,** 579-593.

KIM, S.-H., KAMINKER, P. & CAMPISI, J. 1999. TIN2, a new regulator of telomere length in human cells. *Nature genetics,* 23**,** 405-412.

KRAMER, S., BANNERMAN-CHUKUALIM, B., ELLIS, L., BOULDEN, E. A., KELLY, S., FIELD, M. C. & CARRINGTON, M. 2013. Differential localization of the two T. brucei poly (A) binding proteins to the nucleus and RNP granules suggests binding to distinct mRNA pools. *PloS one,* 8**,** e54004.

KRAUS, A. J., VANSELOW, J. T., LAMER, S., BRINK, B. G., SCHLOSSER, A. & SIEGEL, T. N. 2020. Distinct roles for H4 and H2A.Z acetylation in RNA transcription in African trypanosomes. *Nat Commun,* 11**,** 1498.

KUPIEC, M. 2014. Biology of telomeres: lessons from budding yeast. *FEMS microbiology reviews,* 38**,** 144-171.

LEAL, A. Z., SCHWEBS, M., BRIGGS, E., WEISERT, N., REIS, H., LEMGRUBER, L., LUKO, K., WILKES, J., BUTTER, F. & MCCULLOCH, R. 2020. Genome maintenance functions of a putative Trypanosoma brucei translesion DNA polymerase include telomere association and a role in antigenic variation. *Nucleic acids research,* 48**,** 9660-9680.

LEI, M., PODELL, E. R. & CECH, T. R. 2004. Structure of human POT1 bound to telomeric single-stranded DNA provides a model for chromosome end-protection. *Nature structural & molecular biology,* 11**,** 1223-1229.

LI, B., ESPINAL, A. & CROSS, G. A. 2005. Trypanosome telomeres are protected by a homologue of mammalian TRF2. *Molecular and cellular biology,* 25**,** 5011-5021.

LI, B., OESTREICH, S. & DE LANGE, T. 2000. Identification of human Rap1: implications for telomere evolution. *Cell,* 101**,** 471-483.

LI, C. H., IRMER, H., GUDJONSDOTTIR-PLANCK, D., FREESE, S., SALM, H., HAILE, S., ESTEVEZ, A. M. & CLAYTON, C. 2006. Roles of a Trypanosoma brucei 5'->3' exoribonuclease homolog in mRNA degradation. *RNA,* 12**,** 2171-86.

LIANG, X.-H., HARITAN, A., ULIEL, S. & MICHAELI, S. 2003. trans and cis Splicing in Trypanosomatids: Mechanism, Factors, and Regulation. *Eukaryotic cell,* 2**,** 830-840.

LIDANI, K. C. F., ANDRADE, F. A., BAVIA, L., DAMASCENO, F. S., BELTRAME, M. H., MESSIAS-REASON, I. J. & SANDRI, T. L. 2019. Chagas disease: from discovery to a worldwide health problem. *Frontiers in public health,* 7**,** 166.

LIM, C. J. & CECH, T. R. 2021. Shaping human telomeres: from shelterin and CST complexes to telomeric chromatin organization. *Nature Reviews Molecular Cell Biology,* 22**,** 283-298.

LINK, F., BORGES, A. R., JONES, N. G. & ENGSTLER, M. 2021. To the surface and back: exo-and endocytic pathways in Trypanosoma brucei. *Frontiers in Cell and Developmental Biology***,** 2034.

LIU, B., WANG, J., YILDIRIR, G. & ENGLUND, P. T. 2009. TbPIF5 is a Trypanosoma brucei mitochondrial DNA helicase involved in processing of minicircle Okazaki fragments. *PLoS pathogens,* 5**,** e1000589.

LÓPEZ-FARFÁN, D., BART, J.-M., ROJAS-BARROS, D. I. & NAVARRO, M. 2014. SUMOylation by the E3 ligase TbSIZ1/PIAS1 positively regulates VSG expression in Trypanosoma brucei. *PLoS pathogens,* 10**,** e1004545.

LUKEŠ, J., SKALICKÝ, T., TÝČ, J., VOTÝPKA, J. & YURCHENKO, V. 2014. Evolution of parasitism in kinetoplastid flagellates. *Molecular and biochemical parasitology,* 195**,** 115-122.

LUO, K., VEGA-PALAS, M. A. & GRUNSTEIN, M. 2002. Rap1–Sir4 binding independent of other Sir, yKu, or histone interactions initiates the assembly of telomeric heterochromatin in yeast. *Genes & development,* 16**,** 1528-1539.

MACGREGOR, P., SZÖŐR, B., SAVILL, N. J. & MATTHEWS, K. R. 2012. Trypanosomal immune evasion, chronicity and transmission: an elegant balancing act. *Nat Rev Microbiol,* 10**,** 431-8.

MAHAMAT, M. H., PEKA, M., RAYAISSE, J.-B., ROCK, K. S., TOKO, M. A., DARNAS, J., BRAHIM, G. M., ALKATIB, A. B., YONI, W. & TIRADOS, I. 2017. Adding tsetse control to medical activities contributes to decreasing transmission of sleeping sickness in the Mandoul focus (Chad). *PLoS neglected tropical diseases,* 11**,** e0005792.

MAIR, G., SHI, H., LI, H., DJIKENG, A., AVILES, H. O., BISHOP, J. R., FALCONE, F. H., GAVRILESCU, C., MONTGOMERY, J. L. & SANTORI, M. I. 2000. A new twist in trypanosome RNA metabolism: cis-splicing of pre-mRNA. *Rna,* 6**,** 163-169.

MELVILLE, S. E., LEECH, V., NAVARRO, M. & CROSS, G. A. 2000. The molecular karyotype of the megabase chromosomes of Trypanosoma brucei stock 427. *Mol Biochem Parasitol,* 111**,** 261-73.

MILHAUSEN, M., NELSON, R. G., SATHER, S., SELKIRK, M. & AGABIAN, N. 1984. Identification of a small RNA containing the trypanosome spliced leader: a donor of shared 5′ sequences of trypanosomatid mRNAs? *Cell,* 38**,** 721-729.

MIYAKE, Y., NAKAMURA, M., NABETANI, A., SHIMAMURA, S., TAMURA, M., YONEHARA, S., SAITO, M. & ISHIKAWA, F. 2009. RPA-like mammalian Ctc1-Stn1-Ten1 complex binds to single-stranded DNA and protects telomeres independently of the Pot1 pathway. *Molecular cell,* 36**,** 193-206.

MORRISWOOD, B., HAVLICEK, K., DEMMEL, L., YAVUZ, S., SEALEY-CARDONA, M., VIDILASERIS, K., ANRATHER, D., KOSTAN, J., DJINOVIC-CARUGO, K., ROUX, K. J. & WARREN, G. 2013. Novel bilobe components in Trypanosoma brucei identified using proximity-dependent biotinylation. *Eukaryot Cell,* 12**,** 356-67.

MUGNIER, M. R., STEBBINS, C. E. & PAPAVASILIOU, F. N. 2016. Masters of Disguise: Antigenic Variation and the VSG Coat in Trypanosoma brucei. *PLoS Pathog,* 12**,** e1005784.

MUKHERJEE, A., HOSSAIN, Z., ERBEN, E., MA, S., CHOI, J. Y. & KIM, H. S. 2023. Identification of a small-molecule inhibitor that selectively blocks DNA-binding by Trypanosoma brucei replication protein A1. *Nat Commun,* 14**,** 4390.

MÜLLER, L. S., COSENTINO, R. O., FÖRSTNER, K. U., GUIZETTI, J., WEDEL, C., KAPLAN, N., JANZEN, C. J., ARAMPATZI, P., VOGEL, J. & STEINBISS, S. 2018. Genome organization and DNA accessibility control antigenic variation in trypanosomes. *Nature,* 563**,** 121-125.

NANAVATY, V., SANDHU, R., JEHI, S. E., PANDYA, U. M. & LI, B. 2017. Trypanosoma brucei RAP1 maintains telomere and subtelomere integrity by suppressing TERRA and telomeric RNA: DNA hybrids. *Nucleic acids research,* 45**,** 5785-5796.

NARAYANAN, M. S. & RUDENKO, G. 2013. TDP1 is an HMG chromatin protein facilitating RNA polymerase I transcription in African trypanosomes. *Nucleic acids research,* 41**,** 2981-2992.

NAVARRO, M. & GULL, K. 2001. A pol I transcriptional body associated with VSG mono-allelic expression in Trypanosoma brucei. *Nature,* 414**,** 759-63.

NGUYEN, T. H. D., TAM, J., WU, R. A., GREBER, B. J., TOSO, D., NOGALES, E. & COLLINS, K. 2018. Cryo-EM structure of substrate-bound human telomerase holoenzyme. *Nature,* 557**,** 190-195.

NGUYEN, T. N., MULLER, L. S., PARK, S. H., SIEGEL, T. N. & GUNZL, A. 2014. Promoter occupancy of the basal class I transcription factor A differs strongly between active and silent VSG expression sites in Trypanosoma brucei. *Nucleic Acids Res,* 42**,** 3164-76.

NIKITINA, T. & WOODCOCK, C. L. 2004. Closed chromatin loops at the ends of chromosomes. *The Journal of cell biology,* 166**,** 161-165.

OBERHOLZER, M., MORAND, S., KUNZ, S. & SEEBECK, T. 2005. A vector series for rapid PCR-mediated C-terminal in situ tagging of Trypanosoma brucei genes. *Molecular and biochemical parasitology,* 145**,** 117-120.

OUNA, B. A., NYAMBEGA, B., MANFUL, T., HELBIG, C., MALES, M., FADDA, A. & CLAYTON, C. 2012. Depletion of trypanosome CTR9 leads to gene expression defects. *PLoS One,* 7**,** e34256.

OVERATH, P., STIERHOF, Y. D. & WIESE, M. 1997. Endocytosis and secretion in trypanosomatid parasites - Tumultuous traffic in a pocket. *Trends Cell Biol,* 7**,** 27-33.

PAVANI, R. S., DA SILVA, M. S., FERNANDES, C. A., MORINI, F. S., ARAUJO, C. B., FONTES, M. R., SANT'ANNA, O. A., MACHADO, C. R., CANO, M. I., FRAGOSO, S. P. & ELIAS, M. C. 2016. Replication Protein A Presents Canonical Functions and Is Also Involved in the Differentiation Capacity of Trypanosoma cruzi. *PLoS Negl Trop Dis,* 10**,** e0005181.

PAVANI, R. S., VITARELLI, M. O., FERNANDES, C. A. H., MATTIOLI, F. F., MORONE, M., MENEZES, M. C., FONTES, M. R. M., CANO, M. I. N. & ELIAS, M. C. 2018. Replication Protein A-1 Has a Preference for the Telomeric G-rich Sequence in Trypanosoma cruzi. *J Eukaryot Microbiol,* 65**,** 345-356.

PAYS, E., LIPS, S., NOLAN, D., VANHAMME, L. & PÉREZ-MORGA, D. 2001. The VSG expression sites of Trypanosoma brucei: multipurpose tools for the adaptation of the parasite to mammalian hosts. *Molecular and biochemical parasitology,* 114**,** 1-16.

PENA, A. C., PIMENTEL, M. R., MANSO, H., VAZ-DRAGO, R., PINTO-NEVES, D., ARESTA-BRANCO, F., RIJO-FERREIRA, F., GUEGAN, F., PEDRO COELHO, L., CARMO-FONSECA, M., BARBOSA-MORAIS, N. L. & FIGUEIREDO, L. M. 2014. Trypanosoma brucei histone H1 inhibits RNA polymerase I transcription and is important for parasite fitness in vivo. *Mol Microbiol,* 93**,** 645-63.

POLÁKOVÁ, E., ZÁHONOVÁ, K., ALBANAZ, A. T., BUTENKO, A., LUKEŠ, J. & YURCHENKO, V. 2021. Diverse telomeres in trypanosomatids. *Parasitology,* 148**,** 1254-1270.

RABBANI, M., TONINI, M. L., AFRIN, M. & LI, B. 2022. POLIE suppresses telomerase-mediated telomere G-strand extension and helps ensure proper telomere C-strand synthesis in trypanosomes. *Nucleic acids research,* 50**,** 2036-2050.

RAI, R., CHEN, Y., LEI, M. & CHANG, S. 2016. TRF2-RAP1 is required to protect telomeres from engaging in homologous recombination-mediated deletions and fusions. *Nature communications,* 7**,** 1-13.

RAPPSILBER, J., MANN, M. & ISHIHAMA, Y. 2007. Protocol for micro-purification, enrichment, pre-fractionation and storage of peptides for proteomics using StageTips. *Nature protocols,* 2**,** 1896-1906.

REDMOND, S., VADIVELU, J. & FIELD, M. C. 2003. RNAit: an automated web-based tool for the selection of RNAi targets in Trypanosoma brucei. *Molecular and biochemical parasitology,* 128**,** 115-118.

REDON, S., REICHENBACH, P. & LINGNER, J. 2010. The non-coding RNA TERRA is a natural ligand and direct inhibitor of human telomerase. *Nucleic acids research,* 38**,** 5797-5806.

REIS, H. 2017. *Characterization of telomere protein complexes in Trypanosoma brucei.* Universität Würzburg.

REIS, H., SCHWEBS, M., DIETZ, S., JANZEN, C. J. & BUTTER, F. 2018. TelAP1 links telomere complexes with developmental expression site silencing in African trypanosomes. *Nucleic Acids Res,* 46**,** 2820-2833.

RIBES-ZAMORA, A., INDIVIGLIO, S. M., MIHALEK, I., WILLIAMS, C. L. & BERTUCH, A. A. 2013. TRF2 interaction with Ku heterotetramerization interface gives insight into c-NHEJ prevention at human telomeres. *Cell reports,* 5**,** 194-206.

RICO, E., ROJAS, F., MONY, B. M., SZOOR, B., MACGREGOR, P. & MATTHEWS, K. R. 2013. Bloodstream form pre-adaptation to the tsetse fly in Trypanosoma brucei. *Front Cell Infect Microbiol,* 3**,** 78.

ROAKE, C. M. & ARTANDI, S. E. 2020. Regulation of human telomerase in homeostasis and disease. *Nature reviews Molecular cell biology,* 21**,** 384-397.

RODITI, I., SCHWARZ, H., PEARSON, T. W., BEECROFT, R. P., LIU, M. K., RICHARDSON, J. P., BÜHRING, H.-J., PLEISS, J., BÜLOW, R. & WILLIAMS, R. O. 1989. Procyclin gene expression and loss of the variant surface glycoprotein during differentiation of Trypanosoma brucei. *The Journal of cell biology,* 108**,** 737-746.

ROSE, C., CASAS-SÁNCHEZ, A., DYER, N. A., SOLÓRZANO, C., BECKETT, A. J., MIDDLEHURST, B., MARCELLO, M., HAINES, L. R., LISACK, J. & ENGSTLER, M. 2020. Trypanosoma brucei colonizes the tsetse gut via an immature peritrophic matrix in the proventriculus. *Nature microbiology,* 5**,** 909-916.

RUDD, S. G., GLOVER, L., JOZWIAKOWSKI, S. K., HORN, D. & DOHERTY, A. J. 2013. PPL2 translesion polymerase is essential for the completion of chromosomal DNA replication in the African trypanosome. *Mol Cell,* 52**,** 554-65.

RUDENKO, G., BISHOP, D., GOTTESDIENER, K. & VAN DER PLOEG, L. H. 1989. Alpha-amanitin resistant transcription of protein coding genes in insect and bloodstream form Trypanosoma brucei. *EMBO J,* 8**,** 4259-63.

SAHA, A., GAURAV, A. K., PANDYA, U. M., AFRIN, M., SANDHU, R., NANAVATY, V., SCHNUR, B. & LI, B. 2021. Tb TRF suppresses the TERRA level and regulates the cell cycle-dependent TERRA foci number with a TERRA binding activity in its C-terminal Myb domain. *Nucleic acids research,* 49**,** 5637-5653.

SAHA, A., NANAVATY, V. P. & LI, B. 2020. Telomere and subtelomere R-loops and antigenic variation in trypanosomes. *Journal of molecular biology,* 432**,** 4167-4185.

SALE, J. E. 2013. Translesion DNA synthesis and mutagenesis in eukaryotes. *Cold Spring Harbor perspectives in biology,* 5**,** a012708.

SANDHU, R. & LI, B. 2017. Telomerase activity is required for the telomere G-overhang structure in Trypanosoma brucei. *Scientific reports,* 7**,** 1-13.

SANDHU, R., SANFORD, S., BASU, S., PARK, M., PANDYA, U. M., LI, B. & CHAKRABARTI, K. 2013. A trans-spliced telomerase RNA dictates telomere synthesis in Trypanosoma brucei. *Cell research,* 23**,** 537-551.

SCHIMANSKI, B., NGUYEN, T. N. & GUNZL, A. 2005a. Highly efficient tandem affinity purification of trypanosome protein complexes based on a novel epitope combination. *Eukaryot Cell,* 4**,** 1942-50.

SCHIMANSKI, B., NGUYEN, T. N. & GÜNZL, A. 2005b. Highly efficient tandem affinity purification of trypanosome protein complexes based on a novel epitope combination. *Eukaryotic cell,* 4**,** 1942-1950.

SCHOLZ, J., BESIR, H., STRASSER, C. & SUPPMANN, S. 2013. A new method to customize protein expression vectors for fast, efficient and background free parallel cloning. *BMC biotechnology,* 13**,** 1-11.

SCHULZ, D., MUGNIER, M. R., PAULSEN, E. M., KIM, H. S., CHUNG, C. W., TOUGH, D. F., RIOJA, I., PRINJHA, R. K., PAPAVASILIOU, F. N. & DEBLER, E. W. 2015. Bromodomain Proteins Contribute to Maintenance of Bloodstream Form Stage Identity in the African Trypanosome. *PLoS Biol,* 13**,** e1002316.

SCHULZ, D., ZARINGHALAM, M., PAPAVASILIOU, F. N. & KIM, H. S. 2016. Base J and H3.V Regulate Transcriptional Termination in Trypanosoma brucei. *PLoS Genet,* 12**,** e1005762.

SCHUSTER, S., LISACK, J., SUBOTA, I., ZIMMERMANN, H., REUTER, C., MUELLER, T., MORRISWOOD, B. & ENGSTLER, M. 2021. Unexpected plasticity in the life cycle of Trypanosoma brucei. *Elife,* 10**,** e66028.

SHAPIRO, T. A. & ENGLUND, P. T. 1995. The structure and replication of kinetoplast DNA. *Annual review of microbiology,* 49**,** 117-143.

SHAW, P. L., MCADAMS, N. M., HAST, M. A., AMMERMAN, M. L., READ, L. K. & SCHUMACHER, M. A. 2015. Structures of the T. brucei kRNA editing factor MRB1590 reveal unique RNA-binding pore motif contained within an ABC-ATPase fold. *Nucleic acids research,* 43**,** 7096-7109.

SIEGEL, T. N., GUNASEKERA, K., CROSS, G. A. & OCHSENREITER, T. 2011. Gene expression in Trypanosoma brucei: lessons from high-throughput RNA sequencing. *Trends Parasitol,* 27**,** 434-41.

SIEGEL, T. N., HEKSTRA, D. R., KEMP, L. E., FIGUEIREDO, L. M., LOWELL, J. E., FENYO, D., WANG, X., DEWELL, S. & CROSS, G. A. 2009. Four histone variants mark the boundaries of polycistronic transcription units in Trypanosoma brucei. *Genes Dev,* 23**,** 1063-76.

SIEGEL, T. N., HEKSTRA, D. R., WANG, X., DEWELL, S. & CROSS, G. A. 2010. Genome-wide analysis of mRNA abundance in two life-cycle stages of Trypanosoma brucei and identification of splicing and polyadenylation sites. *Nucleic Acids Res,* 38**,** 4946-57.

SIEGEL, T. N., TAN, K. S. & CROSS, G. A. 2005. Systematic study of sequence motifs for RNA trans splicing in Trypanosoma brucei. *Mol Cell Biol,* 25**,** 9586-94.

SMITH, T. K., BRINGAUD, F., NOLAN, D. P. & FIGUEIREDO, L. M. 2017. Metabolic reprogramming during the Trypanosoma brucei life cycle. *F1000Research,* 6.

STEVERDING, D. 2008. The history of African trypanosomiasis. *Parasites & vectors,* 1**,** 1-8.

STROS, M., LAUNHOLT, D. & GRASSER, K. D. 2007. The HMG-box: a versatile protein domain occurring in a wide variety of DNA-binding proteins. *Cell Mol Life Sci,* 64**,** 2590-606.

SUROVTSEVA, Y. V., CHURIKOV, D., BOLTZ, K. A., SONG, X., LAMB, J. C., WARRINGTON, R., LEEHY, K., HEACOCK, M., PRICE, C. M. & SHIPPEN, D. E. 2009. Conserved telomere maintenance component 1 interacts with STN1 and maintains chromosome ends in higher eukaryotes. *Molecular cell,* 36**,** 207-218.

TAYLOR, J. E. & RUDENKO, G. 2006. Switching trypanosome coats: what's in the wardrobe? *Trends Genet,* 22**,** 614-20.

THIVOLLE, A., MEHNERT, A.-K., TIHON, E., MCLAUGHLIN, E., DUJEANCOURT-HENRY, A. & GLOVER, L. 2021. DNA double strand break position leads to distinct gene expression changes and regulates VSG switching pathway choice. *PLoS pathogens,* 17**,** e1010038.

THON, G., BALTZ, T. & EISEN, H. 1989. Antigenic diversity by the recombination of pseudogenes. *Genes & development,* 3**,** 1247-1254.

TOMASKA, L., WILLCOX, S., SLEZAKOVA, J., NOSEK, J. & GRIFFITH, J. D. 2004. Taz1 binding to a fission yeast model telomere: formation of telomeric loops and higher order structures. *Journal of Biological Chemistry,* 279**,** 50764-50772.

TOUBIANA, S. & SELIG, S. 2018. DNA: RNA hybrids at telomeres–when it is better to be out of the (R) loop. *The FEBS journal,* 285**,** 2552-2566.

URWYLER, S., STUDER, E., RENGGLI, C. K. & RODITI, I. 2007. A family of stage‐specific alanine‐rich proteins on the surface of epimastigote forms of Trypanosoma brucei. *Molecular microbiology,* 63**,** 218-228.

VAISMAN, A. & WOODGATE, R. 2017. Translesion DNA polymerases in eukaryotes: what makes them tick? *Crit Rev Biochem Mol Biol,* 52**,** 274-303.

VAN STEENSEL, B. & DE LANGE, T. 1997. Control of telomere length by the human telomeric protein TRF1. *Nature,* 385**,** 740-743.

VAN XONG, H., VANHAMME, L., CHAMEKH, M., CHIMFWEMBE, C. E., VAN DEN ABBEELE, J., PAYS, A., VAN MEIRVENNE, N., HAMERS, R., DE BAETSELIER, P. & PAYS, E. 1998. A VSG expression site–associated gene confers resistance to human serum in Trypanosoma rhodesiense. *Cell,* 95**,** 839-846.

VASSELLA, E., REUNER, B., YUTZY, B. & BOSHART, M. 1997. Differentiation of African trypanosomes is controlled by a density sensing mechanism which signals cell cycle arrest via the cAMP pathway. *Journal of cell science,* 110**,** 2661-2671.

VAUGHAN, S. & GULL, K. 2015. Basal body structure and cell cycle-dependent biogenesis in Trypanosoma brucei. *Cilia,* 5**,** 5.

VINK, C., RUDENKO, G. & SEIFERT, H. S. 2012. Microbial antigenic variation mediated by homologous DNA recombination. *FEMS microbiology reviews,* 36**,** 917-948.

WANG, F., PODELL, E. R., ZAUG, A. J., YANG, Y., BACIU, P., CECH, T. R. & LEI, M. 2007. The POT1–TPP1 telomere complex is a telomerase processivity factor. *Nature,* 445**,** 506-510.

WANG, Q. P., KAWAHARA, T. & HORN, D. 2010. Histone deacetylases play distinct roles in telomeric VSG expression site silencing in African trypanosomes. *Molecular microbiology,* 77**,** 1237-1245.

WANG, Y. & CHAI, W. 2018. Pathogenic CTC1 mutations cause global genome instabilities under replication stress. *Nucleic acids research,* 46**,** 3981-3992.

WEDEL, C., FORSTNER, K. U., DERR, R. & SIEGEL, T. N. 2017. GT-rich promoters can drive RNA pol II transcription and deposition of H2A.Z in African trypanosomes. *EMBO J,* 36**,** 2581-2594.

WICKSTEAD, B., ERSFELD, K. & GULL, K. 2004. The small chromosomes of Trypanosoma brucei involved in antigenic variation are constructed around repetitive palindromes. *Genome Res,* 14**,** 1014-24.

WOLD, M. S. 1997. Replication protein A: a heterotrimeric, single-stranded DNA-binding protein required for eukaryotic DNA metabolism. *Annu Rev Biochem,* 66**,** 61-92.

YANG, Q., ZHENG, Y.-L. & HARRIS, C. C. 2005. POT1 and TRF2 cooperate to maintain telomeric integrity. *Molecular and cellular biology,* 25**,** 1070-1080.

YANG, X., FIGUEIREDO, L. M., ESPINAL, A., OKUBO, E. & LI, B. 2009. RAP1 is essential for silencing telomeric variant surface glycoprotein genes in Trypanosoma brucei. *Cell,* 137**,** 99-109.

ZHOU, Q., LEE, K. J., KURASAWA, Y., HU, H., AN, T. & LI, Z. 2018. Faithful chromosome segregation in Trypanosoma brucei requires a cohort of divergent spindle-associated proteins with distinct functions. *Nucleic acids research,* 46**,** 8216-8231.

ZOMERDIJK, J., OUELLETTE, M., TEN ASBROEK, A., KIEFT, R., BOMMER, A., CLAYTON, C. E. & BORST, P. 1990. The promoter for a variant surface glycoprotein gene expression site in Trypanosoma brucei. *The EMBO journal,* 9**,** 2791-2801.

APPENDIX

Supplementary tables

Table S 1: List of candidates including curated GO components, functions and processes using TriTrypDB.

Name	Input Gene ID	Product Description	Curated GO Components	Curated GO Functions	Curated GO Processes
p53	Tb927.2.6100	hypothetical protein, conserved	cytoplasm; kinetoplast; mitochondrion	telomeric DNA binding	mitochondrial RNA processing; mitochondrial genome maintenance
MRB1590	Tb927.3.1590	mitochondrial RNA binding complex 1 subunit	cytoplasm; mitochondrial mRNA editing complex; mitochondrion; nucleoplasm	RNA binding; mRNA binding	cytidine to uridine editing; mRNA stabilization; mitochondrial RNA processing; mitochondrial mRNA processing
p105	Tb927.3.2140	PHD finger domain protein 4	nucleoplasm; nucleus		
p33	Tb927.3.5150	exonuclease, putative	cytoplasm	telomeric DNA binding	
RPA2	Tb927.5.1700	replication Factor A 28 kDa subunit, putative	DNA replication factor A complex; chromosome, telomeric region; nucleoplasm; nucleus; site of double-strand break	single-stranded DNA binding; telomeric DNA binding	DNA repair; DNA replication; double-strand break repair via homologous recombination; nucleotide-excision repair
UPF1	Tb927.5.2140	regulator of nonsense transcripts 1	cytoplasm; cytoplasmic stress granule	RNA binding; RNA helicase activity	nuclear-transcribed mRNA catabolic process, nonsense-mediated decay
p35	Tb927.6.1190	Plus-3 domain/Zinc finger, C3HC4 type (RING finger), putative	cell tip; ciliary basal body; ciliary pro-basal body; transport vesicle		
TelAP2	Tb927.6.4330	telomere-associated protein	nucleoplasm; nucleus; telomere-telomerase complex	telomeric DNA binding	
PIF5	Tb927.8.3560	DNA repair and recombination helicase protein PIF5	cytoplasm; mitochondrion; nucleolus; nucleoplasm; replication fork	5'-3' DNA helicase activity	DNA duplex unwinding; DNA replication; Okazaki fragment processing; DNA replication, removal of RNA primer
PABP2	Tb927.9.10770	polyadenylate-binding protein 2	P-body; cytoplasm; cytoplasmic stress granule; cytosol; nuclear stress granule; nucleus; polysome; ribonucleoprotein complex	RNA binding; mRNA 3'-UTR binding; poly(A) binding; poly(U) RNA binding; telomeric DNA binding	RNA processing; posttranscriptional regulation of gene expression

Name	Input Gene ID	Product Description	Curated GO Components	Curated GO Functions	Curated GO Processes
TelAP3	Tb927.9.4000	hypothetical protein, conserved	cytoplasm; nucleus; telomere-telomerase complex	telomeric DNA binding	
p52	Tb927.9.5020	HMG-box domain containing protein, putative	kinetoplast	telomeric DNA binding	
DRBD3	Tb927.9.8740	Double RNA binding domain protein 3	cytoplasm;cytosol;nucleoplasm;nucleus;polysome;ribonucleoprotein complex	mRNA 3'-UTR binding; mRNA binding; telomeric DNA binding	RNA processing; mRNA cis splicing, via spliceosome; mRNA stabilization; mRNA trans splicing, via spliceosome; posttranscriptional regulation of gene expression
p88	Tb927.10.1900	DNA topoisomerase IA, putative	antipodal site; cytoplasm	DNA binding; DNA topoisomerase type I (single strand cut, ATP-independent) activity	DNA modification; DNA topological change
p38	Tb927.10.2200	hypothetical protein, conserved	cytoplasm	telomeric DNA binding	
PPL2	Tb927.10.2520	PrimPol-like protein 2	nucleoplasm; nucleus; site of double-strand break; telomere-telomerase complex	DNA primase activity; DNA-directed DNA polymerase activity; telomeric DNA binding	regulation of G2/M transition of mitotic cell cycle; response to UV; response to oxidative stress; translesion synthesis
p34	Tb927.10.4220	hypothetical protein, conserved		telomeric DNA binding	
XRND	Tb927.10.6220	5'-3' exoribonuclease D	nucleolus; nucleus	5'-3' exoribonuclease activity; RNA binding; exonuclease activity; telomeric DNA binding	RNA processing; nuclear-transcribed mRNA catabolic process
p97	Tb927.10.9780	ATP-dependent DEAD/H RNA helicase, putative	nucleolus; nucleus	ATP binding; helicase activity	nucleobase-containing compound metabolic process
p68	Tb927.11.16120	hypothetical protein, conserved	kinetoplast; transport vesicle	telomeric DNA binding	
NOP89	Tb927.11.6790	Nucleolar protein 89	PeBoW complex; nucleolus; nucleus; preribosome, large subunit precursor; spindle	ribonucleoprotein complex binding	maturation of LSU-rRNA from tricistronic rRNA transcript (SSU-rRNA, 5.8S rRNA, LSU-rRNA)
p77	Tb927.11.9920	polyubiquitin, putative	ciliary plasm; cytoplasm; flagella connector; nuclear lumen; nucleus; transport vesicle	protein tag; ubiquitin protein ligase binding	cellular protein modification process; modification-dependent protein catabolic process; protein ubiquitination

Table S 2: List of MS-identified surface VSGs 0 h and Xh (dependent on cell line) post depletion of the protein of interest by RNAi. Wt cells served as control. VSG abundance displayed as average percentage of the LFQ intensities. Induction of RNAi via tetracycline is shown as + (+ tetracycline, induced depletion) or – (- tetracycline, uninduced).

Gene ID	WT	*Tb*RAP1		PolIE		TelAP2		PABP2		PPL2		RPA2		XRND		p53		p77		p97		MRB1590	
tet		+	-	+	-	+	-	+	-	+	-	+	-	+	-	+	-	+	-	+	-	+
VSG-3	0.00101678	0.38785517	0.0105473	0.00118667	0	0	0	0	0	0	0	0	0.0021585	0.0116208	0	0	0	0	0	0	0	0
VSG-6	0	0.03663514	0.0127133	0.00153159	0	0	0	0	0	0	0	0	0	0	0	0	0	0	0	0	0	0
VSG-8	0.11932987	0.24994071	0.0353474	0.30234461	0.203	1.218	0.14033755	0.41992657	0.19893255	0.24987103	0.142	0.485	0.09090837	0.45110981	0.131	0.142	0.43785624	0.20233229	0.216	0.694	0.205	0.116
VSG-9	0.0017512	0.03346351	0.01179907	0.00082654	0.004	0.003	0	0	0	0	0.004	0	0	0	0.006	0.003	0	0	0.004	0.002	0.002	0.004
VSG-11	0.00746731	0.08148097	0.0134489	0.0025911	0	0	0	0	0	0	0	0	0.00641813	0.16160219	0	0	0	0	0	0	0	0
VSG-13	0.00130416	0	0	0	0	0	0	0	0	0	0	0	0	0	0	0	0	0	0	0	0	0
VSG-15	0.00144627	0.08278183	0.0117917	0.00094589	0.518	1.25	0	0	0	0	0.004	0.002	0.00260999	0.00275899	0.005	0.003	0	0	0	0	0.003	0.003
VSG-17	0.00136344	0.05383726	0.0113481 6	0.00079244	0.012	0.026	0	0	0	0	0.005	0.013	0.01986952	0.07768205	0.005	0.002	0.00969705	0.00336444	0.007	0.013	0.013	0.005
VSG-18	0.00130758	0	0	0	0.006	0.029	0	0	0	0	0.01	0.072	0.00341031	0.001429	0.004	0.004	0.02687562	0.02160755	0.008	0	0.018	0.004
VSG-21	0	0.02641636	0.0121216 2	0.00083763	0	0	0	0	0	0	0	0	0	0	0	0	0	0	0	0	0	0
VSG-397	0.00127315	0.44285383	0.0120550 7	0.73136181	0.006	0.112	0	0	0	0	0.005	0.118	0	0	0.005	0.003	0.00284347	0.0031584	0.006	0.023	0.005	0.004
VSG-531	0.00423909	2.88690892	0.0117581 8	0.92373424	0.007	0.233	0.00164881	0.00871479	0.00302117	0.00534161	0.003	0.095	0.00204584	0.00596058	0.004	0.002	0.00768475	0.00662983	0.006	0.069	0.012	0.004

Gene ID	WT	TbRAP1	PolIE	TelAP2	PABP2	PPL2	RPA2	XRND	p53	p77	p97	MRB1590	
VSG-559	0	0.002 62234	0.010 91402	0.018 1287	0	0	0	0	0	0	0	0	0
VSG-582	0	0.001 99249	0.011 86029	0.002 88371	0	0	0	0	0	0	0	0	0
VSG-636	0.001 06851	0.006 0846	0.011 87796	0.273 81782	0.005	0.089	0	0	0	0.005	0.003	0	0.004	0.004	0.004	0.003	0.004
VSG-653	0.005 04023	2.871 4331	0.016 5866	0.434 93766	0.006	0.012	0	0	0.004	0.13	0	0.005	0.006	0.002 42511	0.003 45618	0.009	0.041	0	0
VSG-1954	0.002 15737	0.002 43598	0.012 43674	0.508 35753	0.005	0.205	0	0	0.005	0.018	0	0.005	0.003	0	0	0	0.006	0.003	0.004
VSG-3591	0.001 08562	0.022 11819	0.016 14987	0.001 26929	0.009	0.031	0	0	0.004	0	0	0.006	0.003	0	0	0	0	0.004	0.004
VSG-322	0.000 97712	1.040 07367	0.013 18077	0.002 11066	0.003	0.407	0	0	0.004	0.001	0	0.005	0.002	0	0	0.003	0.006	0.002	0.007
VSG-336	0.059 18313	0.001 87603	0.011 20139	0.184 56727	0.063	0.109	0.001 87047	0.008 18801	0.128 42066	0.113 58864	0.075	0.065	0.083 809	0.027 7667	0.079	0.006 46798	0.005 75661	0.067	0.108	0.036	0.033
VSG-775	0.001 45107	0.027 09208	0.013 09226	0.001 00339	0.003	0.03	0	0	0	0	0.004	0.057	0	0	0.003	0	0	0.004	0	0.003	0.003
VSG-1828	0.014 37759	0.006 8113	0.014 36931	0.000 85103	0.01	0.01	0	0	0.002 95529	0.028 13829	0.013	0.019	0.003 44309	0.004 70769	0.021	0.119 09426	0.084 71576	0.007	0.023	0.014	0.003
VSG-3233	0.003 05552	0	0	0	0.004	0	0	0	0	0	0.005	0.002	0.002 59257	0.002 28335	0.005	0.003	0.011 62784	0.011 21516	0.006	0	0.007	0.006
VSG-417	0	0.051 84699	0.011 37466	0.001 40063	0	0	0	0	0	0	0	0	0	0	0	0	0	0	0	0	0	0
VSG-545	0	0.003 31984	0.010 31684	0.037 45916	0.004	0.004	0	0	0.088 2183	0.083 83535	0.005	0.007	0.002 87853	0.002 44417	0.005	0.003	0.011 80134	0.022 11155	0.004	0.002	0.003	0.003
VSG-1158	0	0	0	0	0.004 9926	0.003 40044	0	0	0	0.003 66611	0.005	0.001 48208	0	0	0.004 41108	0.002 49496	0	0.006 40182	0.004 34303	0.004	0.002 92431	0.003 12735
VSG-1666	0.008 18213	0	0	0	0.008	0.008	0	0	0.004 21669	0.008 13385	0.004	0.001	0	0	0.004	0.002	0.009 08139	0.008 05387	0.005	0.006	0.006	0.006
VSG-1747	0.026 77157	0	0	0	0.029	0.027	0.021 84965	0.011 18363	0.010 57193	0.006 70392	0.038	0.02	0.009 99565	0.007 33637	0.026	0.011	0.031 90679	0.046 14278	0.034	0.007	0.034	0.028

Gene ID	WT	*Tb*RAP1		PolIE		TelAP2		PABP2		PPL2		RPA2		XRND		p53		p77		p97		MRB1590	
VSG-2085	0.01061203	0	0	0	0.003	0	0	0	0.03332391	0.01857995	0.004	0	0.00243004	0.00206685	0.004	0.01	0	0	0	0	0.003	0.004
VSG-3036	0	0	0	0	0	0	0	0	0	0	0	0	0.00288489	0.00203712	0	0	0	0	0	0	0	0
VSG-3240	0.02938924	0	0	0	0.045	0.055	0.00833237	0.01117425	0.05127759	0.06262524	0.049	0.021	0.01988848	0.02209161	0.034	0.065	0.05757941	0.06400839	0.042	0.047	0.043	0.055
VSG-3255	0	0	0	0	0.003	0.003	0	0	0.00428421	0.00484436	0.004	0.002	0	0	0.005	0.004	0.00232096	0.00376364	0.005	0.006	0.007	0.006

Table S 3: List of MS-identified surface VSGs 0 h and Xh post depletion of the protein of interest by RNAi. Wt cells served as control. VSG abundance displayed as average percentage of the LFQ intensities. Induction of RNAi via tetracycline is shown as + (+ tetracycline, induced depletion) or – (- tetracycline, uninduced cell line).

Gene ID	NOP89		PIF5		TelAP3		UPF1		p33		p34		p35		p38		p52		p68		p88		p105	
tet	-	+	-	+	-	+	-	+	-	+	-	+	-	+	-	+	-	+	-	+	-	+	-	+
VSG-3	0.00287394	0.00349316	0.00362504	0.00349799	0	0	0	0	0.00395891	0.00405061	0.00367061	0.00385906	0.00401363	0.00345149	0.00364126	0.00202877	0.00359185	0.00320038	0.00345329	0.00323937	0.00353991	0.00261392	0.00360462	0.00307996
VSG-6	0	0	0	0	0	0	0	0	0	0	0	0	0	0	0	0	0	0	0	0	0	0	0	0
VSG-8	0.11864844	0.12348263	0.07378911	0.10945436	0.08870135	0.13541832	0.04053649	0.06371466	0.11661196	0.13259244	0.04338691	0.09784126	0.08601741	0.11917914	0.10009963	0.09696376	0.02462015	0.01601866	0.27589334	0.20265233	0.14589159	0.13000666	0.13073427	0.20740495
VSG-9	0	0	0	0	0	0	0	0	0	0	0	0	0	0	0	0	0	0	0	0	0	0	0	0
VSG-11	0.004428 4	0.00741364	0.00273281	0.00618021	0	0	0	0	0.00386691	0.00486414	0.00321814	0.00433 89	0.00400366	0.00321351	0.00335501	0.00278979	0.00294098	0.00294289	0.00252163	0.00834434	0.01080129	0.00758141	0.00550 39	0.00473437
VSG-13	0	0	0	0	0	0	0	0	0	0	0	0	0	0	0	0	0	0	0	0	0	0	0	0

Gene ID	NOP89		PIF5		TelAP3		UPF1		p33		p34		p35		p38		p52		p68		p88		p105	
VSG-15	0.002972	0.003412	0.004055	0.002816	0	0	0	0	0.004041	0.003407	0.003773	0.004174	0.003546	0.004200	0.004195	0.002582	0.003144	0.003832	0.002746	0.003571	0.003484	0.002008	0.002436	0.003389
VSG-17	0.002806	0.002867	0.003177	0.003912	0	0	0	0	0.003522	0.003821	0.007941	0.006456	0.003723	0.002884	0.004320	0.002171	0.003948	0.002973	0.002965	0.003630	0.045463	0.043221	0.012891	0.016081
VSG-18	0.003354	0.003381	0.003770	0.003337	0	0	0.002676	0.035398	0.003801	0.004519	0.003589	0.003747	0.003402	0.003035	0.003890	0.002954	0.004229	0.003366	0.003217	0.003295	0.047987	0.017318	0.002839	0.002765
VSG-21	0	0	0	0	0	0	0	0	0	0	0	0	0	0	0	0	0	0	0	0	0	0	0	0
VSG-397	0	0	0	0	0	0	0	0	0	0	0	0	0	0	0	0	0	0	0	0	0	0	0	0
VSG-531	0.002728	0.003406	0.003642	0.003528	0	0	0	0	0.003855	0.004319	0.002950	0.004042	0.003915	0.004187	0.003454	0.002303	0.003755	0.003835	0.003398	0.002814	0.002861	0.002772	0.002483	0.003554
VSG-559	0	0	0	0	0	0	0	0	0	0	0	0	0	0	0	0	0	0	0	0	0	0	0	0
VSG-582	0	0	0	0	0	0	0	0	0	0	0	0	0	0	0	0	0	0	0	0	0	0	0	0
VSG-636	0	0	0	0	0	0	0	0	0	0	0	0	0	0	0	0	0	0	0	0	0	0	0	0
VSG-653	0	0	0	0	0	0	0	0	0	0	0	0	0	0	0	0	0	0	0	0	0	0	0	0
VSG-1954	0	0	0	0	0	0	0	0	0	0	0	0	0	0	0	0	0	0	0	0	0	0	0	0
VSG-3591	0	0	0	0	0	0	0	0	0	0	0	0	0	0	0	0	0	0	0	0	0	0	0	0
VSG-322	0	0	0	0	0	0	0	0	0	0	0	0	0	0	0	0	0	0	0	0	0	0	0	0

Gene ID	NOP89		PIF5		TelAP3		UPF1		p33		p34		p35		p38		p52		p68		p88		p105	
VSG-336	0.02	0.05	0.05	0.05	0.01	0.02	0.06	0.02	0.02	0.03	0.02	0.01	0.04	0.04	0.04	0.04	0.00	0.00	0.05	0.06	0.06	0.05	0.07	0.04
	9998	0223	8562	4311	9029	3766	5855	3447	6638	7422	8342	0570	9900	9560	9508	1762	3425	3666	3895	4906	9388	9666	7189	8661
	24	22		26	23	99	26	24	06	86	66	2	44	33	93	76	47	79	3	41	74	37	31	85
VSG-775	0	0	0	0	0	0	0	0	0	0	0	0	0	0	0	0	0	0	0	0	0	0	0	0
VSG-1828	0.00	0.00	0.00	0.00	0	0	0	0	0.00	0.00	0.00	0.00	0.00	0.00	0.00	0.00	0.00	0.00	0.00	0.00	0.00	0.00	0.00	0.00
	2982	3246	3934	3195					9425	8498	3996	3578	3872	2793	3522	2784	3470	3469	3131	3429	2591	2163	2483	2553
	56	4	07	85					24	74	03	65	35	19	57	37	94	19	9	99	45	54	19	96
VSG-3233	0.00	0.00	0.00	0.00	0	0	0	0	0.00	0.00	0.00	0.00	0.00	0.00	0.00	0.00	0.00	0.00	0.00	0.00	0.00	0.00	0.00	0.00
	3064	3333	3532	2861					3668	3695	4049	3721	3910	4224	3156	2691	3104	3521	3407	2550	3559	1916	2868	3675
	92	14	53	38					42	36	52	24	51	38	18	99	09	05	83	11	19	88	09	19
VSG-417	0	0	0	0	0	0	0	0	0	0	0	0	0	0	0	0	0	0	0	0	0	0	0	0
VSG-5452785	0.00	0.00	0.00	0.00	0	0	0.05	0.02	0.00	0.00	0.00	0.00	0.00	0.00	0.00	0.00	0.00	0.00	0.00	0.00	0.00	0.00	0.04	0.03
	2785	3376	3775	2515			4757	6028	3880	4066	4551	3590	3704	3027	3663	2673	4239	3096	2884	3737	3893	2480	7663	8867
	74	43	36	43			25	42	8	08	3	5	83	7	85	91	46	65	39	08	01	9	53	69
VSG-1158	0	0	0	0	0	0	0	0	0	0	0	0	0	0	0	0	0	0	0	0	0	0	0	0
VSG-1666	0	0	0	0	0	0	0	0	0	0	0	0	0	0	0	0	0	0	0	0	0	0	0	0
VSG-1747	0.01	0.01	0.00	0.00	0	0	0	0	0.01	0.02	0.00	0.00	0.02	0.02	0.02	0.01	0.01	0.01	0.01	0.01	0.02	0.01	0.01	0.00
	3845	7532	4665	3424					6268	1467	5927	4872	5365	2292	5233	8449	9245	1546	4370	4596	0325	5823	2295	6912
	01	46	41	77					1	04	7	83	15	95	11	18	47	96	14	04	92	91	43	12
VSG-2085	0.00	0.00	0.00	0.00	0	0	0	0	0.00	0.00	0.00	0.00	0.00	0.00	0.00	0.00	0.00	0.00	0.00	0.00	0.00	0.00	0.00	0.00
	3682	3805	3429	3004					3273	3561	3418	4369	4753	3095	4263	2733	5159	3849	2365	3207	5472	2321	3595	3157
	57	54	08	2					23	83	24	96	31	43	45	12	1	71	36	79	47	54	75	21
VSG	0.00	0.00	0.00	0.00	0	0	0	0	0.00	0.00	0.00	0.00	0.00	0.00	0.00	0.00	0.00	0.00	0.00	0.00	0.00	0.00	0.00	0.00

Gene ID	NOP89	PIF5	TelAP3	UPF1	p33	p34	p35	p38	p52	p68	p88	p105	
- 3036	4511 72	4269 24	3598 2	3477 45			4224 56	4582 09	4412 24	3663 63	4013 92	2931 66	3836 38	3164 29	3533 45	3079 42	4205 98	4261 58	2952 18	2397 36	3007 1	3392 42
VSG - 3240	0.02 4554 4	0.02 5577 96	0.01 7449 08	0.01 7655 79	0	0	0.01 8084 95	0.00 8446 98	0.02 7816 31	0.03 0496 83	0.01 9468 47	0.01 7778 54	0.01 9407 3	0.02 8689 2	0.02 3646 54	0.02 2611 15	0.02 1718 89	0.02 1889 11	0.02 4098 58	0.02 8277 11	0.02 0083 96	0.02 2797 16	0.02 1893 75	0.00 8920 29
VSG - 3255	0	0	0	0	0	0	0	0	0	0	0	0	0	0	0	0	0	0	0	0	0	0	0	0

Publication List

Weisert N., Kreß V., Hartleb L., Luko K., Lototska L., Krapoth N. C., Ulrich H., Janzen C. j., Butter F. (2023). TelAP2 links TelAP1 to the telomere complex in *Trypanosoma brucei*. in preparation, not published yet

Weisert N., Thein K., Reis H., Janzen, C. J. (2021). Quantification of RNA Polymerase I transcriptional attenuation at the active VSG expression site in *Trypanosoma brucei*. bioRxiv 2021.06.21.449234; doi: https://doi.org/10.1101/2021.06.21.449234. preprint.

Leal, A. Z., Schwebs, M., Briggs, E., Weisert, N., Reis, H., Lemgruber, L., Luko, K., Wilkes, J., Butter, F., McCulloch, R., & Janzen, C. J. (2020). Genome maintenance functions of a putative *Trypanosoma brucei* translesion DNA polymerase include telomere association and a role in antigenic variation. Nucleic acids research, 48(17), 9660–9680. https://doi.org/10.1093/nar/gkaa686.

Curriculum vitae